Unconventional Superconductivity in Bose-Fermi Mixtures

Jonatan Melkær Midtgaard

PhD Dissertation

Department of Physics and Astronomy
Aarhus University
Denmark

Jonatan Melkær Midtgaard
Department of Physics and Astronomy
Aarhus University
Ny Munkegade 120, Building 1520
8000 Aarhus C
Denmark

Unconventional Superconductivity in Bose-Fermi Mixtures

A Dissertation Presented to the
Faculty of Science and Technology of Aarhus University
in Partial Fulfillment of the Requirements
for the PhD Degree

by
Jonatan Melkær Midtgaard
October 2019

To my family.

Contents

Abstract

The present thesis is based on five publications and manuscripts. Three of them are on the general subject of p-wave topological superconductors in cold atomic gases, one of them on FFLO-type superconductivity in an atomic gas. The last one, which is unfortunately not quite covered by the title of the thesis, is regarding the microscopic origins of non-hermitian models used to extend the idea of topology into the realm of systems with loss and gain.

The first publication considers a gas of identical fermions, trapped in a 2-dimensional optical lattice and surrounded by a 3-dimensional Bose-Einstein condensate. The condensate acts as a medium for the fermions and leads to an induced, attractive interaction between them that can be tuned in strength and range. We study the system of fermions and find that topological p-wave superfluidity and phase separation are competing orders. While the phase separation is damaging to the superfluidity, the high level of control over the system is shown to be promising.

In the second publication, the same mixed-dimensional Bose-Fermi mixture is considered, but with the fermions being trapped in a bilayer geometry, without an in-plane optical lattice. We find that this system can realize time-reversal invariant topological states and that it is in principle possible to selectively prepare the system in this state, as opposed to non-time-reversal invariant ground states.

The third manuscript concerns the detection of the time-reversal symmetry-breaking states considered in the first and second publication. Analogous to circular dichroism in absorption spectroscopy, we find that the heating rates from clockwise and counter-clockwise circularly oscillating perturbations are different. It is possible to define a probe that follows an approximately topological law and is well suited to detect a topologically non-trivial ground state.

The fourth publication moves away from topological superconductivity and instead discusses superconductivity of the FFLO-type. Here, a density-

imbalanced version of the bilayer system is studied, showing that the long-range interactions and the control over the layer distance allows the FFLO-state to take up a much larger part of the phase diagram than possible for short-range interactions and and other schemes to produce longer-range interactions.

The fifth publication was done in collaboration with Prof. Hui Zhai's group at the Institute for Advanced Study at Tsinghua University in Beijing. Much work has been done there about the extension of topological classification to non-hermitian systems, and in our publication we take a look at how typically used toy models can be derived from system-environment interactions. We prove some identities about the eigenvalues of these effective Hamiltonians and show how to tune the non-hermitian terms by changing the properties of the environment.

Resumé

Denne afhandling er baseret på fem artikler og manuskripter. Tre af dem omhandler p-bølgesuperledere i kolde atomare gasser og én omhandler realiseringen af FFLO-superfluiditet i samme type system. Den sidste, som desværre ikke helt er dækket af afhandlingens titel, omhandler oprindelsen af ikke-hermitiske modeller, som bruges til at udvide konceptet om topologi i fysik til systemer med tab og forstærkning.

Den første udgivelse ser på en gas af identiske fermioner, fanget i et to-dimensionelt optisk gitter og omringet af et tre-dimensionelt Bose-Einstein-kondensat. Kondensatet agerer som et medie for fermionerne, hvilket leder til en induceret vekselvirkning mellem dem. Denne vekselvirkning kan tunes i både styrke og rækkevidde. Vi finder at både topologisk p-bølge superfluiditet og faseseparation er mulige ordener der bekæmper hinanden. Selvom faseseparationen bekæmper superfluiditeten, viser den store grad of kontrol over systemet sig at være lovende.

I den anden udgivelse betragtes den samme Bose-Fermi-blanding, dog med fermionerne fanget i en to-lags geometri, uden et optisk gitter. Dette system kan realisere topologiske tilstande der er invariante overfor tidsomvending, og det er principielt muligt at udvælge denne tilstand fremfor grundtilstande der bryder tidsomvendingssymmetri.

Det tredje manuskript omhandler detektionen de grundtilstande der bryder tidsomvendingssymmetri, betragtet i de to tidligere udgivelser. Analogt til cirkulær dikroisme inden for absorptions-spektroskopi, ser vi at opvarmningsraterne fra en rystelse med og mod urets retning, er forskellige. Det er da muligt at definere en probe der følger en approximativt topologisk kvantiseringslov og kan bruges til at detektere en topologisk grundtilstand.

Den fjerde udgivelse bevæger sig væk fra topologiske systemer og diskuterer i stedet superfluiditet af FFLO-typen. Her studerer vi to-lags systemet fra tidligere, men med forskellige tætheder af partikler i de to lag. Kontrollen over den inducerede vekselvirkning som Bose-Fermi-blandingen giver os, sammen med muligheden for at variere afstanden mellem lagene, tillader

FFLO-tilstanden at være den foretrukne grundtilstand for et langt større område af fasediagrammet end det er muligt for kortrækkende vekselvirkninger.

Den femte udgivelse blev skrevet i samarbejde med prof. Hui Zhais gruppe ved 'Institute for Advanced Study' på Tsinghua Universitet i Beijing. Som et led i deres arbejde på topologisk klassificering af ikke-hermitiske systemer, ser vi på hvordan hyppigt brugte modeller kan udledes fra interaktioner mellem et system og dens omgivelser. Vi beviser nogle matematiske sætninger om egenværdierne af de effektive Hamiltonoperatorer og viser hvordan omgivelsernes egenskaber kan bruges til at tune de ikke-hermitiske dele af systemet.

Acknowledgments

The work in this thesis was carried out in the years 2015-2019 in the group of Georg Bruun at Aarhus University. I began working with Georg during the writing of my Bachelor's thesis where our mutual struggle into the world of topological systems began. Above all, I would like to thank Georg for keeping his door open and letting me drop in at all times to ask questions.

I am also indebted to my friend Zhigang Wu, who has been almost as a second supervisor for me during my studies. Your support has been instrumental in getting me here and I am grateful for the opportunity to visit and work with you in Beijing after you went back to China. In the same vein, I would thank Prof. Hui Zhai for inviting me to stay and work with his group at Tsinghua University for 4 months in 2018, and Yu Chen for teaching me about the great works of Keldysh and just generally being a great guy and collaborator.

I would not have made it through 8 years plus some at Aarhus University without my friends, both inside and outside the walls. In the last couple of years I have been especially grateful for *frokostklubben* and our (sometimes) heated discussions over lunch or coffee. A special thanks to Niels Jakob, who has somehow survived sharing an office with me for as long as I can remember.

While studying for this PhD degree, I have had many chances to try to explain to various family members what it actually *is* I am spending all this time on. Despite my best efforts, I am still not sure anyone knows more than the fact that it's about cold things. Nevertheless, I owe my deepest gratitude to my whole family for their patience in dealing with someone like me.

Jonatan Melkær Midtgaard,
Aarhus, October 21, 2019.

List of Publications

This thesis is based on the following scientific papers:

I Jonatan Melkær Midtgaard, Zhigang Wu, and G. M. Bruun. "Topological superfluidity of lattice fermions inside a Bose-Einstein condensate." In: *Phys. Rev. A* 94 (6 Dec. 2016), p. 063631

II Jonatan Melkær Midtgaard, Zhigang Wu, and G. M. Bruun. "Time-reversal-invariant topological superfluids in Bose-Fermi mixtures." In: *Phys. Rev. A* 96 (3 Sept. 2017), p. 033605

III Jonatan Melkær Midtgaard and Georg M. Bruun. "Stabilizing Fulde-Ferrell-Larkin-Ovchinnikov superfluidity with long-range interactions in a mixed-dimensional Bose-Fermi system." In: *Phys. Rev. A* 98 (1 July 2018), p. 013624

IV Jonatan Melkær Midtgaard, Zhigang Wu, and Yu Chen. "Constraints on the energy spectrum of non-Hermitian models in open environments." In: *Eur. Phys. J. B (accepted)* (2019)

V Jonatan Melkær Midtgaard, Zhigang Wu, and G. M. Bruun. "Detecting Topological Superfluidity with a Dichroism probe." In: *(in preparation)* (2019)

In addition to the work presented in this thesis, I am a co-author on the following scientific paper:

VI Oleksandr V. Marchukov, Emil H. Eriksen, Jonatan M. Midtgaard, Alex A.S. Kalaee, Dmitri V. Fedorov, Aksel S. Jensen, and Nikolaj T. Zinner. "Computation of local exchange coefficients in strongly interacting one-dimensional few-body systems: local density approximation and exact results." In: *The European Physical Journal D* 70.2 (Feb. 2016), p. 32

— 1 —

Introduction

1.1 Structure of the Thesis

This thesis is mainly a so-called *paper-based* thesis. This means that published articles, accepted manuscripts as well as manuscripts in preparation has been copied in and forms the bulk of the thesis. In the case of published material, this has been copied in as it appears in the publications. In the case of accepted manuscripts and those in preparation, they are presented in a form close to what is intended for publication. At the same time, I have tried to introduce concepts and physics in appropriate places before they appear in the manuscripts. My hope is that this maintains the narrative strength of the more typical monograph-like thesis.

In accordance with GSST rules and regulations, parts of this thesis was also used in the progress report for the qualifying examination. This applies mainly to figures and wordings in the manuscripts from Chapters 2 and 3.

The remainder of the thesis is divided into five chapters, each corresponding to one of five published papers or prepared manuscripts. This is followed by a short summary. Throughout the thesis, $\hbar$ has been set to 1.

1.2 Ultracold Atoms

The field of ultracold atomic gases has seen tremendous growth in recent years as new experimental techniques have become available. Compared to solid-state materials, cold atomic gases offer a clean testbed for many-body physics and excellent tunability of system parameters.

The start of the rapid developments for bosons is arguably the first realisations of a Bose-Einstein Condensate by Anderson *et al.* [7] and Ketterle [8] in 1995. Not many years after, in 1999, De Marco and Jin [9] succeeded in cooling down a gas of fermionic ^{40}K to quantum degeneracy. Soon, this was followed also by several groups cooling down ^{6}Li [10, 11], and quantum

degeneracy has since been achieved with also alkaline and rare earth metals as well.

Optical Traps

In most experiments with cold atomic gases, beams of light are used to control the spatial distribution of the atom cloud. When an atom is exposed to an electric field, $\mathbf{E}(\mathbf{r})$, the field induces a dipole moment, $\mathbf{d}$, between the electron cloud and the nucleus. When the field is oscillating, as is the case for a laser, the AC Stark shift describes the shift of the ground state energy. This is a second-order effect, since the dipole moment of the atom is not constant. If we imagine the atom as a two-level system, the shift of the ground state energy is

$$V(\mathbf{r}) = |\Omega(\mathbf{r})|^2 \frac{\delta}{\Gamma^2 + 4\delta^2} \tag{1.1}$$

where $\Omega(\mathbf{r}) = \langle e|\mathbf{d} \cdot \mathbf{E}(\mathbf{r})|g\rangle$ is the Rabi frequency, and Γ is the lifetime of the excited state. δ is the detuning of the light from the resonant frequency between the two states. So with red-detuned light (negative δ) the atom is attracted to maxima in the light intensity and for blue-detuned light (positive δ) the atom is pushed away from the intensity maxima.

Optical Lattices

By applying two counter-propagating beams of light (or retro-reflecting a single beam), a standing wave can be created. This means the potential for the atom becomes (for a lattice along the z-direction)

$$V(\mathbf{r}) = V_{\text{lat}} \sin^2(kz) \tag{1.2}$$

where $k = 2\pi/\lambda$ with λ being the laser wavelength. A convenient scale for the lattice depth, V_{lat}, is often the recoil energy, $E_R = k^2/2m$, where m is the atom mass. In a sufficiently cold gas, the movement of atoms are restricted to the nodes (or possibly the anti-nodes) of the lattice. A tight-binding approximation can then be employed to recast the Hamiltonian in terms of lattice site occupations and hopping terms. This procedure can be repeated in other orientations to produce 1-, 2-, and 3-dimensional optical lattices.

To make the (quasi-) 2-dimensional systems considered in this thesis, it is possible to load an atomic cloud in an optical lattice in the z-direction, creating a "stack of pancakes" of 2D layers. For experiments with e.g. quantum gas microscopes it is often necessary to prepare only a single layer of atoms. This can then be done by applying a magnetic field gradient in

the z-direction along with a microwave field [12]. Only the layer in the correct position along the gradient is unchanged, whereas the atoms in the other layers are transferred to a different hyperfine state which can then be removed from the lattice.

Feshbach Resonances

In an ultracold, dilute gas af atoms, the only relevant scattering parameter is the s-wave scattering length, a_0. Higher orders of scattering are "frozen out" due to the low energy available. There might be bound states of two atoms at some lower energy, but due to energy conservation, these can not be accessed for two-particle collisions. However, if the magnetic moment of the bound state is different from the combined magnetic moment of the two free atoms, the energy difference between the "open" and "closed" channel can be changed by applying a magnetic field, B.

At resonance, B_0, the closed channel has the same energy as the two free atoms, leading to a divergence in scattering length. This is known as a magnetic Feshbach resonance. A simple expression for the scattering length is [13, 14]

$$a(B) = a_0 \left(1 - \frac{W}{B - B_0}\right) \tag{1.3}$$

where W is the resonance width. Around the resonance there is clearly both an attractive and repulsive regime. When these Feshbach resonances are available, they offer unprecedented freedom to choose a suitable interaction strength in an experiment. Due to this, we will often consider the interaction strength to be freely tunable in simulations.

1.3 Superconductivity in Atomic Gases

A many-body Hamiltonian for an ultracold atomic gas is usually truncated to only consider 2-body interaction. Due to the low density, 3- and 4- body interactions are exceedingly rare and usually negligible. For an interacting, two-component gas of fermions, ψ, with mass m, the Hamiltonian is

$$\begin{aligned} H = &\sum_{\sigma} \int \mathrm{d}\mathbf{r}\ \psi_\sigma^\dagger(\mathbf{r}) \left(\frac{-\nabla^2}{2m} + V(\mathbf{r}) - \mu_\sigma\right) \psi_\sigma(\mathbf{r}) \\ &+ \frac{1}{2} \sum_{\sigma\sigma'} \int \mathrm{d}\mathbf{r}\mathrm{d}\mathbf{r}'\ \psi_\sigma^\dagger(\mathbf{r}) \psi_{\sigma'}^\dagger(\mathbf{r}') U(\mathbf{r} - \mathbf{r}') \psi_{\sigma'}(\mathbf{r}') \psi_\sigma(\mathbf{r}) \end{aligned} \tag{1.4}$$

Within mean-field theory, the quartic term is approximated by a sum of quadratic terms

$$\begin{aligned}\psi^\dagger_\sigma(\mathbf{r})\psi^\dagger_{\sigma'}(\mathbf{r}')U(\mathbf{r}-\mathbf{r}')\psi_{\sigma'}(\mathbf{r}')\psi_\sigma(\mathbf{r}) \approx \\ 2U(\mathbf{r}-\mathbf{r}')\left\langle\psi^\dagger_{\sigma'}(\mathbf{r}')\psi_{\sigma'}(\mathbf{r}')\right\rangle\psi^\dagger_\sigma(\mathbf{r})\psi_\sigma(\mathbf{r}) \\ -2U(\mathbf{r}-\mathbf{r}')\left\langle\psi^\dagger_{\sigma'}(\mathbf{r}')\psi_\sigma(\mathbf{r})\right\rangle\psi^\dagger_\sigma(\mathbf{r})\psi_{\sigma'}(\mathbf{r}') \\ +\{U(\mathbf{r}-\mathbf{r}')\left\langle\psi_{\sigma'}(\mathbf{r}')\psi_\sigma(\mathbf{r})\right\rangle\psi^\dagger_\sigma(\mathbf{r})\psi^\dagger_{\sigma'}(\mathbf{r}'\} + \text{h.c.})\end{aligned} \tag{1.5}$$

where the two first terms are the Hartree and Fock terms, respectively. For the Hartree term we see that it is a coupling to the particle density

$$n_\sigma(\mathbf{r}) = \left\langle\psi^\dagger_\sigma(\mathbf{r})\psi_\sigma(\mathbf{r})\right\rangle. \tag{1.6}$$

The last two terms are the superconducting pairing terms,

$$\Delta_{\sigma\sigma'}(\mathbf{r},\mathbf{r}') = U(\mathbf{r}-\mathbf{r}')\left\langle\psi_{\sigma'}(\mathbf{r}')\psi_\sigma(\mathbf{r})\right\rangle \tag{1.7}$$

This is the Bardeen-Cooper-Schrieffer (BCS) approximation, as an extension to the usual Hartree-Fock approximation of many-body systems. $\Delta_{\sigma\sigma'}$ is usually referred to as the pairing field or the gap function. The Hamiltonian is now bilinear in the field operators and can be diagonalized by by a unitary Bogoliubov transformation. If we go to momentum space, the Bogoliubov transformation defines new fields as a linear combination of particles and holes

$$\gamma_{\mathbf{k}\sigma} = u_{\mathbf{k},\sigma}\psi_{\mathbf{k},\sigma} + v_{\mathbf{k},\bar{\sigma}}\psi^\dagger_{\mathbf{k},\bar{\sigma}} \tag{1.8}$$

and the ground state is defined as the vacuum state, $\gamma\left|\Omega\right\rangle = 0$, of these operators. These Bogoliubov modes are the excited states of the system, and a specific case is particularly interesting. If the Bogoliubov mode has zero energy, it turns out to be an even mixture of particle and hole, causing it to be its own antiparticle. This is known as a Majorana mode and is intimately related to the notion of topological superconductors as we shall see below.

The correct many-body ground state of the system in Eq. (1.4) with (1.5) is found by minimizing the grand canonical potential, $\Omega = \langle H\rangle - TS$, where the chemical potential has been included in the Hamiltonian to keep the number of particles constant. The reason for using the grand canonical ensemble, when most experiments are done with a fixed particle number, is that for large systems in a shallow trap one region will exchange particles with another region. So the local particle number fluctuates, and the quantity that is kept constant through out the trap is the chemical potential. Minimizing the grand canonical potential gives a set of coupled, self-consistent equations for the self-energy, superconducting pairing, as well as the number equation.

These can typically be solved in an approximate manner, or iteratively from some initial guess.

For now, we focus on the pairing terms. If the interaction U is a contact interaction, there is no interaction between like components and hence no pairing, so $\Delta_{\sigma\sigma} = 0$, due to Pauli exclusion. With a longer-range interaction, however, we can have pairing between the same components. If we interpret σ as a spin-polarization, then along with the spin wavefunction $|\sigma\sigma'\rangle$, the pairing function $\Delta_{\sigma\sigma'}$ constitutes the wavefunction of the *Cooper pairs* that condense in the superconducting ground state.

In momentum space, the pairing usually happens between pairs of fermions with opposite momenta, $\mathbf{k}$ and $-\mathbf{k}$, such that the Cooper pair with the gap function $\Delta_{\mathbf{k}}$ has no total, center-of-mass momentum. Knowledge of the spin-components then allows us to make assumptions on the symmetry properties of $\Delta_{\mathbf{k}}$, since the total wavefunction must be antisymmetric under particle exchange.

A gas of interacting fermions show strikingly different behaviour on different sides of a Feshbach resonance. Above, we have described the behaviour for weak to moderate negative scattering lengths. On the other side of the resonance, for positive scattering lengths, the ground state is a Bose-Einstein condensate of tightly bound fermion dimers [15]. The nature of the ground state as the scattering length diverges across the resonance is known as the BEC-BCS crossover and has received intense study over the years [16–18]. In this thesis we will stick to moderately attractive fermions. Because we work with neutral atomic gases they will also have no charge, so the terms superfluid and superconductor will be used interchangeably and always about behaviour in the BCS regime.

1.4 Topological Systems

The name *Topological systems* refers to classifications of systems that are robust to a certain set of deformations or perturbations. Being robust in this case means that some observable, the conductivity for instance, only takes discrete values and is unchanged even if we perturb the system slightly. This type of classification goes beyond the normal Landau theory of symmetry breaking.

In general there are two main groups of topological systems. A (intrinsic) topological system has long-range order and will be robust to all kinds of perturbations that does not close the energy gap. This might be a weak potential, magnetic order, or the introduction of some other gauge field. The archetypical example is the Fractional Quantum Hall state, which gets its name from the fractional values of the Hall conductance it displays.

The other group of topological systems are known as *Symmetry-Protected Topological states*. The symmetries the name refers to are a set of three *anti-unitary* symmetries which will be explained below. In a sense, these systems are "less" topological than their intrinsically topological cousins, as they only display robust features against perturbations that do not break any of the anti-unitary symmetries the unperturbed Hamiltonian obeys. In the more recent literature, the name 'topological' refers mainly to the first kind of system, but in this thesis it is the second class of topological systems that will be considered in this thesis whenever topology is mentioned.

The three independent anti-unitary symmetries a system can obey are called *time-reversal*, T, *particle-hole*, P, and their combined transformation $S = T \cdot P$ called *chiral* or *sublattice* symmetry. Consider some second-quantized, non-interacting Hamiltonian,

$$\hat{H} = \sum_{ab} \hat{\psi}_a^\dagger H_{ab} \hat{\psi}_b \tag{1.9}$$

We will consider this Hamiltonian to not obey any unitary symmetries, such as translation-invariance. If it does, we can transform to a block-diagonal structure of the Hamiltonian and consider each of the blocks separately. Note that Eq. 1.9 describes an insulator, but the method can easily be extended to Hamiltonians with pairing terms $\sim \psi^\dagger \psi^\dagger$. The matrix H_{ab} must then obey particle-hole symmetry, as defined below.

The time-reversal transformation is defined according to the criteria

$$T\hat{\psi}_a T^{-1} = \sum_b (U_T^\dagger)_{ab} \hat{\psi}_b, \quad TiT^{-1} = -i, \tag{1.10}$$

where U_T is a unitary matrix. So in effect, $T = U_T \cdot K$ for the first-quantized Hamiltonian H_{ab}, where K denotes complex conjugation. If $T\hat{H}T^{-1} = \hat{H}$, then time-reversal is a symmetry of the Hamiltonian. The particle-hole transformation, P, (also sometimes called charge-conjugation, C, in the literature) is defined by

$$P\hat{\psi}_a^\dagger P^{-1} = \sum_b \hat{\psi}_b (U_P^*)_{ba}, \quad PiP^{-1} = i \tag{1.11}$$

where U_P is again a unitary matrix. The matrix U_P has the property that $U_P U_P^* = \pm 1$, and likewise for U_T. After defining these transformations, we can start to classify Hamiltonians. Every Hamiltonian can react in three ways to time-reversal for instance. Either it is not invariant, or it *is* invariant under a time-reversal symmetry that squares to $+1$, or it is invariant under one that squares to -1. With these two symmetries, we have then classified Hamiltonians in 9 different classes. The last possibility is to consider is

their combined operation, $S = T \cdot P$. The transformation under this is only undetermined if the Hamiltonian is not invariant under any of the individual symmetry transformations. The Hamiltonian can then either be or not be invariant under the combined transformation. So this brings us to a total of 10 classes of Hamiltonians, and is the foundation of Kitaev's "periodic table of insulators and superconductors" [19] seen in Fig. 1.1.

Symmetry				Spatial Dimension d								
Class	T	C	S	1	2	3	4	5	6	7	8	$\cdots$
A	0	0	0	0	$\mathbb{Z}$	0	$\mathbb{Z}$	0	$\mathbb{Z}$	0	$\mathbb{Z}$	$\cdots$
AIII	0	0	1	$\mathbb{Z}$	0	$\mathbb{Z}$	0	$\mathbb{Z}$	0	$\mathbb{Z}$	0	$\cdots$
AI	1	0	0	0	0	0	$\mathbb{Z}$	0	$\mathbb{Z}_2$	$\mathbb{Z}_2$	$\mathbb{Z}$	$\cdots$
BDI	1	1	1	$\mathbb{Z}$	0	0	0	$\mathbb{Z}$	0	$\mathbb{Z}_2$	$\mathbb{Z}_2$	$\cdots$
D	0	1	0	$\mathbb{Z}_2$	$\mathbb{Z}$	0	0	0	$\mathbb{Z}$	0	$\mathbb{Z}_2$	$\cdots$
DIII	-1	1	1	$\mathbb{Z}_2$	$\mathbb{Z}_2$	$\mathbb{Z}$	0	0	0	$\mathbb{Z}$	0	$\cdots$
AII	-1	0	0	0	$\mathbb{Z}_2$	$\mathbb{Z}_2$	$\mathbb{Z}$	0	0	0	$\mathbb{Z}$	$\cdots$
CII	-1	-1	1	$\mathbb{Z}$	0	$\mathbb{Z}_2$	$\mathbb{Z}_2$	$\mathbb{Z}$	0	0	0	$\cdots$
C	0	-1	0	0	$\mathbb{Z}$	0	$\mathbb{Z}_2$	$\mathbb{Z}_2$	$\mathbb{Z}$	0	0	$\cdots$
CI	1	-1	1	0	0	$\mathbb{Z}$	0	$\mathbb{Z}_2$	$\mathbb{Z}_2$	$\mathbb{Z}$	0	$\cdots$

Figure 1.1: The tenfold classification of topological superconductors and insulators, by Kitaev [19], and Altland and Zirnbauer [20]. Figure from [21]. Note that they use C as the particle-hole/charge-conjugation transformation, which is denoted as P in the main text.

While the names of the symmetries carry a certain physical intuition, it is important to note that there is a freedom in the exact definitions of these symmetries. For instance, we are used to the time-reversal operation squaring to -1, giving us Kramer's theorem, but we have expanded this definition. The particle-hole symmetry under the above definition might not always coincide with the *physical* definition of particle-hole symmetry, either.

Classification of Ground States

The idea of topological classification is then the realisation that each of these classes are subdivided into families of Hamiltonians which cannot be smoothly connected without closing an energy gap. The rest of this chapter will be a sketch of how this comes about for an Integer Quantum Hall (IQH) state[1]. This is the simplest of the 10 classes and obeys no anti-unitary symmetries.

[1]This part is based on and contains excerpts from notes produced by me for a study group I organized on topological classification.

Consider two mappings $f, g : X \to Y$. The two mappings are homotopic if there exists the smooth interpolating function $h : X \times [0, 1] \to Y$ where $h(x, 0) = f(x)$ and $h(x, 1) = g(x)$. For simple choices of X and Y„ the structure is simple. Consider maps from the circle S^1 to $\mathbb{R}^2$. The maps f and g are then simply closed curves in the plane. Clearly, all maps are homotopic, since all closed curves can be deformed into each other in $\mathbb{R}^2$. But for maps from S^1 to the 2-torus T^2, the situation is different. Here, a closed curve going around one of the basic loops of the torus can never be deformed to one going around the other basic loop. So the space of maps is not path-connected. Indeed, every map is characterized by a set of two integers: Their winding number around each basic loop of the torus. These two integers are topological invariants for a map, in the same way as the Hall conductivity is a topological invariant for the IQH state.

The general idea is to consider Hamiltonians as maps from momentum space to some space of matrices. For a two-dimensional system with translation symmetry, momentum space is a torus, but it turns out to be sufficient to consider it as a 2-sphere, which is quite a bit simpler. For the IQH state with n separate bands, the matrices do not have to obey any special symmetries, so this is simply the space of hermitian matrices of size n. By diagonalisation we can choose to work with the space of unitary matrices $U(n)$, instead. Here we must remember that eigenstates of a Hamiltonian are only uniquely defined up to a phase, so elements of $U(n)$ are only unique up to an element of $DU(n)$, the diagonal, unitary matrices. What this leaves us with, is that in two dimensions, we are interested in classifying the maps from the 2-sphere, S^2, to the coset space $U(n)/DU(n)$.

Classifying these maps is done through the notion of a *homotopy group*. Skipping over some details, $\pi_d(M)$ tells us what topological invariants are associated to maps from the d-sphere to the space M. $\pi_1(M)$ is called the *fundamental group* and is simply a classification of all possible loops in M. The classification associates an element in a group – for our purposes, typically $\mathbb{Z}$ or $\mathbb{Z}_2$ – to each family of homotopic loops. Right now, we are interested in maps from S^2, corresponding to π_2. In the interest of brevity, we will simply state the result, which is that

$$\pi_2(U(n)/DU(n)) = \mathbb{Z}^{n-1} \tag{1.12}$$

There are a few things we can extract from this result. The common interpretation is that we can associate n integers to the Hamiltonian – one for each band – as topological invariants. This turns out to be the first Chern number, which can be calculated individually for each band. The reason that we have one fewer invariants than bands is because of a sum rule. All Chern numbers must sum to 0. So in a 2-band model, we really only

have 1 independent invariant. Another nice result is that if we calculate π_1 or π_3 for the same space of matrices, they turn out to be the trivial group. This is equivalent to the statement that there are no IQH effect in 1 or 3 dimensions.

We must fix one remaining problem, though. No matter how many bands, we expect our quantum Hall state to have only *one* invariant, which is the Hall conductivity. This is because we have classified our Hamiltonians to discriminately. With the construction above, we did not allow ourseves to close an energy gap between *any* bands. But in fact, the only relevant distinction is between filled and empty bands. So let us instead say that we have a model with m empty and n filled bands. Then our space of allowed unitary matrices are $U(m+n)$. But we consider them equivalent up to unitary rotations within the empty or filled manifold, respectively. That is, the target space for our maps is the complex Grassmannian, $G = U(m+n)/[U(m) \times U(n)]$. Calculating the first few homotopy groups for this yields

$$\pi_1(G) = \{1\}, \quad \pi_2(G) = \mathbb{Z}, \quad \pi_3(G) = \{1\}. \tag{1.13}$$

Here, the notation $\{1\}$ denotes the trivial group. This exactly reproduces our expectations of no IQH state in 1 or 3 dimensions, but a single topological invariant in 2 dimensions. For the other classes in the tenfold classification, we could in principle repeat the same calculations. However, the introduction of the anti-unitary symmetries makes the target spaces more complicated and in general the direct calculation of the homotopy groups become intractable. For more information, see e.g. Kitaev [19] and reviews by Ludwig [22] and Ryu *et al.* [23].

The IQH state was chosen for this part because of the relatively simple derivations required and because the chiral superconductors that much of the thesis concerns, are the superconducting analog to this insulating state. The only difference is that the BCS Hamiltonian obeys particle-hole symmetry (with $U_P U_P^* = +1$).

Majorana Edge Modes

Topological systems can have special excitations at the boundary. The boundaries of a topological insulator such as the IQH state carries metallic states at the Fermi level. Similarly, the chiral superconductors considered in this thesis are expected to have Majorana excitations at the edge, which are exitations at the Fermi level composed of an equal mixture of particles and holes as mentioned above. They obey non-Abelian statistics when interchanged, meaning that for some quantum state with two Majorana

modes [24],

$$\psi(\mathbf{r}_1, \mathbf{r}_2) \to e^{i\phi}\psi(\mathbf{r}_2, \mathbf{r}_1) \to e^{i2\phi}\psi(\mathbf{r}_1, \mathbf{r}_2) \tag{1.14}$$

when the modes are interchanged twice. $\phi = 0, \pi$ corresponds to bosons and fermions, respectively. Majorana states can realize other values of ϕ, as an example of an *anyon*. In quantum computation, a system of m Majorana modes would constitute a 2^m-dimensional subspace in which computations are transformations performed by physically braiding the Majorana modes. The non-local nature of the computations make this an intriguing proposal for building a fault-tolerant quantum computer [25, 26].

A further thing to note about realizing Majorana modes in chiral superconductors is that these modes can also appear in the core of Abrikosov vortices [27]. This allows for spatial isolation and control over the location. For a review of the above, see [24].

— 2 —

A p-wave Superconductor in a Lattice

The paper presented in this chapter considers a gas of identical fermions immersed in a Bose-Einstein condensate. Through the exchange of Bogoliubov modes of the BEC, the fermions acquire an attractive, induced interaction that in turn makes the ground state unstable towards superfluidity. The fermions are furthermore constrained into a two-dimensional plane and caught in a square, optical lattice. This ensures that the possible superfluid pairings are chiral. The chapter will start with a brief discussion about the chiral superfluids, and then some relevant background physics, before moving on to the included paper. The induced interaction is obtained by integrating out the bosons from the total system action, but the derivation is outlined in the paper, so it will not be discussed here.

2.1 The $p_x + ip_y$ Superconducting Phase

The chiral superfluid, as realised by the $p_x + ip_y$ state, is perhaps one of the most paradigmatic examples of a topological superconductor, in the same sense as the integer quantum Hall state has been for topological insulators. Also known as the Chern insulator, the integer quantum Hall state has been an archetypical example of topological systems since it was shown to be realised in the Haldane model [28]. It remains a popular starting point for extension into the fractional Quantum Hall effect, non-Hermitian topology and much more [29, 30]. As discussed above, the ground state obeys none of the three anti-unitary symmetries, so the superconductor-equivalent to this state must obey no other symmetries than the particle-hole symmetry intrinsic to the BCS Hamiltonian. These are indeed the *chiral* superconductors, due to the breaking of time-reversal. Going back to Fig. 1.1, we see that this type of system is in class D.

In a chiral, topological superconductor, each Cooper pair has a non-zero angular momentum equal to $-C$, where C is the Chern number of the ground state. For identical fermions, the spin wavefunction of the Cooper

pair is even, so this limits us to odd values of the angular momentum, to ensure that the gap $\Delta_{\mathbf{p}}$, is odd. For systems with cylindrical symmetry we can usually ignore admixtures between different angular momenta, so a useful ansatz is $\Delta_{\mathbf{p}} = \Delta(|p|)e^{i(l\phi_{\mathbf{p}}+\Phi)}$ where $\phi_{\mathbf{p}}$ is the angle of the $\mathbf{p}$-vector and Φ is a global phase. Note that l is an odd integer. For p-wave pairing we choose $l = \pm 1$, which realises the $p_x \pm ip_y$-superfluid state. The name comes from the high-wavelength limit where $\Delta(|p|) \propto |p|$. This state has a Chern number $C = 1$ or $C = -1$, depending on the chirality.

Higher angular momenta, $l = \pm 3, \pm 5, \ldots$ would have higher Chern numbers, but these typically have a higher ground state energy. There are also other choices of ansatz for the pairing that are odd, but not cylindrically symmetric, such as a pure p_x or p_y pairing. These only gap part of the Fermi surface, however, so they will also typically have a higher ground state energy.

In cold atomic gases, proposals to break time-reversal symmetry and realise a chiral superfluid include, among others, p-wave Feshbach resonances, which unfortunately suffer from recombination-losses [31], and spin-orbit-coupling [32]. In the spin-orbit proposal, a background BEC provides s-wave pairing between the fermions and a Raman transition induces the spin-orbit coupling which breaks time-reversal symmetry. In the proposal below we cut out the middle man, so to speak, and let the induced interaction work on a gas of identical fermions. p-wave pairing is then the most energetically favorable type of pairing.

In the following paper, we will consider the fermions to be moving in a square lattice. Capturing the fermions in a lattice does not substantially change the topological properties of the system, but it has several technical advantages. With the advent of quantum gas microscopes [33, 34], it is now possible to probe and control atoms in optical lattices at a single-site level. This would make it possible to directly image the Majorana modes at the edges and provide an unequivocal detection of topological superconductivity, something which has so far eluded us in cold atomic systems.

2.2 Methods

Berezinskii-Kosterlitz-Thouless Melting

The 2-dimensional XY model is a model of vector spins (or rotors) on a 2-dimensional square lattice. The nearest-neighbour interactions are given by

$$F_{XY} = -J \sum_{\langle i,j \rangle} \cos(\theta_i - \theta_j) \tag{2.1}$$

where θ_i is the angle of the spin $\mathbf{S}_i$ on the i'th lattice site. If $J > 0$, it is quite intuitive that the low-temperature behaviour must have all the spins pointing in the same direction, spontaneously breaking the global $U(1)$ symmetry. However, the Mermin-Wagner theorem prohibits this for any non-zero temperature in 2 dimensional systems [35]. The resolution of this apparent paradox is to realize that the low-temperature ground state actually doesn't have perfect long-range order. There are always available spin wave excitations at low energies at high enough wavelengths, meaning that the otherwise ordered spins can twist on long enough length scales. Indeed, for low temperatures, the correlation function drops off as a power function

$$\langle \mathbf{S}_i \cdot \mathbf{S}_j \rangle \propto (\mathbf{r}_i - \mathbf{r}_j)^{-T/2\pi J} \tag{2.2}$$

instead of being a constant, as would be expected for a completely ordered phase. It drops off exponentially at higher temperatures

$$\langle \mathbf{S}_i \cdot \mathbf{S}_j \rangle \propto e^{-|\mathbf{r}_i - \mathbf{r}_j|/\xi} \tag{2.3}$$

where ξ is inversely related to the temperature. Looking at these functions, we can see that the transition between the two must be more subtle than a simple second-order phase transition. As discovered by Berezinskii, Kosterlitz and Thouless (BKT) [36–38], the phase transition is one of infinite order. The transition is intimately connected to the formation and proliferation of vortices in the vector spins, as I will briefly outline. The energy cost of a free vortex scales logarithmically with the system size,

$$E = \pi J \ln \frac{L}{\ell} \tag{2.4}$$

where L is the system side length and ℓ is the lattice length. So in the thermodynamic limit, no free vortices exist in the low-temperature phase. A cheaper possibility is to create a bound vortex-antivortex pair. This always costs a finite energy, so they are present in the low-temperature phase at any non-zero temperature. As the temperature is increased, the vortex-pairs become unbound and destroy the *quasi*-long-range order that was present. Arguments from Kosterlitz and Thouless [39] can estimate the temperature where this happens. Consider the entropy of a free vortex. It can be placed on every lattice site, so the entropy must be

$$S = 2k_B \ln \frac{L}{\ell} \tag{2.5}$$

The temperature where the vortices become unbound must then be the temperature where the free energy cost of the single vortex vanishes. This gives us

$$F = E - TS = 0 \rightarrow T = \frac{\pi}{2} J \tag{2.6}$$

For our purposes, we can map our superfluid systems to this XY model by realising that the global superfluid phase Φ is equivalent to the vector spins in the XY model. The superfluid phase stiffness is then equivalent to the coupling strength J. In the paper below, we calculate this stiffness by imposing a twist in the global phase and calculating the change in free energy.

Phase Separation

Apart from superconductivity, there is another, competing instability of the normal, metallic ground state of the fermions. This is *phase separation* where a range of filling fractions in the lattice become unstable. In the paper, we consider a system of fermions with periodic boundary conditions, but we can use the Maxwell construction to understand how a finite system would behave in some kind of confinement. The Maxwell construction itself is a classic result from thermodynamics that we can adapt to our system, but we will go through the argument here.

Consider a gas in a container, with an equation of state giving us an isotherm line on a $(p - V)$ diagram as in Fig. 2.1(a). Intuitively, this line decreases monotonically. If we push on the sides of the container to lower the volume, we expect the pressure to increase and vice versa. The initial use of the Maxwell construction was for the van der Waals-equation

$$(p + \frac{\tilde{n}^2 a}{V^2})(V - \tilde{n}b) = \tilde{n}RT \tag{2.7}$$

which describes a gas of attractive particles. $\tilde{n} = N/N_A$ is the number of moles of particles, and a and b are the attraction strength and volume of the particles, respectively. The solutions of this behaves as expected for high temperatures. For low temperatures however, the isotherm drops down and changes direction as seen on Fig. 2.1(b). The section of the graph where $\partial p/\partial V$ is positive is clearly unphysical, since this corresponds to a negative compressibility. We could squeeze the sides of the container and cause the pressure of the gas to *drop*. As Maxwell argued [40], it must mean that the intermediate states are not true equilibrium states, but instead corresponds to a phase transition where the gas liquefies to a liquid-gas mixture. We fix this by drawing a horizontal line on the $(p - V)$-diagram as shown in Fig. 2.1(b) and claiming that all the states on the border of the shaded area are unphysical, or at least unstable. The constraint is that the two shaded areas are equal in size. To see this, consider the work done by the gas as we take the system from the high-pressure phase to the low-pressure phase. This cannot depend on whether we take the hypothetical path the van der

Waals equation gives us or our new, straight line. So since

$$W = \int_{V_1}^{V_2} P \mathrm{d}V \tag{2.8}$$

the equal-area rule follows naturally.

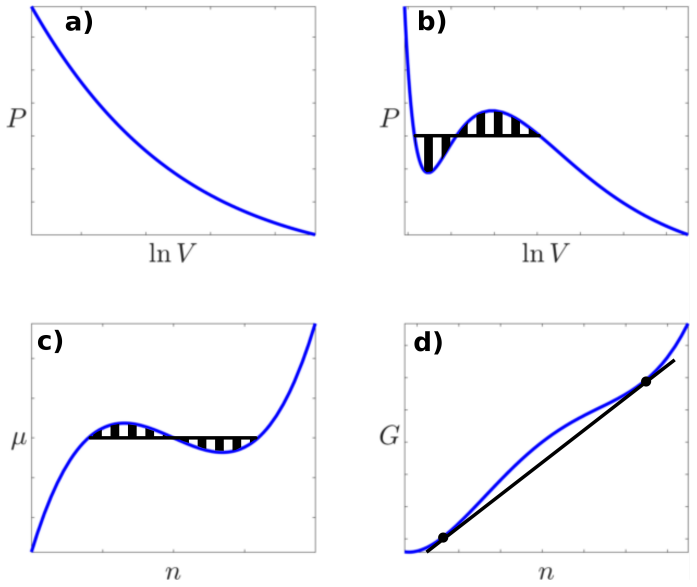

Figure 2.1: (a) and (b) show (P-V)-diagrams for a gas above and below the critical temperatures, respectively. The curves are solutions of Eq. 2.7. In (b), the unstable region with the Maxwell construction is indicated. (c) and (d) show the same situation as (b), but in the grand canonical ensemble with the chemical potential μ and Gibbs free energy G, respectively.

In our system of fermions, we are working in the grand-canonical ensemble and in a lattice, so the natural variables are the chemical potential, μ, and the filling fraction $n = Na^2/V$, where N is the number of fermions, a is the distance between the lattice sites, and V is the system volume. The chemical potential of a gas generally depend logarithmically on pressure, but since we are considering very dilute gases, we can approximate this to be a linear behaviour. This leads us to the conclusion that a proper isothermic line on a $(\mu - n)$-diagram should increase monotonically and when we get a curve that slopes downward, we should interpret it with Maxwell's equal area rule, as in the case of the $(p - V)$-diagram. Se Fig. 2.1(c) for an illustration. In this situation, the system will spontaneously order itself into a high-density phase and a low-density phase with equal chemical potentials.

Another way of considering the phase separation in the $(\mu - n)$-diagram is to recognize that $\mu = (\partial G/\partial N)$, where G is the Gibbs free energy. A

downward-sloping μ means that the energy curve in the $(G-n)$-diagram becomes concave and it is possible to minimize the free energy of the system by splitting up into two phases. The two points must be connected by a common tangent since they have the same chemical potential, as seen in Fig. 2.1(d). We get

$$\frac{G_2 - G_1}{V} = \int_{n_1}^{n_2} \mu \, \mathrm{d}n \tag{2.9}$$

since μ is the partial derivative of G, and

$$\frac{G_2 - G_1}{V} = \mu_1 (n_2 - n_1) \tag{2.10}$$

from the common chemical potential. Together, Eqs. (2.9-2.10) yields the equal-area rule.

2.3 Results

Our analysis showed the 2D lattice system immersed in a 3D BEC indeed had two competing orders in the low-temperature regime: topological $p_x + ip_y$ superfluidity and phase separation. The phase separation is mainly driven by the Hartree-terms in the mean-field theory. Varying the healing length of the BEC is equivalent to varying the range of the induced interaction between the fermions, so it is possible to tune the system towards favoring superfluidity. Given a BEC healing length, there then exists an optimal value for the strength of the Bose-Fermi interaction. It is in a "sweet spot", given by the trade-off between superfluidity and phase separation. As the interaction strength is turned up, phase separation kicks in and the filling fractions around $n = 1/2$ become unstable. These are unfortunately also the most favorable filling fractions for superfluidity. For this reason, it is not possible to achieve a large superfluid pairing gap, even with a Bose-Fermi mixture with a convenient, broad Feshbach resonance. For high enough interaction strengths, all filling fractions between 0 and 1 are phase separated, analogously to a collapse in homogeneous Bose-Fermi mixtures [41]. However, the phase separation only happens for higher interaction strengths than in purely two-dimensional mixtures [42]. This suggests that the mixed-dimensional geometry is suitable for inducing topological superconductivity in 2D systems.

We found that shorter BEC healing lengths tended to favor superfluidity over phase seaparation. Indeed, the healing length should be well below $\sim$1 lattice length for the critical temperature to be within reach of current experiments. However, once we approach the limit where the induced interaction is basically only between nearest-neighbours in the lattice, it is not possible to improve the situation further.

Even in this limit, however, the critical temperature seems to be limited to about $T_{\mathrm{BKT}} \approx 2\mathrm{nK}$. This is for experimentally relevant parameters for a gas of fermionic ^{6}Li trapped in an optical lattice with wavelength $\lambda = 1000\mathrm{nm}$ and a depth of $V_{\mathrm{lat}} = 5E_R$.

This temperature is unfortunately too low to be realised in experiments at the moment. Schäfer *et al.* recently reported [43] reaching temperatures of approximately 80nK, though this was for a heavy-fermion Bose-Fermi mixture. The appearance of phase separation in the lattice system turns out to be quite detrimental to the superfluid order since this makes the most desirable regions of the phase diagram unstable.

From a topological point of view, the lattice system would be quite interesting to study, if realized. If the fermions were confined in a harmonic trap, the phase separation changes the density profile from a smooth Thomas-Fermi-like profile, to a discontinuous 'wedding cake' profile with a high density region in the center of the trap, surrounded by a lower-density ring-shaped region. Because of the behaviour of the system under the particle-hole transformation $Pa_iP^{-1} = a_i^\dagger$, we concluded that at the discontinuity, the Chern number changes from +1 in the center to -1 at the rim. This would seem to imply the existence of zero-energy Majorana modes at the interface. However, two caveats must be mentioned here. The first is that the opposite situation is just as likely ($p_x + ip_y$ and $p_x - ip_y$ are degenerate), which is not that important to the observable zero-modes, since they still exist in this scenario. The second caveat is more severe. It is unclear how much this mapping between a filling fraction n and $n-1$ would translate into a relationship between the high-density inner part and low-density rim. We might always get one of them in a $p_x + ip_y$ state and the other in a $p_x - ip_y$ state, or we might get them in the same state. In this case there would be no zero-modes at the interface. A full real-space calculation with a harmonic trap would be needed to answer which situation, if any, is energetically favorable. In fact, the real-space calculation was the initial plan for this publication but because of the phase separation, the pairing field was quite low compared to finite-size effects in the lattice. This made a calculation through the self-consistent equations untractable. Instead, the next publication [2] in chapter 3 attempts to attack this question from a different angle.

2.4 Contribution

I carried out most of the derivations in the following paper, in particular chapters I through IV. Chapter V was based on previous work by Anne-Louise Gadsbølle with G. M. Bruun [44], which was adapted for use in this

context. I also performed all numerical simulations and I had the main responsibility for writing the paper.

Topological superfluidity of lattice fermions inside a Bose-Einstein condensate

Jonatan Melkær Midtgaard,* Zhigang Wu, and G. M. Bruun
Department of Physics and Astronomy, Aarhus University, Ny Munkegade, DK-8000 Aarhus C, Denmark
(Received 11 October 2016; published 22 December 2016)

We calculate the phase diagram of identical fermions in a two-dimensional lattice immersed in a three-dimensional Bose-Einstein condensate (BEC). The fermions exchange density fluctuations in the BEC, which gives rise to an attractive induced interaction. The resulting zero-temperature phase diagram exhibits topological $p_x + ip_y$ superfluid phases as well as a phase separation region. We show how to use the flexibility of the Bose-Fermi mixture to tune the induced interaction, so that it maximizes the pairing between nearest-neighbor sites, whereas phase separation originating from long-range interactions is suppressed. Finally, we calculate the Berezinskii-Kosterlitz-Thouless critical temperature of the topological superfluid in the lattice and discuss experimental realizations.

DOI: 10.1103/PhysRevA.94.063631

I. INTRODUCTION

Since topological superfluids and superconductors with Majorana modes were predicted to exist [1], detecting them has been a major research goal. Experimental evidence for Majorana modes has been reported in one-dimensional (1D) wires [2–8], and Sr_2RuO_4 is a promising candidate for realizing a two-dimensional (2D) topological superconductor [9–12]. Unambiguous detection of topological superconductivity or superfluidity is, however, still lacking, partly due to the complexity of these condensed matter systems. There have been several proposals to use the clean and highly flexible atomic quantum gases to overcome this difficulty. The first scheme was based on Fermi gases interacting via a p-wave Feshbach resonance [13], but these systems suffer from short lifetimes [14–17]. Other quantum gas proposals include schemes based on optical lattices [18–21], synthetic spin-orbit coupling [22–24], driven dissipation [25,26], dipolar molecules [27–29], and mixed-dimension Fermi-Fermi mixtures [30]. Unfortunately, none of these systems have been realized so far.

Very recently, two of us (Z.W. and G.M.B.) demonstrated that a mixed-dimension Fermi-Bose mixture constitutes a promising system for realization of a 2D topological superfluid [31]. In this proposal, identical fermions are confined in a 2D plane and they interact via density modulations in a surrounding Bose-Einstein condensate (BEC). Due to the high compressibility of the BEC, this induced interaction is strong, and one can, moreover, control the range by varying the BEC coherence length. This flexibility can be used to make the critical temperature of the topological superfluid high, while keeping three-body losses small. The purpose of the present paper is to examine this promising scheme in a setup where the fermions are moving in a 2D optical lattice. Optical lattices offer the particular advantage of single-site resolution spectroscopy [32,33], which presents unique opportunities to detect and manipulate Majorana edge modes [34,35]. We therefore investigate the phase diagram of identical fermions moving in a 2D square lattice immersed in a three-dimensional (3D) BEC, which gives rise to an attractive induced interaction between the fermions. As a result, the ground state of the fermions is a topological $p_x + ip_y$ superfluid, but the system also suffers from a phase separation instability originating from an underlying particle-hole symmetry in the lattice. Taking the competition of these two instabilities into account, we calculate the zero-temperature phase diagram of the fermions as a function of the Bose-Fermi coupling strength and the filling fraction. We show how to use the flexibility of the Bose-Fermi system to tune the interaction in order to maximize the pairing strength, while keeping the system stable against phase separation. The key point in solving this delicate problem turns out to be adjusting the range of the interaction by changing the BEC coherence length, so that it induces pairing at neighboring sites, while it does not lead to significant long-range interaction effects beyond nearest neighbors. We finally calculate the Berezinskii-Kosterlitz-Thouless (BKT) critical temperature for the superfluid phase and discuss experimental realizations.

II. MODEL

We consider fermionic atoms of mass m moving in a 2D square lattice in the xy plane. The lattice is immersed in a 3D BEC consisting of atoms of mass m_B, which are weakly interacting with $n_0 a_B^3 \ll 1$, so that it can be accurately described by Bogoliubov theory. Here n_0 denotes the condensate density and a_B the boson-boson scattering length. The setup is illustrated in Fig. 1. The Hamiltonian is

$$H = -t \sum_{\langle i,j \rangle} (a_i^\dagger a_j + \text{H.c.}) + \sum_{\mathbf{k}} E_{\mathbf{k}} \gamma_{\mathbf{k}}^\dagger \gamma_{\mathbf{k}} + H_{\text{int}}, \quad (1)$$

where t is the hopping matrix element of the fermions between nearest-neighbor sites $\langle i,j \rangle$, $a_i^\dagger$ creates a fermion at lattice site i, and $\gamma_{\mathbf{k}}^\dagger$ creates a Bogoliubov mode in the BEC with momentum $\mathbf{k}$ and energy $E_{\mathbf{k}} = [\epsilon_k^B(\epsilon_k^B + 8\pi n_0 a_B/m_B)]^{1/2}$, where $\epsilon_k^B = k^2/2m_B$. We use units for which $k_B = \hbar = 1$. Within the pseudopotential approximation, the interaction between the fermions and the bosons is

$$H_{\text{int}} = g \int d^3r \; \psi_F^\dagger(\mathbf{r}) \psi_B^\dagger(\mathbf{r}) \psi_B(\mathbf{r}) \psi_F(\mathbf{r}), \quad (2)$$

where $\psi_B(\mathbf{r})$ and $\psi_F(\mathbf{r})$ are the field operator for the bosons and fermions, respectively. The coupling strength is

*midtgaard@phys.au.dk

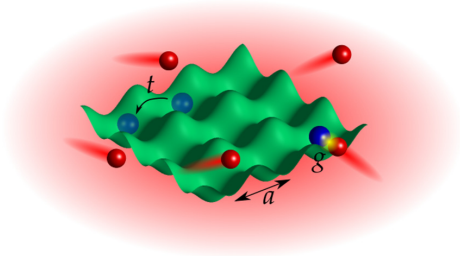

FIG. 1. Illustration of the mixed-dimensional system. Fermions (blue spheres) move in a 2D square lattice in the xy plane with lattice constant a and hopping matrix element t. The lattice is immersed in a 3D BEC (red spheres), and fermions and bosons interact through a contact interaction of strength g.

$g = 2\pi a_I/m_r$, with a_I the Bose-Fermi scattering length and $m_r = mm_B/(m+m_B)$ the reduced mass. For a deep optical lattice, the fermion field operator can be approximated by $\psi_F(\mathbf{r}) = \sum_i \phi_0(\mathbf{r}-\mathbf{r}_i)a_i$ where $\phi_0(\mathbf{r}-\mathbf{r}_i)$ is the lowest Wannier function for site i located at $\mathbf{r}_i$. We approximate the Wannier function by a Gaussian, $\phi_0(\mathbf{r}) = \exp(-r_\perp^2/2\ell_\perp^2 - z^2/2\ell_z^2)/\pi^{3/4}\ell_\perp\sqrt{\ell_z}$, where $\mathbf{r}_\perp = (x,y)$ is a vector in the lattice plane, and ℓ_z and $\ell_\perp$ are the oscillator lengths of the potential wells of the 2D lattice perpendicular and parallel to the plane. Using this in Eq. (1), we obtain

$$H_{\rm int} = \frac{g}{\mathcal{V}}\sum_{i,\mathbf{k},\mathbf{q}} e^{-\frac{1}{4}\ell_z^2 q_z^2} e^{-\frac{1}{4}\ell_\perp^2 q_\perp^2} e^{-i\mathbf{q}_\perp\cdot\mathbf{r}_i} b^\dagger_{\mathbf{k}+\mathbf{q}} b_{\mathbf{k}} a_i^\dagger a_i \quad (3)$$

for the Bose-Fermi interaction, where $\mathcal{V}$ is the system volume and $b^\dagger_{\mathbf{k}}$ creates a boson with momentum $\mathbf{k}$. We have the usual Bogoliubov relation $b_{\mathbf{k}} = u_{\mathbf{k}}\gamma_{\mathbf{k}} - v_{\mathbf{k}}\gamma^\dagger_{-\mathbf{k}}$ with $u^2_{\mathbf{k}} = [1+(\epsilon^B_k + 4\pi n_0 a_B)/E_{\mathbf{k}}]/2$ and $v^2_{\mathbf{k}} = [-1+(\epsilon^B_k + 4\pi n_0 a_B)/E_{\mathbf{k}}]/2$.

III. EFFECTIVE HAMILTONIAN FOR THE FERMIONS

Since the bosons live in three dimensions, whereas the fermions are confined to a 2D lattice, we expect the BEC to be essentially unaffected by the fermions. On the other hand, the fermions interact with each other via the bosons and in this section we derive an effective Hamiltonian describing this. One fermion will either attract or repel the bosons, thereby changing the local density of the BEC, which is felt by the second fermion. This results in the induced interaction

$$V_{\rm ind}(i,j,i\omega_q) = g^2\int\frac{d^3q}{(2\pi)^3} e^{i\mathbf{q}_\perp\cdot(\mathbf{r}_i-\mathbf{r}_j)} e^{-(\ell_z^2 q_z^2 - \ell_\perp^2 q_\perp^2)/2} \times \chi_B(\mathbf{q},i\omega_q) \quad (4)$$

between the fermions, where $\mathbf{q}_\perp = (q_x,q_y)$ is a 2D momentum, $\mathbf{q} = (q_x,q_y,q_z)$ is a 3D momentum, and $i\omega_q$ is a bosonic Matsubara frequency. The density-density correlation function of the BEC is

$$\chi_B(\mathbf{q},i\omega_q) = \frac{q^2}{m_B}\frac{n_0}{(i\omega_q)^2 - E^2_{\mathbf{q}}}. \quad (5)$$

Equation (4) includes an integration over the z component q_z of the boson momentum, since this is not conserved by the Bose-Fermi interaction given by Eq. (3).

For simplicity, we take the limit $\ell_\perp \to 0$ and $\ell_z \to 0$ in the following. We furthermore assume that the speed of sound $c_s = \sqrt{4\pi a_B n_0}/m_B$ in the BEC is much larger than ta, where a is the lattice constant. This means that retardation effects are negligible so that the frequency can be set to 0 in the induced interaction. When c_s becomes comparable to ta, we expect retardation effects to significantly suppress pairing, in analogy with what happens to the corresponding system without a lattice [31]. Ignoring retardation effects by setting $i\omega_q = 0$ in Eq. (4) yields the usual Yukawa interaction [36,37],

$$V_{\rm ind}(i,j) = -g^2\frac{n_0 m_B}{\pi}\frac{e^{-\sqrt{2}|\mathbf{r}_i-\mathbf{r}_j|/\xi_B}}{|\mathbf{r}_i-\mathbf{r}_j|}, \quad (6)$$

where $\xi_B = (8\pi a_B n_0)^{-1/2}$ is the BEC coherence length. It follows from Eq. (6) that the dimensionless parameter determining the strength of the induced interaction between the fermions in the lattice is

$$G = \frac{g^2 n_0 m_B}{\pi a t}. \quad (7)$$

Equation (6) illustrates another important fact: By varying the Bose density n_0 and/or the scattering lengths a_B and a_I, one can experimentally control both the *strength* and the *range* (determined by ξ_B) of the induced interaction between the fermions.

Using the induced interaction, the effective Hamiltonian for the fermions is

$$H_{\rm eff} = -t\sum_{\langle i,j\rangle} a_i^\dagger a_j - \mu\sum_j a_j^\dagger a_j + \sum_{i<j} V_{\rm ind}(i,j)\, a_i^\dagger a_j^\dagger a_j a_i, \quad (8)$$

where $V_{\rm ind}(i,j)$ is given by Eq. (6) and we have subtracted the chemical potential μ as usual. Note that the system is symmetric under the particle-hole transformation $\mathcal{P}a_i\mathcal{P}^{-1} = a_i^\dagger$, where the filling fraction transforms as $n \to 1-n$, the hopping matrix element as $t \to -t$, and the chemical potential as $\mu \to -\mu + \sum_j V_{\rm ind}(0,j)$.

IV. ZERO-TEMPERATURE PHASE DIAGRAM

Using the effective Hamiltonian given by Eq. (8), we now calculate the $T = 0$ phase diagram of the fermions in the lattice. We consider two possible instabilities of the system caused by the induced interaction: a superfluid and a phase separation instability. To do this, we decouple the interaction in the Hartree-Fock and BCS channels. Assuming pairing between $\mathbf{k}$ and $-\mathbf{k}$ states, the mean-field Hamiltonian becomes (apart from a constant)

$$H_{\rm MF} = \frac{1}{2}\sum_{\mathbf{k}}\begin{bmatrix} a^\dagger_{\mathbf{k}} & a_{-\mathbf{k}}\end{bmatrix}\begin{bmatrix}\xi_{\mathbf{k}} & \Delta_{\mathbf{k}} \\ \Delta^*_{\mathbf{k}} & -\xi_{\mathbf{k}}\end{bmatrix}\begin{bmatrix} a_{\mathbf{k}} \\ a^\dagger_{-\mathbf{k}}\end{bmatrix}, \quad (9)$$

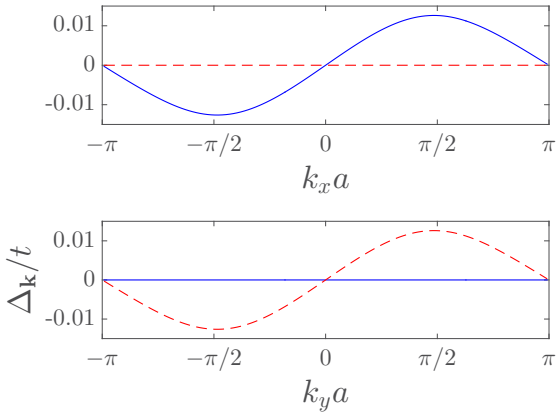

FIG. 2. The gap parameter $\Delta_{\mathbf{k}}$ as a function of the momentum $\mathbf{k}$ for the coupling strength $G = 3$, BEC coherence length $\xi_B/a = 1$, and filling fraction $n = 0.2$. The solid blue line shows the real part of the gap parameter, while the dashed red line shows the imaginary part. In the upper panel, $k_y = 0$; in the lower panel, $k_x = 0$.

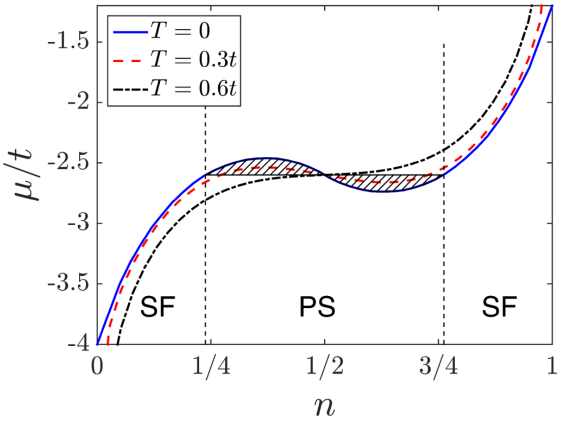

FIG. 3. Plot of the chemical potential μ as a function of the filling fraction n for $G = 3, \xi_B/a = 1$, and different temperatures. The solid blue curve for $T = 0$ has the Maxwell construction indicated, where the system is unstable towards phase separation for filling fractions between the dashed vertical lines and superfluid outside that region. The dashed red curve for $T = 0.3t$ and the dot-dashed black curve for $T = 0.6t$ show how the phase separation region shrinks and, finally, disappears with increasing temperature.

where $\xi_{\mathbf{k}} = \epsilon_{\mathbf{k}} + \Sigma_{\mathbf{k}} - \mu$. Here, $\epsilon_{\mathbf{k}} = -2t(\cos k_x a + \cos k_y a)$ is the kinetic energy dispersion of the 2D lattice and

$$\Sigma_{\mathbf{k}} = \frac{1}{2\mathcal{V}} \sum_{\mathbf{k}'} [V_{\rm ind}(0) - V_{\rm ind}(\mathbf{k} - \mathbf{k}')] \times \left[1 - \frac{\xi_{\mathbf{k}'}}{E_{\mathbf{k}'}} \tanh\left(\frac{E_{\mathbf{k}'}}{2T}\right)\right] \tag{10}$$

is the Hartree-Fock self-energy. The Fourier transform $V_{\rm ind}(\mathbf{k})$ is given by

$$V_{\rm ind}(\mathbf{k}) = \frac{1}{N} \sum_{i \neq 0} V_{\rm ind}(0,i) e^{i\mathbf{k}\cdot\mathbf{r}_i}, \tag{11}$$

where N is the number of lattice sites. The quasiparticle dispersion is $E_{\mathbf{k}} = (\xi_{\mathbf{k}}^2 + |\Delta_{\mathbf{k}}|^2)^{1/2}$, with the gap parameter determined by

$$\Delta_{\mathbf{k}} = -\frac{1}{2\mathcal{V}} \sum_{\mathbf{k}'} V_{\rm ind}(\mathbf{k} - \mathbf{k}') \frac{\Delta_{\mathbf{k}'}}{E_{\mathbf{k}'}} \tanh\left(\frac{E_{\mathbf{k}'}}{2T}\right). \tag{12}$$

As usual, we solve Eqs. (10) and (12) self-consistently together with the number equation

$$n = \frac{1}{2}\left[1 - \frac{1}{N} \sum_{\mathbf{k}} \frac{\xi_{\mathbf{k}}}{E_{\mathbf{k}}} \tanh\left(\frac{E_{\mathbf{k}}}{2T}\right)\right], \tag{13}$$

which gives the filling fraction $0 \leqslant n \leqslant 1$ of the lattice. Our numerical calculations are performed on an $N = 121 \times 121$ lattice of $\mathbf{k}$ values in the first Brillouin zone.

A. Topological $p_x + ip_y$ superfluid

At zero temperature, we find a solution characterized by a gap with $p_x + ip_y$ symmetry. Indeed, the gap is very close to the pure $l = 1$ angular momentum form $\Delta_{\mathbf{k}} \propto \sin k_x a + i \sin k_y a$ as illustrated in Fig. 2.

This solution is the most stable energetically, as it fully gaps the Fermi surface, in contrast to, for instance, a solution with p_x symmetry [38]. The $p_x + ip_y$ pairing breaks time-reversal symmetry and it is a class D topological superfluid with Majorana modes at its edges [39–42]. The topological invariant is the Chern number,

$$\nu = \frac{1}{4\pi} \int_{\rm BZ} d^2k [\hat{\mathbf{s}}(\mathbf{k}) \cdot (\partial_{k_x} \hat{\mathbf{s}}(\mathbf{k}) \times \partial_{k_y} \hat{\mathbf{s}}(\mathbf{k}))], \tag{14}$$

where $\hat{\mathbf{s}}(\mathbf{k}) = \mathbf{S}(\mathbf{k})/|\mathbf{S}(\mathbf{k})|$. Here $\mathbf{S}(\mathbf{k})$ is defined as usual by writing the BCS Hamiltonian as $\left[\begin{smallmatrix} \xi_{\mathbf{k}} & \Delta_{\mathbf{k}} \\ \Delta_{\mathbf{k}}^* & -\xi_{\mathbf{k}} \end{smallmatrix}\right] = \mathbf{S}(\mathbf{k}) \cdot \sigma$, with $\sigma = (\sigma_x, \sigma_y, \sigma_z)$ the vector of Dirac spin-1/2 matrices. For our model, the Chern number is $\nu = -1$ for a filling fraction $0 < n < 1/2$ and $\nu = 1$ for $1/2 < n < 1$. There is therefore a topological phase transition at half-filling, $n = 1/2$, where the spectral gap closes at the points $(k_x, k_y) = (0, \pm\pi/a)$ and $(k_x, k_y) = (\pm\pi/a, 0)$ in the Brillouin zone.

B. Phase separation

The system becomes unstable towards phase separation when the induced interaction between the fermions is too attractive, which originates from the underlying particle-hole symmetry due to the lattice. The instability arises from the compressibility $\kappa = n^{-2}\partial_\mu n$ being negative for certain filling fractions. As an example, we plot in Fig. 3 the chemical potential μ as a function of the filling fraction n for coupling strength $G = 3$, range $\xi_B/a = 1$, and temperatures $T = 0$, $T = 0.3t$, and $T = 0.6t$. For $T = 0$ and $T = 0.3t$, we see that μ decreases with n for a range of filling fractions, which corresponds to a negative compressibility, signaling that the system is unstable towards phase separation. The region of phase separation can be determined by the Maxwell construction. Due to the particle-hole symmetry, this simplifies into the condition that a system with average filling fraction n phase separates into regions with filling fractions $n_1 < n$ and

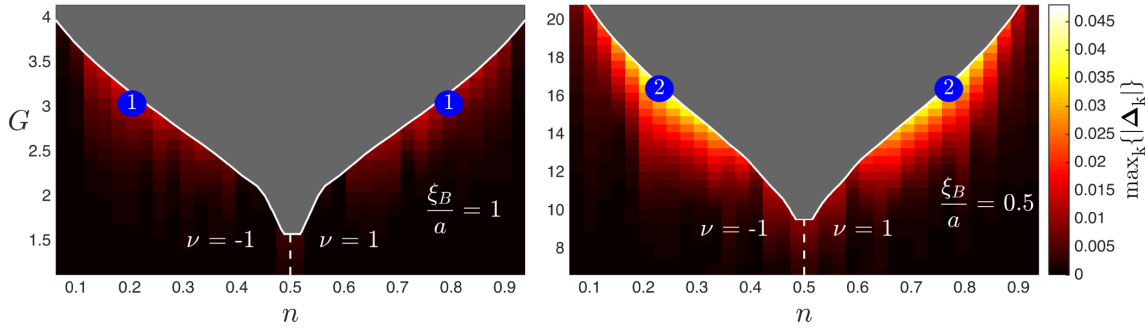

FIG. 4. Zero-temperature phase diagram of the fermions as a function of the filling fraction n and coupling strength G for $\xi_B/a = 1$ (left) and $\xi_B/a = 1/2$ (right). The color code indicates the maximal magnitude of the gap parameter in the Brillouin zone for a given set of (n,G). The central gray regions indicate phase separation, and they are centered around half-filling. The numbered circles indicates the values (n,G) where the pairing is maximal in the phase diagram. The kinks in the bottom of the phase separation regions are due to the finite resolution of the G axis. Inspection of the phase separation condition shows that the region's boundary must be smooth and have a vanishing derivative at the bottom. The dashed vertical lines indicate a topological phase transition between a phase with Chern number $\nu = -1$ and a phase with $\nu = 1$.

$n_2 = 1 - n_1 > n$ determined by $\mu(n_1) = \mu(1/2) = \mu(n_2)$. The resulting range of filling fractions where the system phase separates is shown in Fig. 3 for $T = 0$. We also see from Fig. 3 that this range shrinks with increasing temperature. Indeed, the system does not separate at all for $T = 0.6t$. The reason is that the entropy of mixing stabilizes the system against phase separation for a nonzero temperature.

C. Phase diagrams

We now present $T = 0$ phase diagrams taking the pairing and phase separation instabilities into account. In Fig. 4, we plot phase diagrams as a function of the filling fraction n and the Bose-Fermi coupling strength G for two values of the BEC coherence length: $\xi_B/a = 1$ and $\xi_B/a = 1/2$. The system is phase separated in the gray regions, whereas it is in the $p_x + ip_y$ superfluid state in the other regions, with the color code indicating the maximum value of $|\Delta_{\mathbf{k}}|$ in the Brillouin zone. The vertical line at half-filling indicates a topological phase transition between a superfluid state with Chern number $\nu = -1$ and $\nu = 1$. As expected, an increasing coupling strength G increases the pairing. However, it also increases the range of densities where the system phase separates. Because of this competition, it is not simply a matter of increasing G in order to increase the pairing. If the attraction becomes too strong, the system simply phase-separates into regions with filling fractions close to $n = 0$ and $n = 1$, which strongly suppresses pairing. Instead, one has to tune G to an intermediate value to optimize the pairing. For a given G, one should choose an average filling fraction n in the phase-separated region, i.e., $n_1 \leqslant n \leqslant 1 - n_1$. The system will then phase-separate into two superfluid regions with filling fractions n_1 and $1 - n_1$, which have the same pairing strength. An important conclusion from Fig. 4 is that a shorter coherence length ξ_B allows one to obtain a higher pairing strength by tuning (n,G). Indeed, the maximum value of the pairing one can achieve by tuning (n,G) is $\max_{\mathbf{k}} |\Delta_{\mathbf{k}}| = 0.0142t$ for $(\xi_B/a,G) = (1,3)$ and $n_1 < n < 1 - n_1$ with $n_1 = 0.2$, compared to $\max_{\mathbf{k}} |\Delta_{\mathbf{k}}| = 0.0382t$ for $(\xi_B/a,G) = (1/2,16.4)$ and $n_1 < n < 1 - n_1$ with $n_1 = 0.23$. The positions (n_1,G) and $(1 - n_1,G)$ of the maxima are indicated by the numbered circles ① for $\xi_B/a = 1$ and ② for $\xi_B/a = 1/2$ in Fig. 4. The reason that one can achieve a larger pairing for smaller ξ_B/a is that it determines the range of the induced interaction. Since phase separation is mainly driven by long-range interactions, whereas pairing is mainly driven by nearest-neighbor interactions, a smaller range will suppress pairing less than it suppresses phase separation. As a result of this delicate competition, a small coherence length effectively favors pairing, since it allows a higher coupling strength before the system phase separates. This shows that our proposed system is very useful for realizing a topological superfluid in a lattice, since it allows the tuning of both the strength and the range of the induced interaction.

V. CRITICAL TEMPERATURE OF THE SUPERFLUID PHASE

Since the Fermi system is 2D, the superfluid phase melts via the BKT mechanism [43–46]. In this section, we calculate the critical temperature T_{BKT} of this transition following the approach in Ref. [47]. The melting is determined by the phase stiffness of the order parameter, which can be calculated from the free energy cost associated with imposing a phase twist on the system. If the overall phase (in addition to the $p_x + ip_y$ phase winding) of the order parameter changes by a small amount $\delta\theta$ between neighboring sites along the x direction, the corresponding change in the free energy is

$$F_\theta - F_0 = N\frac{J_x}{2}\delta\theta^2, \tag{15}$$

where J_x is the phase stiffness along the x direction. Imposing such a linear phase twist on the system is equivalent to using periodic boundary conditions in a system described by the gauge-transformed Hamiltonian [48],

$$H_{\mathrm{eff}}(\theta) = e^{-i\frac{\delta\theta}{2}\sum_l x_l/a} H_{\mathrm{eff}} e^{-i\frac{\delta\theta}{2}\sum_l x_l/a}. \tag{16}$$

Here, x_l is the x coordinate of particle l and we gauge-transform each particle with half the angle $\delta\theta/2$, since the

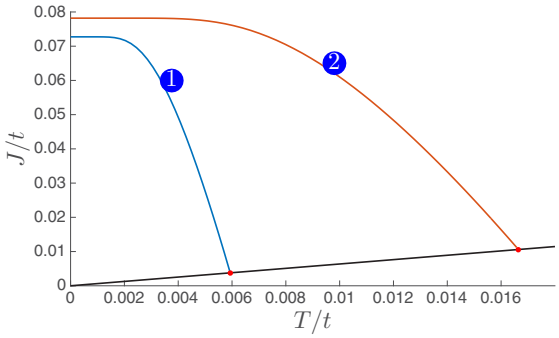

FIG. 5. Phase stiffness given by Eq. (17) as a function of temperature for the two optimal parameter sets ① and ② shown in Fig. 4. The critical temperature is determined when $J(T)$ crosses the line $2T/\pi$, which is also plotted.

order parameter $\Delta_{\mathbf{k}}$ involves two particles. From Eq. (15), it is sufficient to calculate the energy shift due to the gauge transformation to second order in $\delta\theta$ to determine the superfluid stiffness. Expanding Eq. (16) to second order in $\delta\theta$, and calculating the corresponding corrections to the energy, yields, after a lengthy but straightforward calculation [47],

$$J_x = \frac{t}{2N}\sum_{\mathbf{k}}\left[n_{\mathbf{k}}\cos k_x a - \frac{2t}{T}f_{\mathbf{k}}(1-f_{\mathbf{k}})\sin^2 k_x a\right] \quad (17)$$

for the superfluid stiffness along the x direction. Here, $n_{\mathbf{k}} = \langle a^\dagger_{\mathbf{k}} a_{\mathbf{k}}\rangle = |u_{\mathbf{k}}|^2 f_{\mathbf{k}} + |v_{\mathbf{k}}|^2(1-f_{\mathbf{k}})$ is the number of fermions with momentum $\mathbf{k}$ and $f_{\mathbf{k}} = (\exp\beta E_{\mathbf{k}} + 1)^{-1}$ is the Fermi function. An equivalent formula holds for the phase stiffness along the y direction. We find that $J_x = J_y = J$ for $p_x + ip_y$ pairing. The critical temperature for the superfluid phase can now be determined by the BKT condition [43–46]

$$J(T_{\mathrm{BKT}}) = \frac{2}{\pi}T_{\mathrm{BKT}}. \quad (18)$$

In Fig. 5, we plot the calculated phase stiffness $J(T)$ as a function of the temperature for the two parameter sets ① and ② shown in Fig. 4. The critical temperature is determined from Eq. (18) by the crossing of $J(T)$ with the line $2T/\pi$, which is also plotted in Fig. 4. This condition yields the BKT transition temperatures $0.006t$ and $0.017t$ for $(\xi_B/a, n, G) = (1, 0.2, 3)$ and $(\xi_B/a, n, G) = (1/2, 0.23, 16.4)$, respectively. In these calculations, we use that the critical temperature T_c of the BEC typically is much higher than T_{BKT}, so that we can set $T = 0$ when calculating the induced interaction mediated by the BEC. It is straightforward to include nonzero temperature effects on the BEC if necessary.

VI. DISCUSSION

Despite the fact that we have used the flexibility of the Bose-Fermi system to optimize the interaction for topological pairing, the obtained BKT critical temperatures are still fairly low. As an example, if one takes ^{6}Li atoms in an optical lattice with a wavelength of 1000 nm and a lattice depth of $V_0 = 5E_R$, the critical temperature is $T_{\mathrm{BKT}} \simeq 2$ nK using the parameters corresponding to ② in Fig. 4. The reason for this rather low temperature is that phase separation in the lattice prohibits the use of too strong an interaction. One could of course obtain a higher absolute value of the critical temperature by tuning the lattice parameters or by decreasing the coherence length, but here we have chosen to use commonly used experimental values as an example. Another possibility is to use subwavelength lattices in order to increase the energy scales [49–51]. Finally, it is tempting to suppress phase separation by increasing the temperature, but as we saw from the discussion in connection with Fig. 3, the phase separation instability is unfortunately essentially unaffected by the low temperatures $T \leqslant T_{\mathrm{BKT}}$, since $T_{\mathrm{BKT}} \ll t$. We note, however, that the critical temperatures one can obtain in the present system in general are higher than in other lattice proposals, since one can tune both the strength and the range of the interaction. For instance, we find a much lower critical temperature for the system of rotating dipoles in an optical lattice considered in Ref. [28], when the density is the same [52].

Since the Bose-Fermi mixture is a very tunable system compared to other proposals, the fact that we obtain rather low critical temperatures indicates that it will be experimentally challenging to realize a topological superfluid using atoms in an optical lattice. This should be compared with the similar Bose-Fermi system without a lattice, where high critical temperatures can be achieved [31]. The advantage, however, of using an optical lattice is the available schemes for directly detecting the Majorana edge states. Current experiments with single-site resolution [32,33] could specifically image the edge states using, for instance, their time evolution in real space [53,54] or radio-frequency spectroscopy [34]. Intriguingly, we note that since the two phase-separated regions with filling fractions n_1 and $1 - n_1$ have Chern numbers $\nu = -1$ and $\nu = 1$, respectively, there will be topologically robust edge states at the boundary between these two phases.

VII. CONCLUSIONS

In this paper, we have analyzed the phase diagram of identical fermions in a 2D square lattice immersed in a 3D BEC. The attractive induced interaction between the fermions mediated by the BEC was shown to give rise to topological $p_x + ip_y$ pairing as well as phase separation. We calculated the phase diagram at zero temperature as a function of the Bose-Fermi coupling strength and the filling fraction. The Bose-Fermi mixture was demonstrated to allow one to maximize topological superfluid pairing by tuning the range of the interaction, so that it favors pairing between nearest-neighbor fermions, while long-range interaction effects leading to phase separation are suppressed. We have then calculated the BKT critical temperature for the superfluid phase and, finally, discussed the prospect of an experimental realization of a topological superfluid in the present system.

ACKNOWLEDGMENTS

J.M.M. wishes to acknowledge the support of the Danish Council of Independent Research|Natural Sciences via Grant No. DFF – 4002-00336. Z.W. wishes to acknowledge the support of the Villum Foundation via Grant No. VKR023163.

[1] A. Y. Kitaev, Phys. Usp. **44**, 131 (2001).
[2] V. Mourik, K. Zuo, S. M. Frolov, S. R. Plissard, E. P. A. M. Bakkers, and L. P. Kouwenhoven, Science **336**, 1003 (2012).
[3] M. T. Deng, C. L. Yu, G. Y. Huang, M. Larsson, P. Caroff, and H. Q. Xu, Nano Lett. **12**, 6414 (2012).
[4] A. Das, Y. Ronen, Y. Most, Y. Oreg, M. Heiblum, and H. Shtrikman, Nat. Phys. **8**, 887 (2012).
[5] L. P. Rokhinson, X. Liu, and J. K. Furdyna, Nat. Phys. **8**, 795 (2012).
[6] A. D. K. Finck, D. J. Van Harlingen, P. K. Mohseni, K. Jung, and X. Li, Phys. Rev. Lett. **110**, 126406 (2013).
[7] S. Nadj-Perge, I. K. Drozdov, J. Li, H. Chen, S. Jeon, J. Seo, A. H. MacDonald, B. A. Bernevig, and A. Yazdani, Science **346**, 602 (2014).
[8] S. M. Albrecht, A. P. Higginbotham, M. Madsen, F. Kuemmeth, T. S. Jespersen, J. Nygård, P. Krogstrup, and C. M. Marcus, Nature **531**, 206 (2016).
[9] K. Ishida, H. Mukuda, Y. Kitaoka, K. Asayama, Z. Q. Mao, Y. Mori, and Y. Maeno, Nature **396**, 658 (1998).
[10] K. D. Nelson, Z. Q. Mao, Y. Maeno, and Y. Liu, Science **306**, 1151 (2004).
[11] F. Kidwingira, J. D. Strand, D. J. Van Harlingen, and Y. Maeno, Science **314**, 1267 (2006).
[12] J. Xia, Y. Maeno, P. T. Beyersdorf, M. M. Fejer, and A. Kapitulnik, Phys. Rev. Lett. **97**, 167002 (2006).
[13] V. Gurarie and L. Radzihovsky, Ann. Phys. **322**, 2 (2007).
[14] K. Günter, T. Stöferle, H. Moritz, M. Köhl, and T. Esslinger, Phys. Rev. Lett. **95**, 230401 (2005).
[15] J. P. Gaebler, J. T. Stewart, J. L. Bohn, and D. S. Jin, Phys. Rev. Lett. **98**, 200403 (2007).
[16] J. Levinsen, N. R. Cooper, and V. Gurarie, Phys. Rev. Lett. **99**, 210402 (2007).
[17] M. Jona-Lasinio, L. Pricoupenko, and Y. Castin, Phys. Rev. A **77**, 043611 (2008).
[18] A. Bühler, N. Lang, C. V. Kraus, G. Möller, S. D. Huber, and H. P. Büchler, Nat. Commun. **5**, 4504 (2014).
[19] P. Massignan, A. Sanpera, and M. Lewenstein, Phys. Rev. A **81**, 031607 (2010).
[20] L. Mathey, S.-W. Tsai, and A. H. Castro Neto, Phys. Rev. Lett. **97**, 030601 (2006).
[21] Y.-J. Wu, J. He, C.-L. Zang, and S.-P. Kou, Phys. Rev. B **86**, 085128 (2012).
[22] C. Zhang, S. Tewari, R. M. Lutchyn, and S. Das Sarma, Phys. Rev. Lett. **101**, 160401 (2008).
[23] M. Sato, Y. Takahashi, and S. Fujimoto, Phys. Rev. Lett. **103**, 020401 (2009).
[24] L. Jiang, T. Kitagawa, J. Alicea, A. R. Akhmerov, D. Pekker, G. Refael, J. I. Cirac, E. Demler, M. D. Lukin, and P. Zoller, Phys. Rev. Lett. **106**, 220402 (2011).
[25] C.-E. Bardyn, M. A. Baranov, E. Rico, A. İmamoğlu, P. Zoller, and S. Diehl, Phys. Rev. Lett. **109**, 130402 (2012).
[26] S. Diehl, E. Rico, M. A. Baranov, and P. Zoller, Nat. Phys. **7**, 971 (2011).
[27] N. R. Cooper and G. V. Shlyapnikov, Phys. Rev. Lett. **103**, 155302 (2009).
[28] B. Liu and L. Yin, Phys. Rev. A **86**, 031603 (2012).
[29] A. K. Fedorov, S. I. Matveenko, V. I. Yudson, and G. V. Shlyapnikov, Sci. Rep. **6**, 27448 EP (2016).
[30] Y. Nishida, Ann. Phys. **324**, 897 (2009).
[31] Z. Wu and G. M. Bruun, Phys. Rev. Lett. **117**, 245302 (2016).
[32] J. F. Sherson, C. Weitenberg, M. Endres, M. Cheneau, I. Bloch, and S. Kuhr, Nature **467**, 68 (2010).
[33] W. S. Bakr, J. I. Gillen, A. Peng, S. Folling, and M. Greiner, Nature **462**, 74 (2009).
[34] S. Nascimbène, J. Phys. B **46**, 134005 (2013).
[35] N. Goldman, J. C. Budich, and P. Zoller, Nat. Phys. **12**, 639 (2016).
[36] L. Viverit, C. J. Pethick, and H. Smith, Phys. Rev. A **61**, 053605 (2000).
[37] M. J. Bijlsma, B. A. Heringa, and H. T. C. Stoof, Phys. Rev. A **61**, 053601 (2000).
[38] P. W. Anderson and P. Morel, Phys. Rev. **123**, 1911 (1961).
[39] A. Altland and M. R. Zirnbauer, Phys. Rev. B **55**, 1142 (1997).
[40] A. P. Schnyder, S. Ryu, A. Furusaki, and A. W. W. Ludwig, Phys. Rev. B **78**, 195125 (2008).
[41] A. Kitaev, AIP Conf. Proc. **1134**, 22 (2009).
[42] J. Alicea, Rep. Prog. Phys. **75**, 076501 (2012).
[43] V. L. Berezinskii, Sov. Phys. JETP **34**, 610 (1972).
[44] J. M. Kosterlitz and D. J. Thouless, J. Phys. C **6**, 1181 (1973).
[45] J. M. Kosterlitz, J. Phys. C **7**, 1046 (1974).
[46] P. Chaikin and T. Lubensky, *Principles of Condensed Matter Physics* (Cambridge University Press, Cambridge, UK, 2000).
[47] A.-L. Gadsbølle and G. M. Bruun, Phys. Rev. A **86**, 033623 (2012).
[48] E. H. Lieb, R. Seiringer, and J. Yngvason, Phys. Rev. B **66**, 134529 (2002).
[49] B. Dubetsky and P. R. Berman, Phys. Rev. A **66**, 045402 (2002).
[50] S. Nascimbene, N. Goldman, N. R. Cooper, and J. Dalibard, Phys. Rev. Lett. **115**, 140401 (2015).
[51] W. Yi, A. J. Daley, G. Pupillo, and P. Zoller, New J. Phys. **10**, 073015 (2008).
[52] In Ref. [28], the authors present higher critical temperatures for the dipolar system than what we find in the present paper for the Bose-Fermi mixture. However, when using their dipolar interaction in our formalism, we find that they use parameter sets where the system is phase-separated.
[53] N. Goldman, J. Dalibard, A. Dauphin, F. Gerbier, M. Lewenstein, P. Zoller, and I. B. Spielman, Proc. Natl. Acad. Sci. USA **110**, 6736 (2013).
[54] N. Goldman, G. Jotzu, M. Messer, F. Görg, R. Desbuquois, and T. Esslinger, Phys. Rev. A **94**, 043611 (2016).

— 3 —

Time-Reversal-Invariant Superconductors

In chapter 2, we found that in the lattice the fermions had the possibility of ordering into domains of different topological states ($C = \pm 1$). This happened along with phase separation into a high-density and low-density phase, which raised the question of whether the configuration where one domain had $C = 1$ and another $C = -1$ was the preferred configuration. The paper presented at the end of this chapter attempts to look at this question from a different angle, studying the interaction between two physically separated, topological domains.

3.1 Time-Reversal

In publication I in the previous chapter, the two domains were connected through a particle-hole transformation. This is somewhat reminiscent of a different class of topological superconductors that obey time-reversal symmetry. In these systems, there are typically two components/subsystems of fermions, where one subsystem transforms into the other under the time-reversal operation. The kind of time-reversal we will consider is the one that squares to -1. The physical time-reversal operation for fermions encountered in Kramer's theorem, for instance, is an example of this transformation.

To gain an intuition for these systems, let us again consider the analogous insulating systems. The topological insulator that most resembled the $p_x + ip_y$ superfluid state was the Quantum Hall state, since these both broke time-reversal symmetry. To restore time-reversal symmetry in a topological insulator, the Quantum Spin Hall state considers two copies of a Quantum Hall state with opposite helicities. A time-reversal operator can then be defined that transforms between the two subsystems. An example of this is the Kane-Mele model of graphene that contains two copies of a Haldane model [45] with Chern number $+1$ for spin-up electrons and -1 for spin-down electrons.

We can imagine the same thing for the superconducting systems: a subsystem realizing a $p_x + ip_y$-state and another realizing a $p_x - ip_y$-state. If they are uncoupled, this system will obey time-reversal symmetry. Instead of a single branch of chiral edge modes, this system has helical edge modes with one branch running in each direction. As long as time-reversal is obeyed, Kramer's theorem ensures a pair of zero-energy Majorana modes on the boundary. Further details of this are given in Publication II.

With a time-reversal invariant system, the topological invariant to consider is no longer the Chern number. This is because the ground state contains two filled bands with opposite Chern numbers, $C_{1,2} = \pm 1$ so the total Chern number is always zero, $C = C_1 + C_2 = 0$. Instead, a $\mathbb{Z}_2$ invariant can be defined as $\nu = (C_1 - C_2)/2 \,(\mathrm{mod}\ 2)$. For insulators, this is known as the Spin Chern number, or the Fu-Kane-Mele invariant in class AII. Since superconductors also obey particle-hole symmetry, these systems are in class DIII. Note that the simple expression for the $\mathbb{Z}_2$ invariant in terms of the individual Band Chern numbers is a limiting case that relies on the two subsystems being uncoupled. More general expressions exist when this is not the case[46].

3.2 The Bilayer System

In Publication II, we propose a different Bose-Fermi system, with the fermions captured in a bilayer geometry instead of a single layer, again immersed in a BEC. The method for preparing single layers of atoms discussed in the introduction is easy to generalize to several layers. Because of the phase separation in the lattice, we consider homogenous fermion layers from now on. Apart from the intralayer superfluid pairing, which was studied in-depth in [47] there can now also be pairing between fermions in different layers, as seen in Fig. 3.1.

Neglecting the speed of propagation in the BEC, the induced pairing follows the Yukawa form as before,

$$V(r) \propto \frac{e^{-\sqrt{2}r/\xi_B}}{r}, \tag{3.1}$$

where ξ_B is the healing length of the BEC and r is the particle distance. Because of the minimum distance, d, between fermions in different layers the interlayer pairing, Δ_{12}, is suppressed for distances $d > \xi_B$. Since it is between *distinguishable* fermions, however, it will be an s-wave pairing. So we would in turn expect the interlayer pairing to dominate over the intralayer p-wave pairings, Δ_{11} and Δ_{22}, for small layer distances.

By choosing different ansatzes for the intralayer pairings, the bilayer setup allows us to study the time-reversal invariant $(p_x+ip_y)\times(p_x-ip_y)$-state

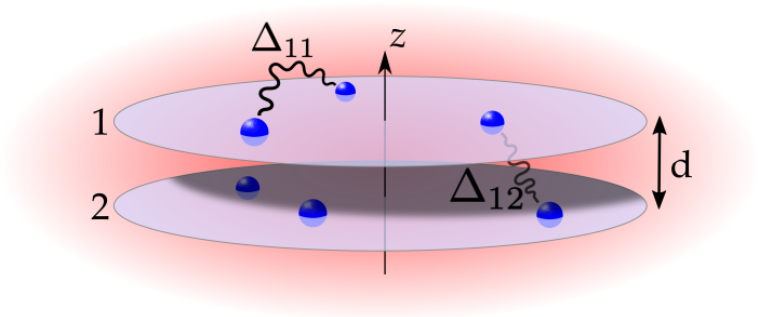

Figure 3.1: The Bose-Fermi mixture with a bilayer geometry for the fermions. Several pairing fields are possible: p-wave intralayer pairings Δ_{11} in layer 1 and Δ_{22} in layer 2 (omitted for clarity). Also possible is an s-wave interlayer pairing Δ_{12}.

as well as the time-reversal breaking states, e.g.the $(p_x + ip_y) \times (p_x + ip_y)$-state. An interesting question is how robust the time-reversal invariance is when the two layers are free to establish interlayer pairing. The motivation is a bit subtle. When the time-reversal operator is defined, the bilayer system in the $(p_x + ip_y) \times (p_x - ip_y)$-state can be shown to be invariant under this transformation in a certain gauge. This corresponds to choosing a certain global phase of the intralayer pairings by a gauge transformation. The correct phase ensures that the complex conjugation in the time-reversal operation does not break the invariance.

However, when the interlayer pairing coexists with the intralayer pairing the relative phase difference can not be gauged away. This is important because an imaginary part on the interlayer pairing breaks time-reversal-symmetry. A purely real interlayer pairing, however, respects time-reversal symmetry and the system remains topological. Looking at the superfluid gap equations, there is not an immediate reason to expect a specific phase difference.

3.3 Results

By numerically solving the gap equations, we investigate the behaviour of the $(p_x + ip_y) \times (p_x - ip_y)$-state and the $(p_x + ip_y) \times (p_x + ip_y)$-state when we vary the layer distance. The behaviour of the $(p_x + ip_y) \times (p_x + ip_y)$-state turns out to be quite boring; no intralayer and interlayer pairing coexists at any time. The transition from a topological state with Chern number $C = -2$ and the trivial state with only interlayer pairing happens abruptly in a first order phase transition.

The $(p_x + ip_y) \times (p_x - ip_y)$-state turns out to have more structure. At intermediate layer distances, the intralayer and interlayer pairing coexist, causing a second order phase transition. However, the interlayer pairing always appears to be imaginary, breaking the time-reversal invariance of the $(p_x + ip_y) \times (p_x - ip_y)$-state. This turned out to be the only self-consistent solution.

By applying a local density approximation, we extracted the edge modes from a low-energy approximate Hamiltonian. When the layers were far apart, the solution was two opposite-moving branches, each localized on a single layer. These are exactly the helical edge modes we expected. When the layers were moved closer together to introduce the interlayer pairing, the edge modes acquired an energy gap immediately, signaling the transition to a topologically trivial phase. This was accompanied by a spatial mixing of the states, such that the lowest-lying edge states were split evenly between the layers.

It is perhaps unfortunate that the time-reversal invariant state is not more robust to perturbations. But it does mean that for intermediate layer distances, the broken $(p_x + ip_y) \times (p_x - ip_y)$-state has a lower ground-state energy than the $(p_x + ip_y) \times (p_x + ip_y)$-state. So it is possible, at least in principle, to select for this state when preparing the system, and then restore time-reversal-symmetry by moving the layers apart afterwards.

3.4 Contribution

I performed all numerical calculations and made all figures. I also wrote the first draft of the paper. The derivation of the induced interaction was based on previous work by Zhigang Wu.

Time-reversal-invariant topological superfluids in Bose-Fermi mixtures

Jonatan Melkær Midtgaard,[1] Zhigang Wu,[2] and G. M. Bruun[1]
[1]*Department of Physics and Astronomy, Aarhus University, Ny Munkegade, DK-8000 Aarhus C, Denmark*
[2]*Institute for Advanced Study, Tsinghua University, Beijing 100084, China*
(Received 29 May 2017; published 5 September 2017)

A mixed dimensional system of fermions in two layers immersed in a Bose-Einstein condensate (BEC) is shown to be a promising setup to realize topological superfluids with time-reversal symmetry (TRS). The induced interaction between the fermions mediated by the BEC gives rise to a competition between p-wave pairing within each layer and s-wave pairing between the layers. When the layers are far apart, intralayer pairing dominates and the system forms a topological superfluid either with or without TRS. With decreasing layer separation or increasing BEC coherence length, interlayer pairing sets in. We show that this leads either to a second-order transition breaking TRS where the edge modes gradually become gapped or to a first-order transition to a topologically trivial s-wave superfluid. Our results provide a realistic road map for experimentally realizing a topological superfluid with TRS in a cold atomic system.

DOI: 10.1103/PhysRevA.96.033605

I. INTRODUCTION

The search for superfluids and superconductors with nontrivial topological properties has experienced an explosion of activities in recent years. One reason is that these systems can host gapless edge (Majorana) modes with possible applications in quantum computation [1,2]. Excitingly, evidence for topological superconductivity and gapless edge states has been reported in nanowires [3–9]. So far the focus has predominantly been placed on superfluids [10] without time-reversal symmetry (TRS), which belong to the symmetry class D in the tenfold classification scheme of topological insulators and superfluids [11–13]. However, superfluids with TRS, belonging to the class DIII, can also host gapless Majorana mode pairs, which are protected by the Kramers theorem. There are also several proposals to realize such systems in the laboratory, both in condensed-matter systems [14–21] and in cold atomic systems [22–24]. One example of such intriguing systems is the superfluid ^{3}He B phase, the topological properties of which have been studied recently [25,26]. However, one has yet to observe a topological superfluid with TRS in a cold atomic system.

Recently, we showed that a mixed dimensional atomic gas system consisting of a two-dimensional (2D) layer of fermions immersed in a three-dimensional (3D) Bose-Einstein condensate (BEC) constitutes a promising system for realizing a $\mathbb{Z}$ topological superfluid in class D with a high critical temperature [27,28]. Here, we show that an analogous system with two layers of fermions, first studied in Ref. [29], is naturally suited to realize a $\mathbb{Z}_2$ topological superfluid with TRS. Fermions in the layers interact attractively via an induced interaction mediated by the BEC. The relative strengths of the intra- and interlayer induced interaction result in a competition between $p_x \pm ip_y$-wave pairing involving fermions in the same layer, and s-wave pairing involving fermions in different layers. For large distance between the layers, intralayer pairing dominates and one has either a $(p_x + ip_y) \times (p_x - ip_y)$ system with TRS or a $(p_x + ip_y) \times (p_x + ip_y)$ system without TRS. With decreasing layer distance or increasing BEC coherence length, we show that interlayer s-wave pairing occurs in a second-order transition for the $(p_x + ip_y) \times (p_x - ip_y)$ system, which breaks TRS thereby gradually gapping the edge modes without closing the bulk gap. For short layer distance, the system ends up in a topologically trivial s-wave superfluid, resembling the case of a single layer with two spin components [30]. On the other hand, the transition from the topological $(p_x + ip_y) \times (p_x + ip_y)$ to the trivial s-wave superfluid is of the first order.

II. MODEL

We consider identical (spin polarized) fermions of mass m in two layers located at $z = 0$ and d (see Fig. 1). The fermions are immersed in a 3D gas of bosons with mass m_B and density n_B. The partition function of the system at temperature T is

$$\mathcal{Z} = \int \mathcal{D}(\bar{\psi}_F, \psi_F, \psi_B^*, \psi_B)\, e^{-(S_F + S_B + S_{\rm int})}, \tag{1}$$

where $\psi_B(\mathbf{r},\tau)$ and $\psi_F(\mathbf{r},\tau)$ are the bosonic and fermionic fields at point $\mathbf{r}$ and imaginary time τ. The bosons form a weakly interacting BEC that be described by Bogoliubov theory, which yields

$$S_B = \beta \sum_{\mathbf{p}\neq 0, l} \gamma_p^*(-i\omega_l + E_{\mathbf{p}})\gamma_p \tag{2}$$

for the bosonic part of the action, where $\beta = 1/T$; $\omega_l = 2l\pi T$ where $l = 0, \pm 1, \pm 2, \ldots$ are the Bose Matsubara frequencies; and γ_p describes the quasiparticle with momentum $\mathbf{p} = (p_x, p_y, p_z)$ and energy $E_{\mathbf{p}}$. Here we have defined $p \equiv (\mathbf{p}, i\omega_l)$. The Bogoliubov spectrum is $E_{\mathbf{p}} = \sqrt{\epsilon_{\mathbf{p}}(\epsilon_{\mathbf{q}} + 2g_B n_B)}$, where $\epsilon_{\mathbf{p}} = \mathbf{p}^2/2m_B$ and $g_B = 4\pi a_B/m_B$, where a_B is the boson scattering length. The fermion part of the action is

$$S_F = \beta \sum_{\sigma} \sum_{\mathbf{k}_\perp, j} \bar{a}_{k_\perp \sigma}(-i\omega_j + \xi_{\mathbf{k}_\perp}) a_{k_\perp \sigma} \tag{3}$$

where $a_{k_\perp\sigma}$ are the Grassmann fields for the fermions in layer $\sigma = 1,2$. The effective 2D action for the fermions results from the fact that the vertical trapping potentials are sufficiently tight that the fermions reside only in the lowest trap levels $\phi_0(z)$ and $\phi_0(z-d)$ along the z direction. We have defined $k_\perp \equiv (\mathbf{k}_\perp, i\omega_j)$ with $\mathbf{k}_\perp = (k_x, k_y)$ as the in-plane momentum; $\omega_j = (2j+1)\pi T$ where $j = 0, \pm 1, \pm 2, \ldots$ are the Fermi Matsubara frequencies; and $\xi_{\mathbf{k}_\perp} = \mathbf{k}_\perp^2/2m - \mu$ where μ is the

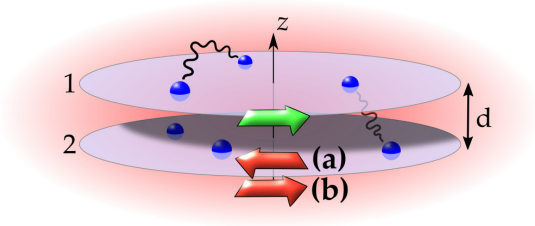

FIG. 1. In the proposed experimental setup, fermions (blue spheres) confined to two layers with distance d interact with the surrounding BEC (red background). This results in induced intralayer and interlayer interactions (illustrated by black wiggly lines). The green and red arrows indicate the edge modes in the two layers, respectively. The intralayer p-wave pairings are either of (a) different chirality, realizing a $\mathbb{Z}_2$ topological superfluid, or of (b) the same chirality, realizing a $\mathbb{Z}$ topological superfluid.

chemical potential of the fermions. We take μ to be the same in each layer which contains an equal number of fermions. Finally, the Bose-Fermi interaction is

$$S_{\rm int} = g \int d^3r \int_0^\beta d\tau\, \bar{\psi}_F \psi_F \psi_B^* \psi_B, \tag{4}$$

where g is the boson-fermion interaction strength. Using the Bogoliubov theory to write $\psi_B(\mathbf{r},\tau) = \mathcal{V}^{-1/2}\sum_p (u_{\mathbf{p}}\gamma_p - v_{\mathbf{p}}\gamma_{-p}^*)\exp[i(\mathbf{p}\cdot\mathbf{r} - \omega_l\tau)]$ with $u_{\mathbf{p}}^2, v_{\mathbf{p}}^2 = [(\epsilon_{\mathbf{p}} + g_B n_B)/E_{\mathbf{p}} \pm 1]/2$, and expanding the fermionic fields as $\psi_F(\mathbf{r},\tau) = \sum_{p_\perp,\sigma} a_{p_\perp\sigma}\exp\{i(\mathbf{p}\cdot\mathbf{r}_\perp - \omega_j\tau)\phi_0[z-(\sigma-1)d]/\sqrt{\mathcal{A}}\}$, we find

$$S_{\rm int} = \frac{g}{T}\sqrt{\frac{n_B}{\mathcal{V}}}\sum_{\substack{\mathbf{p}\neq 0\\ l,\sigma}} \sqrt{\frac{\epsilon_{\mathbf{p}}}{E_{\mathbf{p}}}}(\gamma_p + \gamma_p^*)\rho_{p_\perp\sigma} e^{-ip_z d(\sigma-1)} \tag{5}$$

where $\mathcal{V}$ is the BEC volume, $\mathcal{A}$ is the area of the Fermi layer, $\rho_{p_\perp\sigma} = \sum_{k_\perp}\bar{a}_{k_\perp - p_\perp\sigma}a_{k_\perp\sigma}$, and $p_\perp \equiv (\mathbf{p}_\perp, i\omega_l)$.

Integrating out the quadratic Bose fields in the action in Eq. (1) yields the effective action

$$S_{\rm eff} = S_F + \frac{\beta}{2\mathcal{A}}\sum_{\substack{p_\perp\\ \sigma,\sigma'}} \rho_{-p_\perp\sigma} V_{\rm ind}^{\sigma\sigma'}(p_\perp)\rho_{p_\perp\sigma'}, \tag{6}$$

where the induced interaction between the fermions, mediated by the bosons, is

$$V_{\rm ind}^{\sigma\sigma'}(p_\perp) = g^2\int \frac{dp_z}{2\pi} e^{ip_z d(\sigma-\sigma')}\chi_{\rm BEC}(p). \tag{7}$$

Here, $\chi_{\rm BEC}(p) = n_B\mathbf{p}^2 m_B^{-1}/[(i\omega_l)^2 - E_{\mathbf{p}}^2]$ is the density-density correlation function for the BEC and the p_z integration in Eq. (7) is due to the fact that the momentum along the z direction is not conserved in the boson-fermion scattering due to the mixed dimensional setup. We note that the induced interaction in Eq. (7) is obtained with the assumption that the 3D BEC is not affected by the 2D Fermi gases. This is justified in our mixed dimensional setup because the properties of the 3D BEC will only be affected locally in the vicinity of the 2D layers. Since the induced interaction between the fermions is determined by the overall bulk properties of the BEC, we expect that these local effects on the 3D BEC will only lead to small corrections to the induced interaction given by Eq. (7). For zero frequency, $i\omega_l = 0$, performing the p_z integrals yields

$$V_{\rm ind}^{\sigma\sigma'}(\mathbf{p}_\perp,0) = -\frac{2g^2 n_B m_B}{\sqrt{\mathbf{p}_\perp^2 + 2/\xi_B^2}} e^{-d|\sigma-\sigma'|\sqrt{\mathbf{p}_\perp^2 + 2/\xi_B^2}}, \tag{8}$$

where $\xi_B = (8\pi n_B a_B)^{-1/2}$ is the BEC coherence length. The interlayer ($\sigma \neq \sigma'$) interaction is suppressed compared to the intralayer ($\sigma = \sigma'$) interaction by an exponential factor related to the layer distance d. Fourier transforming Eq. (8) yields a Yukawa interaction $V(\mathbf{r}) = -g^2 n_B m_B \pi^{-1}\exp(-\sqrt{2}r/\xi_B)/r$ in real space with a range determined by ξ_B [28,31–33]. Here $r = |\mathbf{r}|$ is the distance between the particles, which can reside in the same plane or in different planes.

III. GAP EQUATIONS

Since the induced interaction given by Eq. (8) is attractive, fermions with opposite momenta can form Cooper pairs within each layer (intralayer pairing) as well as between different layers (interlayer pairing). The BCS Hamiltonian describing such parings is

$$H_{\rm BCS} = \frac{1}{2}\sum_{\mathbf{p}} \Psi^\dagger(\mathbf{p})\mathcal{H}(\mathbf{p})\Psi(\mathbf{p}), \tag{9}$$

where $\Psi(\mathbf{p}) = (a_{\mathbf{p}1}, a_{-\mathbf{p}1}^\dagger, a_{\mathbf{p}2}, a_{-\mathbf{p}2}^\dagger)^T$ and

$$\mathcal{H}(\mathbf{p}) = \begin{bmatrix} \xi_{\mathbf{p}} & \Delta_{11}(\mathbf{p}) & 0 & \Delta_{12}(\mathbf{p}) \\ \Delta_{11}^*(\mathbf{p}) & -\xi_{\mathbf{p}} & -\Delta_{12}^*(\mathbf{p}) & 0 \\ 0 & -\Delta_{12}(\mathbf{p}) & \xi_{\mathbf{p}} & \Delta_{22}(\mathbf{p}) \\ \Delta_{12}^*(\mathbf{p}) & 0 & \Delta_{22}^*(\mathbf{p}) & -\xi_{\mathbf{p}} \end{bmatrix}. \tag{10}$$

Here the $\perp$ subscript is dropped since we are dealing only with 2D momenta of the fermions from now on, and $a_{\mathbf{p}\sigma}$ are the Fermi annihilation operators for layer $\sigma = 1,2$. We neglect retardation effects and use only the zero-frequency component of the induced interaction. Retardation effects are small when the Fermi velocity v_F in the layers is much smaller than the speed of sound in the BEC, while for larger v_F they suppress the magnitude of the pairing without changing the qualitative behavior [27]. The pairing fields are determined self-consistently as

$$\Delta_{\sigma\sigma'}(\mathbf{p}) = -\sum_{\mathbf{k}} V_{\rm ind}^{\sigma\sigma'}(\mathbf{p}-\mathbf{k},0)\langle a_{\mathbf{k}\sigma}a_{-\mathbf{k}\sigma'}\rangle. \tag{11}$$

We take the interlayer pairing to be s-wave so that $\Delta_{12}(\mathbf{p}) = \Delta_{12}(-\mathbf{p}) = -\Delta_{21}(\mathbf{p})$ and the Fermi antisymmetry dictates that $\Delta_{\sigma\sigma}(\mathbf{p}) = -\Delta_{\sigma\sigma}(-\mathbf{p})$ for the intralayer pairing. Since the system has rotational symmetry with respect to the z axis, we take the intralayer pairing to be of the $p_x \pm ip_y$ form, as this fully gaps the Fermi surface [34], i.e., $\Delta_{\sigma\sigma}(\mathbf{p}) = \Delta_\sigma(|\mathbf{p}|)e^{i\phi_\sigma(\mathbf{p})}$ where $\phi_\sigma(\mathbf{p}) = \phi_{0\sigma} \pm \varphi_{\mathbf{p}}$ with $\varphi_{\mathbf{p}}$ being the azimuthal angle of $\mathbf{p}$. Furthermore, for identical layers we assume that $\Delta_1(|\mathbf{p}|) = \Delta_2(|\mathbf{p}|)$ and we thus have $\Delta_{22}(\mathbf{p}) = \Delta_{11}(\mathbf{p})e^{i[\phi_2(\mathbf{p})-\phi_1(\mathbf{p})]}$. We diagonalize Eq. (9) by introducing new pairing fields $\Delta_\pm(\mathbf{p}) = \Delta_{11}(\mathbf{p}) \pm \Delta_{12}(\mathbf{p})e^{-i[\phi_2(\mathbf{p})-\phi_1(\mathbf{p})-\pi]/2}$. Equation (11) then yields

a set of gap equations in a symmetrical form as

$$\Delta_\nu(\mathbf{p}) = -\sum_{\nu',\mathbf{k}} V_{\nu\nu'}(\mathbf{p}-\mathbf{k})\frac{\Delta_{\nu'}(\mathbf{k})}{2E_{\mathbf{k},\nu'}}\tanh\left(\frac{E_{\mathbf{k},\nu'}}{2T}\right). \quad (12)$$

Here $\nu = \pm$, $E_{\mathbf{p},\pm} = \sqrt{\xi_{\mathbf{p}}^2 + |\Delta_\pm(\mathbf{p})|^2}$, and

$$V_{\nu\nu'}(\mathbf{p}-\mathbf{k}) \equiv \frac{1}{2}\big[V_{\rm ind}^{11}(\mathbf{p}-\mathbf{k}) + \mathrm{sgn}(\nu,\nu')e^{-i[\phi_2(\mathbf{p})-\phi_1(\mathbf{p})]/2} \times V_{\rm ind}^{12}(\mathbf{p}-\mathbf{k})e^{i[\phi_2(\mathbf{k})-\phi_1(\mathbf{k})]/2}\big], \quad (13)$$

where $\mathrm{sgn}(\nu,\nu) = 1$ and $\mathrm{sgn}(\nu,-\nu) = -1$. Finally, the number equation is $N = \sum_{\nu,\mathbf{p}}[1 - \xi_{\mathbf{p}}\tanh(E_{\mathbf{p},\nu}/2T)/E_{\mathbf{p},\nu}]/2$ and the BCS ground-state energy is

$$E_{\rm BCS} - \mu N = \frac{1}{2}\sum_{\nu,\mathbf{p}}[\xi_{\mathbf{p}} - E_{\mathbf{p},\nu} + |\Delta_{\mathbf{p},\nu}|^2/2E_{\mathbf{p},\nu}]. \quad (14)$$

We note that when the s- and p-wave order parameters coexist their relative phase is important. It cannot be gauged away contrary to the case of a single order parameter. The relative phase therefore has physical consequences, and we shall see that it determines whether the system has a time-reversal symmetry or not.

IV. SYMMETRIES AND TOPOLOGICAL PROPERTIES

The topological properties of the bilayer system are determined by its symmetries and 2D dimensionality [11–13]. Consider first the limit where the two layers are uncoupled, which corresponds to the layer distance being much larger than the range of the induced interaction given by the BEC coherence length, i.e., $d \gg \xi_{\rm B}$. There is then only particle-hole symmetry for each layer, and they each form a topological $p_x \pm ip_y$ superfluid in symmetry class D, which supports chiral edge states. Consider now the case when the two layers are brought closer to each other so that they interact. The topological properties and the fate of the edge states then depend on whether the Cooper pairs in the two layers have opposite or the same angular momentum, corresponding to $(p_x + ip_y)\times(p_x - ip_y)$ or $(p_x + ip_y)\times(p_x + ip_y)$ pairing, respectively.

For $(p_x + ip_y)\times(p_x - ip_y)$ pairing illustrated in Fig. 1(a), which we refer to as the $(+,-)$ case, the system possesses in addition to particle-hole symmetry the time-reversal symmetry

$$\mathcal{T}(a_{\mathbf{p}1}, a_{\mathbf{p}2})\mathcal{T}^{-1} = (a_{-\mathbf{p}2}, -a_{-\mathbf{p}1}), \quad (15)$$

which swaps particles in the two layers. Note that this antiunitary symmetry operation is different from the usual time-reversal symmetry operation, which flips the spin of the particles. Here, the layer index plays the role of a pseudospin. Since $\mathcal{T}^2 = -1$, the bilayer system is then in symmetry class DIII, and its ground state is a $\mathbb{Z}_2$ topological superfluid, which supports helical edge modes in analogy with the quantum spin Hall state [35–37]. The counterpropagating edge modes in the two layers are related by TRS and protected by the Kramers theorem. However, when the layers are sufficiently close together, the s-wave interlayer pairing ($\Delta_{12}(\mathbf{p}) \neq 0$) will dominate, and the system forms a topologically trivial s-wave superfluid. Thus, the edge states must become gapped at some critical interlayer distance. Without solving the gap equation, one can envision two ways this can happen: either the interlayer pairing explicitly breaks TRS thereby gapping the edge modes as soon as $\Delta_{12}(\mathbf{p}) \neq 0$, or the interlayer pairing respects TRS and the edge states become gapped only when the bulk energy gap is closed. By analyzing the properties of the interlayer gap under time reversal, we find that these two scenarios correspond to $\Delta_{12}(\mathbf{p})$ being imaginary and real, respectively. Our numerical results (see later) show that $\Delta_{12}(\mathbf{p})$ is in fact imaginary and the first scenario describes the physical transition.

For $(p_x + ip_y)\times(p_x + ip_y)$ pairing illustrated in Fig. 1(b), which we refer to as the $(+,+)$ case, the system only has the particle-hole symmetry and is a $\mathbb{Z}$ topological superfluid in class D, which supports chiral edge modes propagating in the same direction in the two layers. When the layer distance is decreased, the possible onset of interlayer pairing coexisting with the intralayer pairing will not gap these edge modes as long as the bulk gap remains nonzero, since this pairing does not break any symmetry. However, we shall see later that such a coexisting scenario does not occur for the $(+,+)$ case. Similar to the $(+,-)$ case, the system ends up in the topologically trivial interlayer s-wave superfluid for small interlayer distances. We shall demonstrate below that this happens via a first-order phase transition.

The topological $\mathbb{Z}$ and $\mathbb{Z}_2$ invariants of class D and DIII, respectively, can be calculated from the two energy bands $E_{\mathbf{p},+}$ and $E_{\mathbf{p},-}$ of the bilayer system [38]. If the two layers are uncoupled, these bands are degenerate and the invariant for class D is simply given by the sum $C = C_1 + C_2$ of the Chern numbers C_σ of each layer, whereas it is given by the difference $\nu = C_1 - C_2 \pmod 2$ for class DIII. This is consistent with the fact that the $(+,-)$ state has $C_1 = -1, C_2 = 1$ and is therefore topological in class DIII, whereas it is trivial in class D. Therefore, if the TR symmetry is broken for the $(+,-)$ state by an imaginary $\Delta_{12}(\mathbf{p})$ that mixes the two bands, the system is in class D and it is no longer topological.

V. EDGE STATES

In this section, we show explicitly how the edge states of the $(+,-)$ system become gapped with the onset of interlayer s-wave pairing $\Delta_{12}(\mathbf{p})$ which is imaginary. We consider the following low-energy Hamiltonian in real space:

$$H = \int d^2\mathbf{r}\,\Psi^\dagger(\mathbf{r})\mathcal{H}(\mathbf{r})\Psi(\mathbf{r})$$

where $\Psi(\mathbf{r}) = (\psi_1, \psi_1^\dagger, \psi_2, \psi_2^\dagger)^T$ and

$$\mathcal{H}(\mathbf{r}) = \begin{pmatrix} -\mu(\mathbf{r}) & \Delta_{11}e^{-i\phi_0}(-\partial_x + i\partial_y) & 0 & \Delta_{12} \\ \Delta_{11}e^{i\phi_0}(\partial_x + i\partial_y) & \mu(\mathbf{r}) & -\Delta_{12}^* & 0 \\ 0 & -\Delta_{12} & -\mu(\mathbf{r}) & \Delta_{11}e^{i\phi_0}(-\partial_x - i\partial_y) \\ \Delta_{12}^* & 0 & \Delta_{11}e^{-i\phi_0}(\partial_x - i\partial_y) & \mu(\mathbf{r}) \end{pmatrix}.$$

Assuming that we can apply a local-density approximation, we take $\mu(\mathbf{r}) = \mu(r)$ to be positive within the radius R, and negative outside. Solutions to the eigenvalue equation $\mathcal{H}(\mathbf{r})\chi(\mathbf{r}) = E\chi(\mathbf{r})$ with definite angular momentum can then be found, and we use the following ansatz in the usual polar coordinates:

$$\chi(\mathbf{r}) = \kappa e^{in\theta} \begin{pmatrix} e^{-i\phi/2}[A(r) + iB(r)] \\ e^{i\phi/2}[A(r) - iB(r)] \\ e^{i\phi/2}[C(r) + iD(r)] \\ e^{-i\phi/2}[-C(r) + iD(r)] \end{pmatrix}$$

where κ is a normalization constant. The real functions A, B, C, D satisfy a set of four coupled equations, and for a large system with tightly confined edge modes we can find solutions with the energy $\pm E = \pm\sqrt{(\Delta_{11} n/R)^2 + |\Delta_{12}|^2}$. Here, n is a half integer related to the angular momentum of the edge state. These solutions require Δ_{12} to be real. If it is imaginary, it is possible to show that the edge modes do not acquire a gap. When finding the specific solutions for the edge states, care should be taken to choose the solution that is normalizable and confined to the edge. As an example, consider the physical, positive branch of energies, $+E$. A possible solution is given by $A(r) = D(r) = 0$ and

$$B(r) = \exp\left\{\frac{1}{\Delta_{11}} \int_0^r \mu(r')dr'\right\}$$
$$C(r) = \alpha B(r)$$

with

$$\alpha = \frac{\Delta_{11} n}{|\Delta_{12}| R} - \sqrt{\left(\frac{\Delta_{11} n}{|\Delta_{12}| R}\right)^2 + 1}.$$

We see that the edge states lowest in energy are localized on both layers when the two gap parameters coexist. The states higher in energy approach the solutions for uncoupled layers, which are only localized on a single layer.

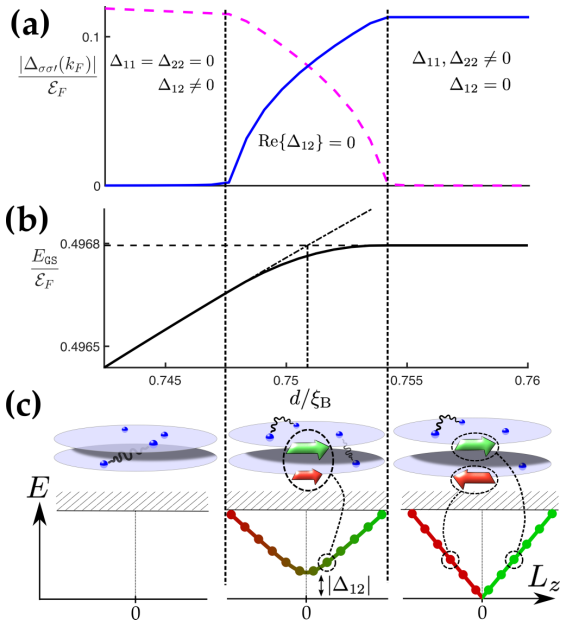

FIG. 2. (a) The magnitude of the interlayer s-wave pairing (dashed line) and intralayer p-wave pairing (solid line) as a function of the layer distance for the $(+,-)$ system. (b) The corresponding ground-state energy per particle (solid line). The dashed lines indicate the energy of states with only inter- or intralayer pairing. The dashed vertical line at $d \simeq 0.751\xi_B$ indicates where the two solutions have the same energy. (c) The edge modes of the $(+,-)$ system and their spectrum. For $d \gtrsim 0.754\xi_B$ (right column) the counter clockwise and clockwise edge modes are localized in the upper and lower layer, respectively. For $0.747\xi_B \lesssim d \lesssim 0.754\xi_B$ (middle column), the low-lying edge modes are localized in both layers and they acquire a gap. For $d \lesssim 0.747\xi_B$ (left column), there are no edge modes.

VI. NUMERICAL SOLUTION OF THE GAP EQUATION

We now numerically solve the gap equations (12) along with the number equation at $T = 0$. The $(+,-)$ case corresponds to $\phi_2(\mathbf{p}) - \phi_1(\mathbf{p}) = \pi - 2\varphi_{\mathbf{p}}$, while the $(+,+)$ case corresponds to $\phi_2(\mathbf{p}) - \phi_1(\mathbf{p}) = \pi$.

A. $(+,-)$ system

In Fig. 2(a), we plot the magnitude of the pairing fields at the Fermi surface as a function of the layer distance d for the $(+,-)$ system. Here $k_F = \sqrt{4\pi n_F}$ is the Fermi momentum with n_F the density of fermions in each layer. We have chosen a relatively weak Bose-Fermi coupling strength $g = 2\pi a/\sqrt{m_r m_B}$ with $k_F a = 0.1$, where a is the 2D-3D mixed dimensional scattering length [39]. The gas parameter of the BEC is $(n_B a_B^3)^{1/3} = 0.01$ and the ratio of the Fermi and Bose interparticle distances is $n_F^{1/2}/n_B^{1/3} = 0.2$. The energy of the system is plotted in Fig. 2(b).

For layer distances $d \gtrsim 0.754\xi_B$, there is no interlayer pairing and the two layers are uncoupled, each realizing a $p_x \pm ip_y$ topological superfluid. The corresponding edge states, illustrated in Fig. 2(c), propagate in opposite directions in the two layers and are related by the TRS operator $\mathcal{T}$. We have chosen a circular boundary with radius R to illustrate the typical geometry formed by the harmonic trap in an atomic gas experiment. As the layer distance decreases, interlayer pairing sets in for $d \lesssim 0.754\xi_B$ via a second-order transition and it coexists with the intralayer pairing. We find numerically that the interlayer pairing $\Delta_{12}(\mathbf{k})$ is purely imaginary and it therefore breaks TRS. The edge modes in the two layers mix and become gapped as illustrated in Fig. 2(c). More precisely, the dispersion of the edge modes is $E = \sqrt{(\Delta_{11} n/R)^2 + |\Delta_{12}|^2}$, where $|\Delta_{12}| \simeq |\Delta_{12}(0)|$ and $\Delta_{11}(\mathbf{p}) \simeq \Delta_{11}(p_x + ip_y)$ give the magnitude of the inter- and intralayer pairing at low momenta, as seen above. The low-energy edge states with small n are hybridized between the two layers; for larger n, the edge states become increasingly localized in a single layer, approaching those for the uncoupled layers. Finally, for layer distances $d \lesssim 0.747\xi_B$ the intralayer pairing is completely suppressed by the interlayer pairing and the system is a topologically trivial s-wave superfluid with no edge modes. We have not been

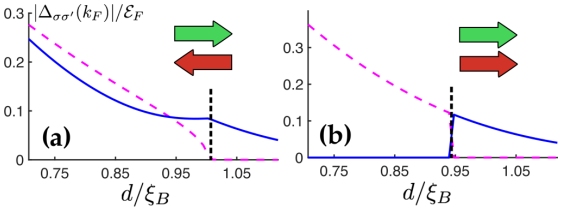

FIG. 3. The intra- (solid line) and interlayer (dashed line) pairing as a function of the BEC coherence length for the (a) $(+,-)$ and (b) $(+,+)$ system.

able to find a numerical solution with a real interlayer pairing coexisting with intralayer pairing, which would preserve TRS and support the gapless edge modes. While the coexistence region shown here is quite narrow, the width can be tuned by altering the parameters (see below).

B. (+,+) system

For the $(+,+)$ system, our numerical results show that the transition between the topological and trivial phase is first order. The transition occurs at the critical layer distance $d \simeq 0.751\xi_B$ when the phases with only one type of pairing have the same energy, as indicated by the vertical line in Fig. 2(b). We do not find numerical solutions with both types of pairing coexisting. Instead, the intralayer pairing and the associated gapless edge modes disappear and the interlayer pairing appears abruptly.

VII. VARYING THE COHERENCE LENGTH

Experimentally, it might be easier to change the BEC coherence length, which determines the range of the induced interaction, by varying a_B using a Feshbach resonance, instead of changing the layer distance. To examine this case, we plot in Fig. 3 the magnitudes of the intra- and interlayer pairings as a function of ξ_B with $k_F a = 0.12$, $k_F d = 1.0$, and $n_F^{1/2}/n_B^{1/3} = 0.2$. The coherence length is varied by changing a_B keeping n_B fixed. For a small ξ_B, the two layers are uncoupled forming the $(+,-)$ or the $(+,+)$ topological superfluid. The $(+,-)$ system undergoes a second-order phase transition to a state where intra- and interlayer pairings coexist for $\xi_B \gtrsim 1d$. Note that contrary to decreasing the distance d the system does not end up in a pure s-wave state for large ξ_B. The reason is that for a large interaction range the suppression of the p-wave channel compared to the s-wave channel is small, and intra- and interlayer pairings therefore coexist. The $(+,+)$ system on the other hand again undergoes a first-order transition between the topological and the trivial phases at $\xi_B \sim 1.05d$.

VIII. DISCUSSION

All the ingredients in the proposed setup have been realized experimentally. Bose-Fermi mixtures as well as species selective optical potentials to produce mixed dimensional systems have been reported [40–42]. It was moreover shown in Ref. [27] that the Berezinskii-Kosterlitz-Thouless critical temperature for the $p_x \pm ip_y$ superfluid in the present Bose-Fermi setup can be as high as $T_{\mathrm{BKT}} = \mathcal{E}_F/16$, which is within experimental reach [43]. We expect the critical temperature of the phase with s-wave pairing to be even higher. The edge modes can be observed for instance by direct imaging or by the response to an external drive in analogy with topological insulators [44–46].

An intriguing question concerns the robustness of the edge modes beyond mean-field BCS theory. To investigate this, one could analyze the coupling between the edge modes forming a Luttinger liquid [47,48], which is an interesting future project.

IX. CONCLUSION

We demonstrated that a mixed dimensional system consisting of two layers of fermions in a BEC is a powerful setup to realize topological superfluids with TRS. The induced interaction between the fermions mediated by the BEC leads to a competition between p-wave pairing within each layer and s-wave pairing between the layers. For large layer separation or short BEC coherence length, intralayer pairing dominates and the system forms a topological superfluid either with or without TRS. In the case of TRS, the system goes from a $\mathbb{Z}_2$ topological superfluid to a topologically trivial superfluid via a second-order transition where s-wave pairing gradually gaps the edge modes. When there is no TRS, the transition from a $\mathbb{Z}$ topological superfluid to a topologically trivial superfluid is first order. These results show how cold atomic gases offer a realistic path to realizing topological superfluids with TRS.

ACKNOWLEDGMENTS

We wish to acknowledge the support of the Villum Foundation via Grant No. VKR023163 and the Danish Council of Independent Research—Natural Sciences via Grant No. DFF-4002-00336. We acknowledge useful discussions with Alexandre Dauphin and Alessio Recati.

[1] J. Alicea, Rep. Prog. Phys. **75**, 076501 (2012).
[2] C. Nayak, S. H. Simon, A. Stern, M. Freedman, and S. Das Sarma, Rev. Mod. Phys. **80**, 1083 (2008).
[3] V. Mourik, K. Zuo, S. M. Frolov, S. R. Plissard, E. P. A. M. Bakkers, and L. P. Kouwenhoven, Science **336**, 1003 (2012).
[4] M. T. Deng, C. L. Yu, G. Y. Huang, M. Larsson, P. Caroff, and H. Q. Xu, Nano Lett. **12**, 6414 (2012).
[5] A. Das, Y. Ronen, Y. Most, Y. Oreg, M. Heiblum, and H. Shtrikman, Nat. Phys. **8**, 887 (2012).
[6] L. P. Rokhinson, X. Liu, and J. K. Furdyna, Nat. Phys. **8**, 795 (2012).
[7] A. D. K. Finck, D. J. Van Harlingen, P. K. Mohseni, K. Jung, and X. Li, Phys. Rev. Lett. **110**, 126406 (2013).
[8] S. Nadj-Perge, I. K. Drozdov, J. Li, H. Chen, S. Jeon, J. Seo, A. H. MacDonald, B. A. Bernevig, and A. Yazdani, Science **346**, 602 (2014).
[9] S. M. Albrecht, A. P. Higginbotham, M. Madsen, F. Kuemmeth, T. S. Jespersen, J. Nygård, P. Krogstrup, and C. M. Marcus, Nature (London) **531**, 206 (2016).

[10] We shall from now on refer to superfluids only. It is implicitly understood that this also refers to superconductors.
[11] A. P. Schnyder, S. Ryu, A. Furusaki, and A. W. W. Ludwig, Phys. Rev. B **78**, 195125 (2008).
[12] A. Kitaev, AIP Conf. Proc. **1134**, 22 (2009).
[13] A. Altland and M. R. Zirnbauer, Phys. Rev. B **55**, 1142 (1997).
[14] C. L. M. Wong and K. T. Law, Phys. Rev. B **86**, 184516 (2012).
[15] S. Deng, L. Viola, and G. Ortiz, Phys. Rev. Lett. **108**, 036803 (2012).
[16] F. Zhang, C. L. Kane, and E. J. Mele, Phys. Rev. Lett. **111**, 056402 (2013).
[17] S. Nakosai, J. C. Budich, Y. Tanaka, B. Trauzettel, and N. Nagaosa, Phys. Rev. Lett. **110**, 117002 (2013).
[18] A. Keselman, L. Fu, A. Stern, and E. Berg, Phys. Rev. Lett. **111**, 116402 (2013).
[19] E. Gaidamauskas, J. Paaske, and K. Flensberg, Phys. Rev. Lett. **112**, 126402 (2014).
[20] J. Klinovaja, A. Yacoby, and D. Loss, Phys. Rev. B **90**, 155447 (2014).
[21] C. Schrade, A. A. Zyuzin, J. Klinovaja, and D. Loss, Phys. Rev. Lett. **115**, 237001 (2015).
[22] Z. Yan, X. Yang, and S. Wan, Eur. Phys. J. B **86**, 347 (2013).
[23] X. Yang, B. Huang, and H.-Q. Lin, J. Phys. B **46**, 205302 (2013).
[24] B. Huang, P. H. Chui, J. Liu, C. Zhang, and M. Gong, arXiv:1511.01713.
[25] G. E. Volovik, JETP Lett. **90**, 587 (2009).
[26] Y. Makhlin, M. Silaev, and G. E. Volovik, Phys. Rev. B **89**, 174502 (2014).
[27] Z. Wu and G. M. Bruun, Phys. Rev. Lett. **117**, 245302 (2016).
[28] J. M. Midtgaard, Z. Wu, and G. M. Bruun, Phys. Rev. A **94**, 063631 (2016).
[29] Y. Nishida, Phys. Rev. A **82**, 011605 (2010).
[30] T. Anzai and Y. Nishida, Phys. Rev. A **95**, 051603 (2017).
[31] M. J. Bijlsma, B. A. Heringa, and H. T. C. Stoof, Phys. Rev. A **61**, 053601 (2000).
[32] L. Viverit, C. J. Pethick, and H. Smith, Phys. Rev. A **61**, 053605 (2000).
[33] D. Suchet, Z. Wu, F. Chevy, and G. M. Bruun, Phys. Rev. A **95**, 043643 (2017).
[34] P. W. Anderson and P. Morel, Phys. Rev. **123**, 1911 (1961).
[35] C. L. Kane and E. J. Mele, Phys. Rev. Lett. **95**, 146802 (2005).
[36] C. L. Kane and E. J. Mele, Phys. Rev. Lett. **95**, 226801 (2005).
[37] X.-L. Qi, T. L. Hughes, S. Raghu, and S.-C. Zhang, Phys. Rev. Lett. **102**, 187001 (2009).
[38] J. de Lisle, S. De, E. Alba, A. Bullivant, J. J. Garcia-Ripoll, V. Lahtinen, and J. K. Pachos, New J. Phys. **16**, 083022 (2014).
[39] Y. Nishida and S. Tan, Phys. Rev. Lett. **101**, 170401 (2008).
[40] G. Lamporesi, J. Catani, G. Barontini, Y. Nishida, M. Inguscio, and F. Minardi, Phys. Rev. Lett. **104**, 153202 (2010).
[41] D. C. McKay, C. Meldgin, D. Chen, and B. DeMarco, Phys. Rev. Lett. **111**, 063002 (2013).
[42] G. Jotzu, M. Messer, F. Görg, D. Greif, R. Desbuquois, and T. Esslinger, Phys. Rev. Lett. **115**, 073002 (2015).
[43] R. Onofrio, Phys. Usp. **59**, 1129 (2017).
[44] N. Goldman, J. Dalibard, A. Dauphin, F. Gerbier, M. Lewenstein, P. Zoller, and I. B. Spielman, Proc. Natl. Acad. Sci. USA **110**, 6736 (2013).
[45] D. T. Tran, A. Dauphin, A. G. Grushin, P. Zoller, and N. Goldman, Sci. Adv. **3**, e1701207 (2017).
[46] N. Goldman, G. Jotzu, M. Messer, F. Görg, R. Desbuquois, and T. Esslinger, Phys. Rev. A **94**, 043611 (2016).
[47] C. Xu and J. E. Moore, Phys. Rev. B **73**, 045322 (2006).
[48] Y. Tanaka and N. Nagaosa, Phys. Rev. Lett. **103**, 166403 (2009).

— 4 —

Detection of Topological Superfluidity with Dichroism

The project described in this chapter is still not completed, although most numerical calculations are finished. After a brief introduction, I will start by discussing the results so far and then discuss the plans for the remainder of the manuscript. The work was initiated along with Nathan Goldman, whose similar work for topological insulators [48] served as an inspiration for this project.

4.1 Detecting Superfluidity

A detection of topological superfluidity has been the holy grail of condensed matter physics for a while. Recently, several reports of topological superfluidity in 1D nanowires has been announced [49–51], where zero-energy states at the wire ends have been observed. This is consistent with the Majorana modes predicted to be present there, but it is to my knowledge still hotly debated whether the observations are conclusive.

Even more so, a detection of chiral superfluidity in a 2D system remains elusive. In the condensed matter field, signatures of an exotic type of superconductivity in Sr_2RuO_4 were long hoped to be the $p_x + ip_y$-state, but recently this was shown to not be the case [52]. In fact, the nature of the pairing in this material continues to bewilder researchers [53]. Cold atomic gases could very well be a more successful place for a conclusive detection.

Detecting superfluidity in a gas of neutral atoms is in itself not an easy feat. Thermodynamic measurements and generation of vortices are the main detection schemes. Other schemes, such as rf spectroscopy only provide an indirect probe of the pairing gap [54] It stands to reason that distinguishing different types of superfluid pairing will not be easy either, so conclusively detecting a topological superfluid would represent a great leap forward.

In cold atom experiments, several detection schemes have been proposed and implemented for topological insulators, such as state tomography [55] and direct imaging of edge states which has been implemented in systems

with synthetic dimensions [56]. Many of these are unfortunately not suitable for detecting topological superconductors, which is the major motivation for this work. In this manuscript we show how to detect the chirality of a superfluid using a probe that has recently been implemented and shown to reproduce the Chern number for a topological insulator [57]. As a test, we calculate the response on the 2D chiral superfluid studied in [47]. This is basically the same system we considered in chapter 2, but without the square optical lattice for the fermions, or just a single-layer version of the system considered in chapter 3.

4.2 The Dichroism Probe

In contrast to a Chern insulator, the (charge) Hall conductance of a chiral superconductor is not necessarily quantized, due to the breaking of charge conservation. While the Hall conductance is non-vanishing in some cases and there have been proposals to extract signatures of topology from it [58], they require the possibility of realizing the system in different topological phases to see the *changes* in phase. This is not always feasible, however. The system we are considering is a mixed-dimensional Bose-Fermi mixture. Realizing a topologically trivial phase for the fermions would require the superfluid to be on the topologically trivial BEC side of the BCS-BEC crossover. This in turn would require a very strong Bose-Fermi interaction, limiting the possible pairs of atomic species that would be suitable to those with very broad Feschbach resonances. Even then, very strong Bose-Fermi interactions lead to phase separation of the mixture [41] so that sets an upper limit on how strong the induced interaction can be.

A probe that directly captures the Chern number would thus be very useful. We consider subjecting the superfluid to a potential, circularly oscillating in-plane. This is akin to a clockwise or counter-clockwise shaking of the confining trap. This shaking heats up the gas, causing excited states to be populated. In this case, the excited states are Bogoliubov modes, corresponding to a breaking of Cooper pairs, which will happen at some rate, Γ. Because of the broken chiral symmetry, the system can respond differently to a clockwise and counter-clockwise oscillation. The probe is then defined as the difference in heating rates, integrated over all oscillation frequencies,

$$\Delta\Gamma = \int_0^\infty \Gamma_+(\omega) - \Gamma_-(\omega)\,\mathrm{d}\omega \tag{4.1}$$

where $\Gamma_+(\omega)$ ($\Gamma_-(\omega)$) is the heating rate for a (counter)-clockwise oscillation at frequency ω.

4.3 Results

The probe defined above is shown to be equivalent to a measurement of the transverse current-current correlation function in the limit

$$\lim_{\mathbf{q}\to 0}\lim_{\omega\to 0}\chi_{j_x,j_y}(\mathbf{q},\omega)/i\omega \tag{4.2}$$

This is reminiscent of the Hall conductivity, but crucially the order of the limits are reversed from the typical definition.

In contrast to the similar calculation for an insulator, the current-current correlation for the superconductor is trickier to calculate, however. Within the BCS approximation, the limit in Eq. (4.2) vanishes, so we are forced to go beyond mean-field and include fluctuations of the global phase of the superconducting order parameter. This is elegantly done using path integral techniques. For a thorough introduction to this technique, see chapters 3 and 4 in [59]. In this formalism, integrating out the phase involves performing a simple Gaussian integral, but would require more involved summations of Feynman diagrams with a diagrammatic technique.

In the end, when fluctuations of the phase are included, the probe's largest contribution turns out to be the Chern number of the system. By the continuity equation, this limit of the current-current correlation function can be related to the density-current correlation. Here the probe is proportional to

$$\lim_{\mathbf{q}\to 0}\lim_{\omega\to 0}\chi_{j_x,n}(\mathbf{q},\omega)/iq_y. \tag{4.3}$$

Surprisingly, this function captures the non-zero result at the BCS level, leading to a simpler way of calculating the expected difference in heating rates.

There is another contribution, apart from the Chern number, to the difference in heating rates. This non-topological contribution goes as $\propto |\Delta|^2$, so it is negligible for a weak superfluid pairing. Both this contribution and the topological contribution is calculated for a range of oscillation frequencies and summed together, and we find that for all parameters, the topological contribution is the dominating part.

A thing to note is that the non-topological contribution is due to breaking of the *physical* particle-hole symmetry, whereas the ground-state still obeys the particle-hole symmetry of the BCS Hamiltonian. Recall from chapter 1 that these transformations do not necessarily have to be identical. Also note that in the topological superconductor, as opposed to the topological insulator, a topological ground state do not necessarily imply a quantized conductivity.

The critical temperature of the superfluid can be as high as the maximum allowed by BKT theory, $T_{\mathrm{BKT}} = T_F/16$, by varying the gas parameter of the

BEC and the strength of the Bose-Fermi interaction. The typical behaviour is that critical temperature and difference in heating rates are inversely related, but we find that a stronger Bose-Fermi interaction allows the critical temperature to be high, while still keeping the non-topological contribution to the probe small. This effect is subtle, however, and it seems possible to extract the Chern number from most realistic experimental parameters with only a small non-topological deviation.

4.4 Further Studies

There are a couple of things we wish to further examine in relation to this manuscript. The most notable one concerning the detection of the Chern number relates to the edges of the atomic cloud.

In the above, we have mostly assumed that we could probe the translation-invariant bulk without considering the edges of the system. Tran *et al.* argues in [48] that for a topological insulator, a charge current will flow on the edge exactly opposite to the current in the bulk, when open boundaries are considered. This means that the total contribution to the probe is zero, no matter the value of the Chern number. They go on to present methods for removing the edge-contribution.

A crucial consideration in our case is whether or not this also happens in the superconducting case. Recall that the Majorana edge modes are equal superpositions of particles and holes, so they only carry a heat current, not a charge current. We hope to either confirm whether this means that the edge contribution to the probe is negligible or in the other case, consider if the methods for removing the edge-state contributions considered in the paper above can also be adapted to the superconducting case.

Lastly, another strategy would be to measure the angular momentum of the fermi gas. As the Cooper pairs all carry one quantum of angular momentum, the gas should acquire a non-zero angular momentum on the topological superfluid phase. An experimental procedure for measuring this might be easier than measuring heating rates, and we would also like continue this line of inquiry.

4.5 Contribution

As it stands, I wrote the first draft of the manuscript and have made all figures. Calculations of the dichroic response were done by me, while the critical temperatures were calculated by Zhigang Wu, who also wrote Appendix D.

Detecting Topological Superfluidity with a Dichroism probe

J. M. Midtgaard,[1] Zhigang Wu,[2,3] and G. M. Bruun[1,4]

[1] *Department of Physics and Astronomy, Aarhus University, Ny Munkegade, DK-8000 Aarhus C, Denmark.*
[2] *Shenzhen Institute for Quantum Science and Engineering (SIQSE) and Department of Physics, Southern University of Science and Technology (SUSTech), Shenzhen 518055, China*
[3] *Center for Quantum Computing, Peng Cheng Laboratory, Shenzhen 518055, China*
[4] *Shenzhen Institute for Quantum Science and Engineering and Department of Physics, Southern University of Science and Technology, Shenzhen 518055, China*

(Dated: June 2019)

Several promising detection methods are known for topological insulators in cold atom contexts but detection schemes for superfluids remain elusive. Motivated by this, we propose a probe that utilizes the dichroic response of a chiral superfluid. The probe is equivalent to the measurement of an unconventional Hall conductivity, where the order of limits are reversed. It is shown to accurately reproduce the Chern number of the system within a weak-coupling regime and we demonstrate the use of this probe with calculations for a mixed-dimensional Bose-Fermi mixture.

I. THE DICHROISM PROBE

We consider a 2D system subjected to a clockwise or counterclockwise rotating force. Our analysis is largely equivalent to that in Ref. [1], but we will emphasize more the connection to transverse current-current as well as current-density correlation functions evaluated in the "static" limit.

The Hamiltonian H of the system is

$$H = \int d^2r\psi^*(\mathbf{r})[\frac{1}{2m}(-i\nabla - \mathbf{A})^2 + A_0]\psi(\mathbf{r}) + \frac{1}{2}\iint d^2r d^2r' \psi^\dagger(\mathbf{r})\psi^\dagger(\mathbf{r}')V(\mathbf{r}-\mathbf{r}')\psi(\mathbf{r}')\psi(\mathbf{r}) \quad (1)$$

where $\psi(\mathbf{r})$ is the fermion field and $V(\mathbf{r}-\mathbf{r}')$ is the interaction giving rise to $p_x + ip_y$ pairing. Here and in the following we use units where the system area and $\hbar$ both equal unity. Even though we eventually will consider a neutral atomic system, we have included the gauge potential $A = (A_0, \mathbf{A})$ so that the relevant current-current and current-density correlation functions can be obtained by functional derivatives.

A force rotating clockwise/counter-clockwise gives rise to the perturbation $H'_\pm(\mathbf{q},t) = \int \mathrm{d}^2\mathbf{r} n(\mathbf{r})V_\pm(\mathbf{r},t)$ with $n(\mathbf{r}) = \psi^\dagger(\mathbf{r})\psi(\mathbf{r})$ being the density operator and the potential

$$V_\pm(\mathbf{r},t) = 2E\left(\frac{\sin q_x x}{q_x}\cos\omega t \pm \frac{\sin q_y y}{q_y}\sin\omega t\right). \quad (2)$$

Here, E is the strength of the "electric" field acting on the particles, and we shall take the limit $\mathbf{q}\to 0$ at the end of the calculation corresponding to a uniform force. Following Ref. [1], we go to a rotating frame using the unitary transformation

$$R_\pm(\mathbf{q},t) = e^{i2E(\frac{\sin q_x x}{q_x}\sin\omega t \mp \frac{\sin q_y y}{q_y}\cos\omega t)/\omega}. \quad (3)$$

It is easy to show that if $|\psi\rangle$ obeys the Schrödinger equation $i\partial_t|\psi\rangle = [H + H'_\pm(t)]|\psi\rangle$, then $|\tilde\psi\rangle = R(t)|\psi\rangle$ obeys $i\partial_t|\tilde\psi\rangle = [H + \tilde H'_\pm(t)]|\tilde\psi\rangle$ with the modified perturbation given by

$$\tilde H'_\pm(\mathbf{q},t) = -\frac{2E}{\omega}\left[\tilde j_x(q_x)\sin\omega t \mp \tilde j_y(q_y)\cos\omega t\right] \quad (4)$$

to linear order in E. Here, $\tilde j_x(q_x) = [j_x(q_x) + j_x(-q_x)]/2$ with

$$j_x(q_x) = \frac{1}{2mi}\int d^2r\, e^{iq_x x}[\psi^\dagger(\mathbf{r})\partial_x\psi(\mathbf{r}) - \text{h.c.}] \quad (5)$$

the Fourier transform of the current along the x-direction. Likewise, $\tilde j_y(q_y) = [j_y(q_y) + j_y(-q_y)]/2$.

The excitation $\Gamma_\pm(\mathbf{q},\omega)$ rate out of the ground state $|g\rangle$ of H induced by $H'_\pm(\mathbf{q},t)$ can be calculated using Fermi's golden rule. We define $\Delta\Gamma = \lim_{q\to 0}\int_0^\infty d\omega[\Gamma_+(\mathbf{q},\omega) - \Gamma_-(\mathbf{q},\omega)]/2$ giving the difference in the excitation rate coming from a clockwise/anti-clockwise rotating force integrated over all frequencies. A straightforward calculation gives

$$\Delta\Gamma = 4\pi i E^2 \lim_{q\to 0}\sum_f \frac{\langle g|j_x(\mathbf{q})|f\rangle\langle f|j_y(-\mathbf{q})|g\rangle - (x\leftrightarrow y)}{(E_f - E_g)^2} = 4\pi E^2 \lim_{q\to 0}\lim_{\omega\to 0}\frac{\chi_{j_x,j_y}(\mathbf{q},\omega)}{i\omega} \quad (6)$$

where $|f\rangle$ denotes an excited eigenstate of H with energy E_f, and $\chi_{A,B}(\mathbf{q},\omega)$ is the Fourier transform of the retarded transverse current-current correlation function

$$\chi_{A,B}(\mathbf{q},t-t') = -i\theta(t-t')\langle[A(\mathbf{q},t), B(-\mathbf{q},t')]\rangle \quad (7)$$

with $\theta(x)$ the Heaviside function. This explicitly demonstrates that $\Delta\Gamma$ is given by the "static" limit $\lim_{q\to 0}\lim_{\omega\to 0}$ of the transverse current-current correlation function. This is crucial, since the standard order $\lim_{\omega\to 0}\lim_{q\to 0}$ for the Hall conductivity gives zero for a translationally invariant system [2]. The continuity equation $\partial_t n + \nabla\cdot j$ implies the relation

$$\omega\chi_{j_\alpha,n}(\mathbf{q},\omega) = q_\beta\chi_{j_\alpha,j_\beta}(\mathbf{q},\omega) + \langle[j_\alpha, n]\rangle(\mathbf{q},\omega) \quad (8)$$

between the current-current and current-density correlation function. Using this, we can rewrite Eq. (6) as

$$\Delta\Gamma = 4\pi E^2 \lim_{q\to 0}\lim_{\omega\to 0}\frac{\chi_{j_x,n}(\mathbf{q},\omega)}{iq_y}. \quad (9)$$

II. MEAN-FIELD BCS THEORY

In this section, we derive an effective action for the p_x+ip_y superfluid from which the correlation functions $\chi_{j_x,n}$ and χ_{j_x,j_y} can be obtained by functional derivatives. We focus here on mean-field BCS theory deriving an explicit formula for the Chern number, which will be useful later. The inclusion of phase fluctuations, which is necessary to restore particle conservation and therefore to obtain consistent results from Eq. (6) and Eq. (9), is postponed to Sec. (III).

Using the path integral, the partition function of the system without the dichroism probe can be written as

$$\mathcal{Z} = \int \mathcal{D}(\psi^*\psi) e^{-\int_0^\beta d\tau \int d^2 r \psi^*(\partial_\tau - \mu)\psi - H(\psi^*\psi, A)}, \quad (10)$$

where τ is imaginary time. The superfluid pairing field $\Delta(\mathbf{r},\mathbf{r}',\tau)$ can now be introduced via the Hubbard-Stratonovich transformation [3]. We obtain after Fourier transforming to momentum-frequency space

$$\mathcal{Z} = \int \mathcal{D}(\Delta^*\Delta) e^{-[S_0 + \sum_q' \delta S(q)]} \quad (11)$$

with

$$S_{\rm BCS} = -\sum_k \frac{{\rm Tr}\mathcal{G}^{-1}}{2} - \sum_{kk'} \frac{\Delta^*_{k'}\Delta_k}{2TV(\mathbf{k}'-\mathbf{k})} \quad (12)$$

the action of the superconductor in the absence of the gauge field and phase fluctuations of the order parameter. Here, T is the temperature,

$$\mathcal{G}^{-1}(k) = \begin{bmatrix} -i\omega_n + \xi_{\mathbf{k}} & \Delta_k \\ \Delta_k^* & -i\omega_n - \xi_{\mathbf{k}} \end{bmatrix} \quad (13)$$

is the inverse Green's function in Nambu space and $\xi_{\mathbf{k}} = \mathbf{k}^2/2m - \mu$ with μ the chemical potential. We have defined $q = (\mathbf{q}, i\omega_n)$ where $\omega_n = (2n+1)T$ is a fermionic Matsubara frequency. As we shall explain in Sec. (III), phase fluctuations and the gauge field are included in the term $\sum_q' \delta S(q)$.

Mean-field BCS theory is obtained as usual by the stationary phase approximation $\delta \ln \mathcal{Z}/\delta\Delta_k^* = 0$, which yields the Hamiltonian

$$H_{\mathbf{k}} = \mathcal{G}^{-1}(\mathbf{k},0) = \mathbf{h}_{\mathbf{k}}\cdot\boldsymbol{\tau}, \quad (14)$$

where $\mathbf{h}_{\mathbf{k}} = ({\rm Re}\Delta_{\mathbf{k}}, -{\rm Im}\Delta_{\mathbf{k}}, \xi_k)^T$ and $\boldsymbol{\tau} = (\tau_1,\tau_2,\tau_3)^T$ with τ_i the Pauli matrices.

For spin polarised fermions in 2D, a low energy solution to the resulting gap equation has chiral p-wave symmetry, i.e. $\Delta_{\mathbf{k}} = \Delta_{|\mathbf{k}|}e^{i\phi}$, where ϕ is the polar angle of $\mathbf{k}$. This results in a topological phase characterised by a Chern number $C=-1$ for $\mu>0$ whereas $C=0$ for $\mu<0$ [4, 5]. The Chern number C can be expressed explicitly as

$$C = \int \frac{d^2k}{4\pi}\frac{1}{|\mathbf{h}_{\mathbf{k}}|^3}\mathbf{h}_{\mathbf{k}}\cdot\partial_{k_x}\mathbf{h}\times\partial_{k_y}\mathbf{h} = \int\frac{d^2k}{2\pi}\left[\frac{v_x}{E_{\mathbf{k}}^3}{\rm Im}(\Delta^*_{\mathbf{k}}\partial_{k_y}\Delta_{\mathbf{k}}) + \frac{\xi_{\mathbf{k}}}{2}{\rm Im}(\partial_{k_x}\Delta_{\mathbf{k}}\partial_{k_y}\Delta^*_{\mathbf{k}})\right] \quad (15)$$

where $v_x = k_x/m$ and $E_{\mathbf{k}} = \sqrt{\xi_{\mathbf{k}}^2 + |\Delta_{\mathbf{k}}|^2}$ is the BCS quasiparticle energy. The second term in the integrand scales as $\Delta_{\mathbf{k}}^2/\mu^2$ so that the Chern number is given by the first term for $\Delta_{\mathbf{k}} \ll \mu$.

III. PHASE FLUCTUATIONS

As is well-known, BCS theory does not conserve particle number, which is important for our present purpose, since it consequently predicts different results from Eq. (6) and Eq. (9). In order to recover particle conservation and obtain consistent results, we now go beyond mean-field BCS theory and restore the $U(1)$ symmetry of the order parameter Δ by integrating over its phase. Physically, this corresponds to including supercurrents in the continuity equation.

The phase $\Phi(\mathbf{r},\mathbf{r}',\tau)$ of the pairing field is introduced by writing

$$\Delta(\mathbf{r},\mathbf{r}',\tau) = |\Delta(\mathbf{r},\mathbf{r}',\tau)|e^{i\Phi(\mathbf{r},\mathbf{r}',\tau)}. \quad (16)$$

Since the phase is slowly varying on the length scale of the BCS coherence length $\sim v_F/\Delta$ for the relevant low energy degrees of freedom, we can write $\Phi(\mathbf{r},\mathbf{r}',\tau) \simeq \Phi(\mathbf{r},\tau)$. Following Ref. [6, 7], we employ the variable substitution $\psi(\mathbf{r},\tau) \to e^{i\Phi(\mathbf{r},\tau)/2}\psi(\mathbf{r},\tau)$ and $\psi^*(\mathbf{r},\tau) \to e^{-i\Phi(\mathbf{r},\tau)/2}\psi^*(\mathbf{r},\tau)$ with Jacobian one. This absorbs the phase $\Phi(\mathbf{r},\tau)$ into the gauge potentials, which in momentum-frequency space reads

$$\tilde{\mathbf{A}}(q) = \mathbf{A}(q) - i\mathbf{q}\Phi(q)/2$$
$$\tilde{A}_0(q) = A_0(q) + \omega_\gamma\Phi(q)/2. \quad (17)$$

As detailed in App. A, using this transformation in Eq. (10) yields Eq. (11) with

$$\delta S(q) = \frac{1}{2}\sum_k\Big[\tilde{\mathbf{A}}(q)\cdot\mathbf{k}\frac{g_1(k,q)}{m^2}\tilde{\mathbf{A}}(-q)\cdot\mathbf{k} + \tilde{A}_0(q)g_2(k,q)\tilde{A}_0(-q) - \tilde{A}_0(q)\frac{g_3(k,q)}{m}\tilde{\mathbf{A}}(-q)\cdot\mathbf{k} - \tilde{\mathbf{A}}(q)\cdot\mathbf{k}\frac{g_4(k,q)}{m}\tilde{A}_0(-q)\Big]. \quad (18)$$

We have used that $\Delta_k = -\Delta_{-k}$ for the mean-field p-wave solution to eliminate certain terms and defined $g_1(k,q) = {\rm Tr}[\mathcal{G}(k-q/2)\mathcal{G}(k+q/2)]$, $g_2(k,q) = {\rm Tr}[\mathcal{G}(k-$

$q/2)\tau_3\mathcal{G}(k+q/2)\tau_3]$, $g_3(k,q) = \mathrm{Tr}[\mathcal{G}(k-q/2)\tau_3\mathcal{G}(k+q/2)]$, and $g_4(k,q) = g_3(k,-q)$. In Eq. (11), $\sum_q'$ means summing over half the Fourier components of δA, for instance $\sum_{q,q_x>0}$ in order to avoid double counting.

Amplitude oscillations of the order parameter away from its mean-field value have a high energy $\sim 2\Delta$ and can therefore can be neglected for the present purpose. The phase fluctuations on the other hand correspond to low energy excitations giving rise to superflow, which must be included to maintain particle conservation. Keeping the amplitude of the order parameter fixed at its mean-field value, the remaining integral over the phase in Eq. (11) is easily performed yielding

$$\mathcal{Z} \simeq \int \mathcal{D}(\Phi^*\Phi) e^{-S_{\mathrm{eff}}} \propto e^{-S_{\mathrm{BCS}} - S_{1L} + \sum_q' \frac{C(q)^* C(q)}{B(q)}}. \quad (19)$$

Here, $S_{1L}(A)$ is given by Eq. (18) with $\tilde{A}$ replaced by A. Explicit expressions for $B(q)$ and $C(q)$ are given in App. A.

IV. HEATING RATE AND THE CHERN NUMBER

The connected current-density and current-current correlation functions can now be obtained from partition function as $\chi_{j_x,n}(q) = \delta^2 \ln \mathcal{Z}/\delta A_x(q)\delta A_0(-q)$ and $\chi_{j_x,j_y}(q) = -\delta^2 \ln \mathcal{Z}/\delta A_x(q)\delta A_y(-q)$ respectively. Using Eq. (19), we obtain

$$\begin{aligned}\chi_{j_x,n}(q) &= \sum_k \frac{k_x}{2m} g_4(k,q) + \chi^{\mathrm{fluc}}_{j_x,n}(q) \\ \chi_{j_x,j_y}(q) &= \sum_k \frac{k_x k_y}{2m^2} g_1(k,q) - \chi^{\mathrm{fluc}}_{j_x,j_y}(q) \end{aligned} \quad (20)$$

where

$$\chi^{\mathrm{fluc}}_{j_x,j_y}(q) = \frac{\frac{\delta C(q)}{\delta A_x(q)} \frac{\delta C(q)^*}{\delta A_y(-q)}}{B(q)} \quad (21)$$

and likewise for $\chi^{\mathrm{fluc}}_{j_x,n}(q)$ with $\delta C(q)/\delta A_y(-q)$ replaced by $\delta C(q)/\delta A_0(-q)$. The first terms on the right hand sides of the equality signs in Eq. (20) are the BCS (1-loop) approximations χ^{BCS} to the correlation functions, and χ^{fluc} are the contributions from the superfluid phase fluctuations. Explicit expressions for $\chi^{\mathrm{fluc}}_{j_x,n}(q)$ and $\chi^{\mathrm{fluc}}_{j_x,j_y}(q)$ are given in App. B.

The Matsubara sums for the BCS terms in Eq. (20) are easily evaluated. In particular, as shown in App. A.

$$\begin{aligned}\lim_{\mathbf{q}\to 0} \frac{\chi^{\mathrm{BCS}}_{j_x,n}(\mathbf{q},0)}{iq_y} &= \int \frac{d^2k}{8\pi^2} \frac{k_x}{m} \frac{\mathrm{Im}[\Delta^*_{\mathbf{k}} \partial_{k_y} \Delta_{\mathbf{k}}]}{E^3_{\mathbf{k}}} \\ &= -\frac{C}{4\pi} + \mathcal{O}(\Delta^2/\mu^2), \end{aligned} \quad (22)$$

where the last equality is obtained by comparing with Eq. (15). Combining Eq. (22) with Eq. (9) gives

$$\Delta\Gamma = E^2|C| + \mathcal{O}(\Delta^2/\mu^2). \quad (23)$$

Equation (23) is a main result of the present paper. It shows that the heating rate from the dichroism probe is closely related to the Chern number of the superfluid phase. The heating rate should exhibit a discontinuous jump when the superfluid enters the topological phase with $C = -1$, which is given by the Chern number to order $\mathcal{O}(\Delta^2/\mu^2)$. This result is analogous to the case of non-interacting topological insulators, where the heating rate is exactly proportional to the Chern number [1]. Compared to this, there is however a correction term scaling as $\mathcal{O}(\Delta^2/\mu^2)$ for a superfluid, which although it is small in general means that the heating rate from the dichroism probe is *not* strictly topological. This result is directly connected to the fact that the edge current in a finite sample of a chiral p-wave superconductor is not topological as opposed to the presence of edge (Majorana) states [8, 9]. Indeed, the limit $\lim_{\mathbf{q}\to 0} \lim_{\omega\to 0}$ of the current-density correlation function given by Eq. (22) naturally arises when considering currents close to a static edge [10–13].

Note that BCS theory predicts a very small heating rate unrelated to the Chern number and scaling as $\mathcal{O}(\Delta^2/\mu^2)$, if we had evaluated it from the current-current correlation function $\chi^{\mathrm{BCS}}_{j_x,j_y}$ instead by using Eq. (20) in Eq. (6). As discussed above, the reason for this inconsistency is that BCS theory does not conserve particle number, meaning that $\chi^{\mathrm{BCS}}_{j_x,j_y}(q)$ and $\chi^{\mathrm{BCS}}_{j_x,j_y}(q)$ do not obey Eq. (8). This contradiction is resolved when the phase of the order parameter is included as described in Sec. III. Indeed, we again obtain Eq. (23) when using $\chi_{j_x,j_y}(q)$ obtained from Eq. (20) which includes phase fluctuations, in Eq. (6) [6, 7, 14].

V. A MIXED-DIMENSIONAL BOSE-FERMI MIXTURE

The best solid state candidate so far for a 2D chiral $p_x + ip_y$ superconductor is Sr_2RuO_4. However, the precise symmetry of the order parameter in this system is still subject to intense debate [15]. An atomic spin polarised 2D Fermi gas immersed in a 3D BEC has been shown to offer a very promising system for realising a 2D chiral $p_x + ip_y$ superfluid [16–18]. In this system, the fermions interact by exchanging sound modes in the BEC, which leads to an induced attractive interaction and therefore pairing. One can vary both the range and the strength of the induced interaction by changing the Bose-Fermi and the Bose-Bose scattering length. This allows one to tune the system parameters in order to reach the maximal critical temperature $T_c = T_F/16$ allowed for a 2D spin polarised fermionic superfluid, where T_F is the Fermi temperature [16]. Experimentally, a mixed dimensional Bose-Fermi mixture has already been realised using ^{173}Yb-^{7}Li atoms, which constitutes the first important step towards realising a chiral $p_x + ip_y$ superfluid with cold atoms [19].

We therefore now analyse how the dichroism probe can

be used to detect the topological $p_x + ip_y$ pairing in such a ^{173}Yb-^{7}Li mixture. Since the bosons (^{173}Yb) are much heavier than the fermions (^{7}Li), we can ignore retardation effects [20] and the induced interaction takes the Yukawa form

$$V(\mathbf{r}) = -\frac{a_{\text{eff}}^2 n_B m_B}{\pi} \frac{\exp(-\sqrt{2}r/\xi_B)}{r}. \tag{24}$$

Here, n_B, m_B is the density and mass of the bosons, ξ_B is the healing length of the BEC, and a_{eff} is the effective scattering length between the fermions and bosons. The full frequency-dependent Eliashberg equations are given in App. D, but note that when calculating the dichroic response, we only consider the BCS limit.

From this we can solve self-consistently for the superfluid gap parameter. The dichroism probe $\Delta\Gamma$ is the integrated signal over all perturbation frequencies, so to see what frequencies are needed to accurately estimate the Chern number, we define from Eq. (22)

$$\Delta\Gamma(\Omega) = \int \frac{d^2k}{8\pi^2} \frac{k_x}{m} \frac{\text{Im}[\Delta_{\mathbf{k}}^* \partial_{k_y} \Delta_{\mathbf{k}}]}{E_{\mathbf{k}}^3} \theta(\Omega - E_{\mathbf{k}}) \tag{25}$$

where Ω is the perturbation frequency. In this context it also acts as a cutoff for the possible excited states. When all excited states are considered, it is clear that $\Delta\Gamma = \Delta\Gamma(\Omega \to \text{inf})$. The observed difference in heating rate between a clockwise perturbation and a counterclockwise perturbation at a given perturbation frequency is then $\Gamma(\Omega) = \partial_\Omega \Delta\Gamma(\Omega)$. An example can be seen in Fig. 1.

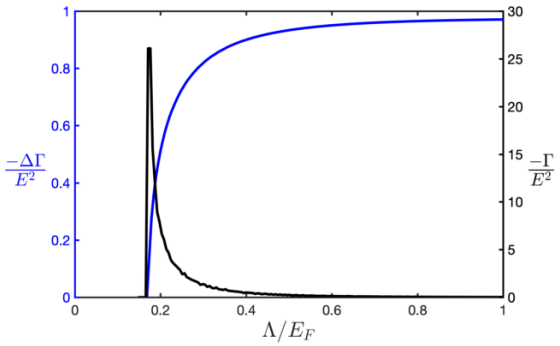

FIG. 1. (Color online). This shows the difference in heating rates between a clockwise and counterclockwise perturbation (black). The scale E is the electric field strength. This is the measured signal from the dichroism probe. The cumulative sum (blue) shows how, when integrating the contributions for frequencies up an appropriate cutoff, the result converges close to the Chern number. Here, an appropriate cutoff would be around the Fermi energy but this depends on the strength of the pairing.

Through this, we can see that probing frequencies from around the energy gap E_{gap} to about $8E_{\text{gap}}$ is sufficient to accurately estimate the effective Chern number. Note that the effective Chern number never quite reaches 1 in Fig. (1). This is due to the second order term in Eq. (23) which grows as the pairing strength grows. To see the influence of this, we can calculate the critical temperature of the superfluid for representative experimental parameters, along with the effective Chern number. In general, the frequency dependence of the induced interaction is important and should be considered when calculating the critical temperature. See App.D and [16] for more details. Fig. 2 shows an example where we have taken the Bose-Fermi coupling to be $n_B a_{\text{eff}} = 0.1$. The density ratio between the fermions and bosons is taken to be $n_F^{1/2}/n_B^{1/3} = 0.5$

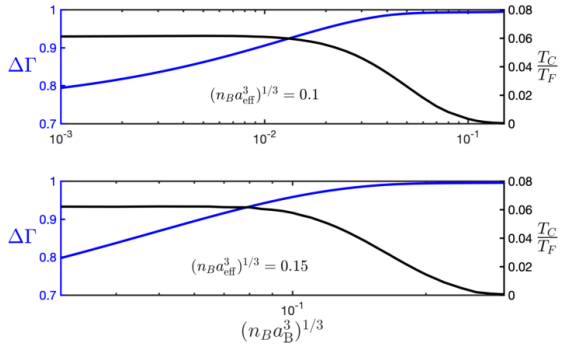

FIG. 2. (Color online). The critical temperature (black) rises when lowering the BEC gas parameter $(n_B a_{\text{B}}^3)^{1/3}$. It rises up to around the highest possible critical temperature for a 2D system. This lowers the effective Chern number (blue), due to the stronger superfluid pairing. The results are shown for two different values of the effective interaction strength between the fermions and the bosons in the BEC, a_{eff}.

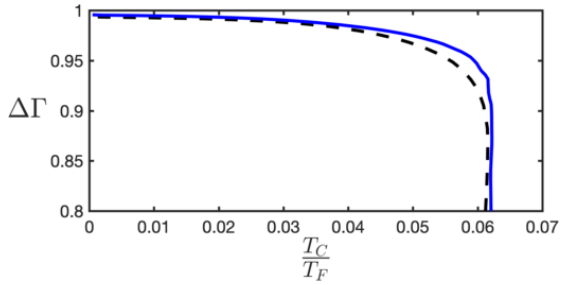

FIG. 3. (Color online). Same data as in Fig. 2 but shows the effect of raising the interaction strength. The dashed (black) line corresponds to the top plot in Fig. 2 with an interaction strength of $(n_B a_{\text{eff}}^3)^{1/3} = 0.1$. Th solid (blue) line corresponds to the bottom plot from Fig. 2 with an interaction strength of 0.15

We see that even for experimental parameters with high critical temperatures, there is an intermediate region where the effective Chern number is close to 1 in

magnitude. To extract the effective Chern number, we have summed contributions up to $8E_{\rm gap}$. Contributions from higher perturbation frequencies could be summed as well but this only changes the curve slightly. The results for the effective Chern number should be seen as a lower bound, especially for lower values of the gas parameter. This is due to the fact that we are restricting ourselves to a slightly naive BCS calculation and not properly including the effect of the full, retarded interaction, when calculating the effective Chern number. Nevertheless, we can see that the behaviour is somewhat universal. The dichroism probe yields a value close to the "topological" value of 1, even for high critical temperatures. The intermediate region where the critical temperature is high, and the probes' deviation from 1 is small, seems to have about the same width for different values of the effective Bose-Fermi interaction strength. However, even a somewhat smaller result make it easy to distinguish between the topological phase and the normal phase, where the dichroic response is 0. Fig. 3 shows the response as a function of critical temperature for two different interaction strengths, $(n_B a_{\rm eff}^3)^{1/3} = 0.1$ and 0.15. In the experiment, we would like to maximise both critical temperature and keep the response to the probe as close to 1 as possible, so we are interested in the knee of the curves. From the figure, it is clear that a stronger Bose-Fermi interaction is beneficial since the solid (blue) line has a sharper knee. However, the difference is small and the lower interaction strength (the dashed line) still provides a response close to 1 at the maximal critical temperature.

VI. CONCLUSION

We have considered how to detect topological superfluidity in a gas of neutral atoms. A dichroism probe can be defined as the difference in heating rates resulting from a clockwise and counter-clockwise perturbation as considered previously for topological insulators. We found that the probe approximates the Chern number for weak pairing strengths and confirmed the viability as a detection method. The probe corresponds to specific limits of the density-current and current-current correlation functions, and it was shown that a number-conserving calculation is needed to obtain correct results for the current-current correlation.

[1] D. T. Tran, A. Dauphin, A. G. Grushin, P. Zoller, and N. Goldman, Science Advances **3** (2017), 10.1126/sciadv.1701207, https://advances.sciencemag.org/content/3/8/e1701207.full.pdf.

[2] G. Giuliani and G. Vignale, *Quantum theory of the electron liquid* (Cambridge University Press, Cambdridge, 2005).

[3] A. Altland and B. Simons, *Condensed Matter Field Theory*, Cambridge books online (Cambridge University Press, 2010).

[4] N. Read and D. Green, Phys. Rev. B **61**, 10267 (2000).

[5] J. Alicea, Reports on Progress in Physics **75**, 076501 (2012).

[6] B. Horovitz and A. Golub, Phys. Rev. B **68**, 214503 (2003).

[7] R. M. Lutchyn, P. Nagornykh, and V. M. Yakovenko, Phys. Rev. B **77**, 144516 (2008).

[8] E. Taylor and C. Kallin, Phys. Rev. Lett. **108**, 157001 (2012).

[9] W. Huang, S. Lederer, E. Taylor, and C. Kallin, Phys. Rev. B **91**, 094507 (2015).

[10] G. E. Volovik, Soviet Journal of Experimental and Theoretical Physics Letters **55**, 368 (1992).

[11] G. E. Volovik, *Soviet Physics - JETP (English Translation)*, **67**, 1804 (1988).

[12] J. Goryo and K. Ishikawa, Physics Letters A **246**, 549 (1998).

[13] M. Stone and R. Roy, Phys. Rev. B **69**, 184511 (2004).

[14] R. Roy and C. Kallin, Phys. Rev. B **77**, 174513 (2008).

[15] A. P. Mackenzie, T. Scaffidi, C. W. Hicks, and Y. Maeno, npj Quantum Materials **2**, 40 (2017).

[16] Z. Wu and G. M. Bruun, Phys. Rev. Lett. **117**, 245302 (2016).

[17] J. M. Midtgaard, Z. Wu, and G. M. Bruun, Phys. Rev. A **94**, 063631 (2016).

[18] J. M. Midtgaard, Z. Wu, and G. M. Bruun, Phys. Rev. A **96**, 033605 (2017).

[19] F. Schäfer, N. Mizukami, P. Yu, S. Koibuchi, A. Bouscal, and Y. Takahashi, Phys. Rev. A **98**, 051602 (2018).

[20] J. J. Kinnunen, Z. Wu, and G. M. Bruun, Phys. Rev. Lett. **121**, 253402 (2018).

[21] H. Bruus and K. Flensberg, *Many-body quantum theory in condensed matter physics* (Oxford University Press,, 2004).

Appendix A: The Topological Superconductor

In this appendix we sketch how to derive the BCS Hamiltonian from the action for a single-component Fermi gas. We then show how the Chern number can be extracted as the density-current correlation function. Lastly we show how the Chern number is also found in the current-current correlation function after integrating out the superfluid phase, in accordance with the continuity equation.

The Hamiltonian of the interacting fermion system (taken to be 2D), along with an external gauge field, is

$$\begin{aligned} H = &\int d^2r\psi^*(\mathbf{r})[\frac{1}{2m}(-i\nabla - \mathbf{A})^2 + A_0]\psi(\mathbf{r}) \\ &+\frac{1}{2}\iint d^2rd^2r'\psi^*(\mathbf{r})\psi^*(\mathbf{r}')V(\mathbf{r}-\mathbf{r}')\psi(\mathbf{r}')\psi(\mathbf{r}) \end{aligned} \tag{A1}$$

where $\psi(\mathbf{r})$ is the fermion field, $A = (A_0, \mathbf{A})$ is the gauge potential for unit charge. Using the path integral, the partition function can be written as

$$\begin{aligned} \mathcal{Z} &= \int \mathcal{D}(\psi^*\psi)e^{-\int_0^\beta d\tau \int d^2r\psi^*(\partial_\tau - \mu)\psi - H(\psi^*\psi, A)} \\ &= \int \mathcal{D}(\psi^*\psi)e^{-S(\psi^*,\psi,A)} \end{aligned} \tag{A2}$$

where τ is imaginary time. We now introduce pairing via the usual Hubbard-Stratonovich transformation, which yields

$$\mathcal{Z} = \iint \mathcal{D}(\psi^*\psi)\mathcal{D}(\Delta^*\Delta)e^{-S(\psi^*\psi,\Delta,\Delta^*,A)} \tag{A3}$$

with the action

$$\begin{aligned} S = &\int_0^\beta d\tau \int d^2r\psi^*(\mathbf{r},\tau)[\partial_\tau - \mu + \frac{(-i\nabla - \mathbf{A})^2}{2m} + A_0]\psi(\mathbf{r},\tau) \\ &- \frac{1}{2}\int_0^\beta d\tau \iint d^2\mathbf{r}d^2\mathbf{r}'[\Delta(\mathbf{r},\mathbf{r}',\tau)^*\Delta(\mathbf{r},\mathbf{r}',\tau)/V(\mathbf{r}-\mathbf{r}') \\ &+ \Delta(\mathbf{r},\mathbf{r}',\tau)\psi^*(\mathbf{r},\tau)\psi^*(\mathbf{r}',\tau) + \Delta^*(\mathbf{r},\mathbf{r}',\tau)\psi(\mathbf{r}',\tau)\psi(\mathbf{r},\tau)]. \end{aligned} \tag{A4}$$

Following the main text, we absorb the phase of the pairing order parameter into the gauge fields, e.g. $\mathbf{A} \to \tilde{\mathbf{A}}$. The effective action for the pairing and the gauge field can then be found while still remaining gauge invariant. Fourier transforming to momentum and frequency space, $\psi(z) = \sum_k e^{ikz}a_k$, where we use the shorthand notation $k = (\mathbf{k}, \omega_n)$ with $\omega_n = (2n+1)T$ a Matsubara frequency, and $kz = \mathbf{k}\cdot\mathbf{r} - \omega_n\tau$. Using this and a similar Fourier transform for the pairing field, and assuming a gauge field of the form $A(z) = A(q)e^{iqz}$ in Eq. (A4), we obtain after some straightforward algebra

$$S = \frac{1}{2}\sum_{k,k'}\begin{bmatrix} a^*_{k'} & a_{-k'} \end{bmatrix}\left[\mathcal{G}_0^{-1}(k',k) - \Sigma(k',k)\right]\begin{bmatrix} a_k \\ a^*_{-k} \end{bmatrix} - \frac{1}{2T}\sum_{kk'}\Delta^*_{k'}V^{-1}(\mathbf{k}'-\mathbf{k})\Delta_k$$

with

$$\mathcal{G}_0^{-1}(k',k) = \delta_{k',k}\begin{bmatrix} -i\omega_n + \xi_k & \Delta_k \\ \Delta^*_k & -i\omega_n - \xi_k \end{bmatrix} \tag{A5}$$

$$\Sigma(k',k) = \delta_{k+q,k}[\frac{1}{m}\tilde{\mathbf{A}}(q)\cdot(\mathbf{k}+\mathbf{q}/2) - \tilde{A}_0(q)\tau_3] + \delta_{k+2q,k}\frac{\tilde{\mathbf{A}}(q)^2}{2m}\tau_3 \tag{A6}$$

where τ_i are the Pauli spin matrices. Here, Δ_k is the solution to the mean-field BCS equations since its phase has been absorbed in the gauge fields. Also, we have omitted convergence factors in $\mathcal{G}_0^{-1}$, which can be important to get finite results for certain calculations [16]. We can now integrate over the fermions. This yields the effective action to second order in the self-energy Σ

$$\mathcal{Z} = \int \mathcal{D}(\Delta^*\Delta)e^{-S_{\text{eff}}} \tag{A7}$$

$$S_{\text{eff}} = S_{\text{BCS}} + \frac{1}{4}\text{Tr}\mathcal{G}_0\Sigma\mathcal{G}_0\Sigma \tag{A8}$$

where Tr denotes the Nambu trace and summation over k, and we have used that $\mathrm{Tr}\mathcal{G}_0\Sigma = 0$. S_{BCS} is given in the main text 12. We evaluate the non-BCS part of the effective action to second order in the gauge potential. We furthermore restrict ourselves to a single frequency component of the gauge field, i.e. $\tilde{A}(q) \neq 0$ and $\tilde{A}(-q) \neq 0$. A long calculation gives for the term involving the gauge potential

$$\begin{aligned}
\frac{1}{4}\mathrm{Tr}\mathcal{G}_0\Sigma\mathcal{G}_0\Sigma = &\frac{1}{2m^2}\sum_k (\tilde{\mathbf{A}}(q)\cdot\mathbf{k})(\tilde{\mathbf{A}}(q)\cdot\mathbf{k})\mathrm{tr}\left[\mathcal{G}_0(k-q/2)\mathcal{G}_0(k+q/2)\right] \\
&+\frac{1}{2}\sum_k \tilde{A}_0(q)\tilde{A}_0(-q)\mathrm{tr}\left[\mathcal{G}_0(k-q/2)\tau_3\mathcal{G}_0(k+q/2)\tau_3\right] \\
&-\frac{1}{2m}\sum_k \tilde{A}_0(q)\tilde{\mathbf{A}}(-q)\cdot\mathbf{k}\mathrm{tr}\left[\mathcal{G}_0(k-q/2)\tau_3\mathcal{G}_0(k+q/2)\right] \\
&-\frac{1}{2m}\sum_k \tilde{\mathbf{A}}(q)\cdot\mathbf{k}\tilde{A}_0(-q)\mathrm{tr}\left[\mathcal{G}_0(k-q/2)\mathcal{G}_0(k+q/2)\tau_3\right] \\
= &\frac{1}{2}\sum_k \Bigg[\tilde{\mathbf{A}}(q)\cdot\mathbf{k}\frac{g_1(k,q)}{m^2}\tilde{\mathbf{A}}(-q)\cdot\mathbf{k} + \tilde{A}_0(q)g_2(k,q)\tilde{A}_0(-q) \\
&-\tilde{A}_0(q)\frac{g_3(k,q)}{m}\tilde{\mathbf{A}}(-q)\cdot\mathbf{k} - \tilde{\mathbf{A}}(q)\cdot\mathbf{k}\frac{g_4(k,q)}{m}\tilde{A}_0(-q)\Bigg]. \qquad \text{(A9)}
\end{aligned}$$

Here, tr[...] on the right hand side means Nambu trace only and we have used that the mean-field solution obeys $\Delta_k = -\Delta_{-k}$ to eliminate certain terms. Before taking functional derivatives to obtain the correlation functions, we plug in the gauge transforms of the potentials, e.g. $\tilde{\mathbf{A}}(q) = \mathbf{A}(q) - i\mathbf{q}\Phi(q)/2$. Plugging this into Eq. (A9) and expanding out yields

$$\frac{1}{4}\mathrm{Tr}\mathcal{G}_0\Sigma\mathcal{G}_0\Sigma = S_{1L}(A) + \sum_q{}' \Phi(q)^* B(q)\Phi(q) + \sum_q{}' [C(q)^*\Phi(q) + \Phi(q)^* C(q)] \qquad \text{(A10)}$$

where we have used that $\Phi(-q) = \Phi(q)$ for a real phase, and $\sum_q'$ denotes sum over half to Fourier components of $\Phi(q)$ in order to avoid double counting, for instance $\sum_q' = \sum_{q,q_x>0}$. The term $S_{1L}(A)$ is given by Eq. (A9) with $\tilde{A}$ replaced by A and contains the one-loop contributions to the correlation functions. We have

$$B(q) = \frac{1}{8}\sum_k \left[(\mathbf{k}\cdot\mathbf{q})^2\frac{g_1(k,q)}{m^2} - \omega_\gamma^2 g_2(k,q) - i\mathbf{q}\cdot\mathbf{k}\frac{g_3(k,q)+g_4(k,q)}{m}\omega_\gamma\right] \qquad \text{(A11)}$$

$$\begin{aligned}
C(q)^* = &\frac{1}{4}\sum_k \Bigg[-i\mathbf{k}\cdot\mathbf{q}\frac{g_1(k,q)}{m^2}\mathbf{A}(-q)\cdot\mathbf{k} + \omega_\gamma g_2(k,q)A_0(-q) \\
&+ i\mathbf{k}\cdot\mathbf{q}\frac{g_4(k,q)}{m}A_0(-q) - \omega_\gamma\frac{g_3(k,q)}{m}\mathbf{A}(-q)\cdot\mathbf{k}\Bigg] \qquad \text{(A12)}
\end{aligned}$$

$$\begin{aligned}
C(q) = &\frac{1}{4}\sum_k \Bigg[i\mathbf{k}\cdot\mathbf{q}\frac{g_1(k,q)}{m^2}\mathbf{A}(q)\cdot\mathbf{k} - \omega_\gamma g_2(k,q)A_0(q) \\
&+ -i\mathbf{k}\cdot\mathbf{q}\frac{g_3(k,q)}{m}A_0(q) + \omega_\gamma\frac{g_4(k,q)}{m}\mathbf{A}(q)\cdot\mathbf{k}\Bigg]. \qquad \text{(A13)}
\end{aligned}$$

Using Eq. (A10), we can now easily integrate over the Fourier components of the phase of the order parameter. We obtain Eq. 19 in the main text

$$\mathcal{Z} \simeq \int \mathcal{D}(\Phi^*\Phi)e^{-S_{\mathrm{eff}}} \propto e^{-S_{\mathrm{BCS}} - S_{1\mathrm{L}}(A) + \sum_q' C(q)^* C(q)/B(q)} \qquad \text{(A14)}$$

Appendix B: Correlation Functions

It is now straightforward from Eq. (A14) to obtain the various correlation functions by taking suitable derivatives with respect to the gauge field. Focusing on the Fourier transform of the transverse current-current correlation

function $\chi_{j_x,j_y}(\mathbf{r}-\mathbf{r}',\tau-\tau') = -\langle T_\tau\{j_x(\mathbf{r},\tau); j_y(\mathbf{r}',\tau')\}\rangle$ where $\mathbf{j}$ is the current operator, we get

$$\chi_{j_x,j_y}(q) = -\frac{\delta^2 \ln \mathcal{Z}}{\delta A_x(q)\delta A_y(-q)} = \chi^{\rm BCS}_{j_x,j_y}(q) - \chi^{\rm fluc}_{j_x,j_y}(q) \tag{B1}$$

where

$$\chi^{\rm BCS}_{j_x,j_y}(q) = \sum_k \frac{k_x k_y}{2m^2} g_1(k,q) \tag{B2}$$

and

$$\chi^{\rm fluc}_{j_x,j_y}(q) = \frac{\frac{\delta C(q)}{\delta A_x(q)}\frac{\delta C(q)^*}{\delta A_y(-q)}}{B(q)} = -\frac{1}{2}\frac{\sum_k \left[i\mathbf{q}\cdot\mathbf{k}\frac{g_1(k,q)}{m^2}k_x + \omega_\gamma \frac{g_4(k,q)}{m}k_x\right]\sum_{k'}\left[i\mathbf{q}\cdot\mathbf{k}'\frac{g_1(k',q)}{m^2}k'_y + \omega_\gamma\frac{g_3(k',q)}{m}k_y\right]}{\sum_k\left[(\mathbf{k}\cdot\mathbf{q})^2\frac{g_1(k,q)}{m^2} - \omega_\gamma^2 g_2(k,q) - i\mathbf{q}\cdot\mathbf{k}\frac{g_3(k,q)+g_4(k,q)}{m}\omega_\gamma\right]} \tag{B3}$$

Here, $\chi^{\rm BCS}_{j_x,j_y}(q)$ is the BCS (1-loop) approximation to the current-current correlation function obtained by letting the functional derivatives act on $S_{1\rm L}(A)$. We can also find the density-current correlation function as

$$\chi_{j_x,n}(q) = \frac{\delta^2 \ln \mathcal{Z}}{\delta A_x(q)\delta A_0(-q)} = \chi^{\rm BCS}_{j_x,n}(q) + \chi^{\rm fluc}_{j_x,n}(q) \tag{B4}$$

where

$$\chi^{\rm BCS}_{j_x,n}(q) = -\sum_{\mathbf{k}} \frac{k_x}{2m} g_4(k,q) \tag{B5}$$

and

$$\chi^{\rm fluc}_{j_x,n}(q) = \frac{\frac{\delta C(q)}{\delta A_x(q)}\frac{\delta C(q)^*}{\delta A_0(-q)}}{B(q)} = \frac{1}{2}\frac{\sum_k \left[i\mathbf{q}\cdot\mathbf{k}\frac{g_1(k,q)}{m^2}k_x + \omega_\gamma \frac{g_4(k,q)}{m}k_x\right]\sum_{k'}\left[\omega_\gamma g_2(k',q) + i\mathbf{q}\cdot\mathbf{k}'\frac{g_4(k',q)}{m}\right]}{\sum_k\left[(\mathbf{k}\cdot\mathbf{q})^2\frac{g_1(k,q)}{m^2} - \omega_\gamma^2 g_2(k,q) - i\mathbf{q}\cdot\mathbf{k}\frac{g_3(k,q)+g_4(k,q)}{m}\omega_\gamma\right]} \tag{B6}$$

In the appropriate static limit, the topological contribution to the correlation functions is then found in $\chi^{\rm BCS}_{j_x,n}$ and $\chi^{\rm fluc}_{j_x,j_y}$, respectively. The remaining terms vanish in this limit.

Appendix C: Chern Number

As an example, we can calculate $\chi^{\rm BCS}_{j_x,n}$ to see how this encodes the Chern number. One way of doing it is by inserting the Green's function on the spectral form, see e.g. [21]

$$\mathcal{G}_0(\mathbf{k}, i\omega_n) = \int_{-\infty}^{\infty}\frac{d\omega}{(-\pi)}\frac{{\rm Im}\mathcal{G}_0(\mathbf{k},\omega)}{i\omega_n - \omega} \tag{C1}$$

where

$${\rm Im}\mathcal{G}_0(\mathbf{k},\omega) = -\frac{\pi}{2E_{\mathbf{k}}}\begin{pmatrix}\omega+\xi_{\mathbf{k}} & -\Delta_{\mathbf{k}}\\ -\Delta^*_{\mathbf{k}} & \omega-\xi_{\mathbf{k}}\end{pmatrix}[\delta(\omega-E_{\mathbf{k}}) - \delta(\omega+E_{\mathbf{k}})] \tag{C2}$$

Inserting this in the BCS part of the density-current correlation and performing the Matsubara sum, we get the limit

$$\chi^{\rm BCS}_{j_x,n}(\mathbf{q},0) = -\frac{1}{\mathcal{V}}\sum_{\mathbf{k}}\frac{k_x}{2m}\frac{\Delta^*_{\mathbf{k}+\mathbf{q}/2}\Delta_{\mathbf{k}-\mathbf{q}/2} - \Delta_{\mathbf{k}+\mathbf{q}/2}\Delta^*_{\mathbf{k}-\mathbf{q}/2}}{E_{\mathbf{k}+\mathbf{q}/2}E_{\mathbf{k}-\mathbf{q}/2}} \times \frac{1}{E_{\mathbf{k}+\mathbf{q}/2}+E_{\mathbf{k}-\mathbf{q}/2}} \tag{C3}$$

For small $\mathbf{q}$, the summand vanishes, so to first order we have

$$\chi^{\rm BCS}_{j_x,n}(\mathbf{q},0) = -\frac{iq_x}{\mathcal{V}}\sum_{\mathbf{k}}\frac{k_x}{2m}\frac{{\rm Im}\Delta_{\mathbf{k}}\partial_{k_x}\Delta^*_{\mathbf{k}}}{E^3_{\mathbf{k}}} - \frac{iq_y}{2\mathcal{V}}\sum_{\mathbf{k}}\frac{k_x}{2m}\frac{{\rm Im}\Delta_{\mathbf{k}}\partial_{k_y}\Delta^*_{\mathbf{k}}}{E^3_{\mathbf{k}}} \tag{C4}$$

The first of these terms vanish, since the summand is odd in k_y. This can be seen if we fix the phase of the gap function and look at, for instance, the simple example $\Delta_{\mathbf{k}} = k_x + ik_y$. With this, it is clear that

$$\lim_{\mathbf{q}\to 0}\frac{\chi^{\rm BCS}_{j_x,n}(\mathbf{q},0)}{iq_y} = \int\frac{d^2\mathbf{k}}{8\pi^2}\frac{k_x}{m}\frac{{\rm Im}[\Delta^*_{\mathbf{k}}\partial_{k_y}\Delta_{\mathbf{k}}]}{E^3_{\mathbf{k}}}. \tag{C5}$$

Appendix D: Calculation of the superfluid transition temperature

In this appendix, we outline the calculation of the superfluid transition temperature for the 2D ^{173}Yb gas immersed in a 3D ^{7}Li gas. First, we solve the following frequency-dependent gap equation at a finite temperature T

$$\Delta(\mathbf{p}, i\omega_n) = -T\sum_m \int \frac{d\mathbf{q}}{(2\pi)^2} V_{\rm ind}(\mathbf{p}-\mathbf{q}, i\omega_n - i\omega_m) \times \frac{\Delta(\mathbf{q}, i\omega_m)}{\omega_m^2 + \mathcal{E}^2(\mathbf{q}, i\omega_m)} \tag{D1}$$

where $\mathcal{E}(\mathbf{q}, i\omega_m) = \sqrt{\xi_{\mathbf{q}}^2 + |\Delta(\mathbf{q}, i\omega_m)|^2}$. Here the frequency-dependent induced interaction $V_{\rm ind}(\mathbf{q}, i\omega_\nu)$ is given by

$$V_{\rm ind}(\mathbf{q}, i\omega_\nu) = -n_B m_B g^2 \left[\left(\frac{1}{\kappa_+} + \frac{1}{\kappa_-} \right) + \frac{1}{\sqrt{1-(\omega_\nu/g_B n_B)^2}} \left(\frac{1}{\kappa_+} - \frac{1}{\kappa_-} \right) \right], \tag{D2}$$

where $\kappa_\pm = \sqrt{2m_B g_B n_B \left[1 \pm \sqrt{1-(\omega_\nu/g_B n_B)^2}\right] + \mathbf{q}^2}$.

Since the Fermi system is 2D, the superfluid transition is described by the BKT theory, where the critical temperature $T_{\rm BKT}$ is determined by the famous Kosterlitz-Thouless condition

$$T_{\rm BKT} = \frac{\pi}{8m_F^2} \rho_s \left(\{\Delta(i\omega_n)\}, T_{\rm BKT} \right). \tag{D3}$$

Here ρ_s is the superfluid mass density and is a function of the gap parameters and the temperature. Neglecting the renormalisation of the vortex pairs, ρ_s can be estimated as

$$\rho_s = \rho_0 + \frac{T}{2}\sum_n \int \frac{d\mathbf{p}}{(2\pi)^2} p^2 \frac{\mathcal{E}^2(\mathbf{p}, i\omega_n) - \omega_n^2}{\left[\omega_n^2 + \mathcal{E}^2(\mathbf{p}, i\omega_n)\right]^2}, \tag{D4}$$

where $\rho_0 = m_F n_F$. Solving Eq. (D3) self-consistently using Eqs. (D4) and the frequency-dependent gap parameters obtained from Eq. (D1), we obtain the superfluid transition temperatures shown in the main text.

— 5 —

FFLO Superconductivity in a Bilayer System

The bilayer system considered in chapter 3 is not only suitable for exploring topological superconductivity. This chapter presents a paper where we use the Bose-Fermi mixture to study the topologically trivial, but still exotic, Fulde-Ferrel-Larkin-Ovchinnikov (FFLO)-type superconductivity. I will start by giving a brief introduction to this type of superconductivity before presenting the context and results of the paper. Vast amounts of literature has been written about this superconducting phase, and it would be impossible to cover all of it here. For a good review as it pertains to cold atomic gases, see [60].

5.1 FFLO Superconductivity

In most cases, a superconducting state is composed of Cooper pairs containing fermions of opposite momenta, $\mathbf{k}$ and $-\mathbf{k}$. As discussed before, Cooper pairs with non-zero center-of-mass momentum are usually not energetically favorable. This is true regardless of the pairing symmetry, s-wave or p-wave or higher orders. We only consider s-wave pairing in the following, however, but interesting work has been done concerning the interplay of the FFLO state and higher order pairing [61], where topological order might also be seen.

Consider a superfluid electron gas with s-wave pairing between its two spin components. Introducing a weak magnetic (Zeeman) field does not change the ground state substantially, but, as argued by Fulde and Ferrel [62], is is quite simple to establish two critical values of the field strength, h, where we expect things to happen. In the case of contact interactions where the pairing Δ is merely a constant, at a field strength $h_{c2} = \Delta$, the cost of breaking a Cooper pair is exactly equal to the energy gained by flipping the spin of one of the electrons. So for field strengths above this limit, there is certainly no superconductivity.

But if we consider the free energy, the paramagnetic exchange energy of the normal state will be greater than the condensation energy of the superconducting state at a field strength $h_{c1} = \Delta/\sqrt{2} \approx 0.7\Delta$. This is also known as the Chandrasekhar-Clogston limit or the Pauli limiting field. Note that we have neglected orbital effects of the magnetic field. In the following paper, the bilayer system mimics the paramagnetic effects of a magnetic field but not the orbital effects.

The ground state for intermediate field strengths, $h_{c1} < h < h_{c2}$, is called the Fulde-Ferrel-Larkin-Ovchinnikov (FFLO) state. To see the structure of this state, consider that the BCS ground state has a vanishing spin susceptibility at $T = 0$, so as long as this state survives, no spins are flipped. But if we consider how the normal state would look for an intermediate field strength, a density imbalance to the favored spin polarization occurs as soon as the field is turned on. This leads to different Fermi surfaces for the two spin components as seen in Fig. 5.1.

We can still have Cooper pairing between the two Fermi surfaces, but each Cooper pair must have a finite center-of-mass (COM) momentum, $(\mathbf{k}+\mathbf{Q}/2)+(-\mathbf{k}+\mathbf{Q}/2) = \mathbf{Q}$. The pairing energy opens up for the possibility of sustaining this type of superconductivity for higher field strengths than the BCS-type superconductivity. The energy cost of the COM momentum quickly grows larger than the pairing energy gained, however. For a 3-dimensional electron gas, for instance, the normal state has lower free energy than the FFLO state above $h \approx 0.75\Delta$. This only leaves a tiny sliver in the phase diagram for the FFLO state, and is the reason why most experimental searches focus on lower-dimensional systems, which are thought to stabilize this phase.

A pairing with non-zero $\mathbf{Q}$ gives a modulation of the pairing in real space, since

$$\Delta_{\mathbf{Q}}(\mathbf{R}) = \Delta e^{i\mathbf{Q}\cdot\mathbf{R}} \tag{5.1}$$

where $\mathbf{R} = (\mathbf{r}_1 + \mathbf{r}_2)/2$ is the center-of-mass position and we take the pairing Δ to be a constant. Depending on the symmetry of the system, many choices of $\mathbf{Q}$-vectors can be equivalent. With full rotational symmetry, all $\mathbf{Q}$-vectors of appropriate length are equivalent, so this symmetry will be spontaneously broken to pick a specific vector. This should remind us of the BKT melting mechanism considered in chapter 2, as it indeed is the correct way to capture the break-up of the FFLO phase at higher temperatures in 2 dimensions. In the paper, we go beyond mean-field theory to calculate the BKT critical temperature, but we do not include fluctuations in $\mathbf{Q}$ in the calculation of the phase diagram. It was shown in [63] that these fluctuations in a 3D Fermi gas do not change the phase diagram significantly.

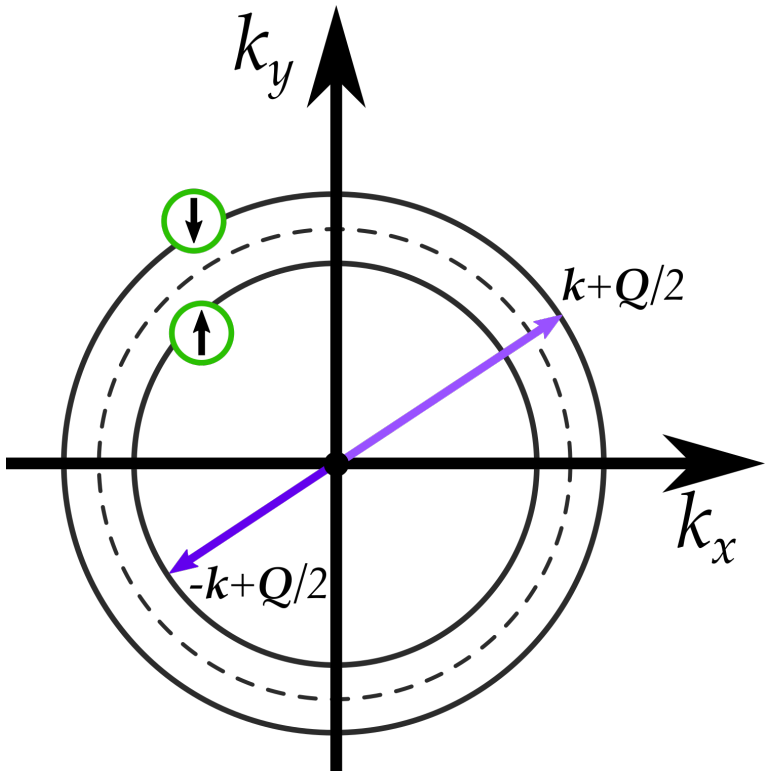

Figure 5.1: Due to a density imbalance, the Fermi surfaces for the two spin components are different. It is thus possible to form Cooper pairs with finite center-of-mass momentum **Q**. Starting out with rotational symmetry as in the illustration, the symmetry is broken to pick a specific **Q**.

The full FFLO state can contain a linear combination of the pairings in Eq. 5.1, for different **Q**'s. Which configurations are energetically most favorable is very dependent on the specifics of the system, however. In 2-dimensional systems, it seems that sums of 3, 4, or 6 different **Q**'s are typically favored [64]. Luckily for our case, we are mostly interested in the upper field limit, h_{c2}, where all configurations are degenerate[64, 65]. This allows us to just consider pairing with a single **Q**-component, sometimes referred to as a plane-wave Fulde-Ferrel state.

5.2 Motivation

By modifying the bilayer system considered in Chapter 3 slightly, we have a great system for realising FFLO superconductivity. As we want to consider the competition between the normal, metallic state, the 'standard' BCS,

s-wave superconductivity and the FFLO state, we keep the layer distance small in our simulations. This ensures that the intralayer p-wave pairing is not in play. We can then impose a difference in chemical potential, $\mu_{\uparrow/\downarrow}$, and consequently a density imbalance, between the layers to emulate the effect of a magnetic field. At some lower value of the imbalance $h = \mu_\uparrow - \mu_\downarrow$, the BCS superfluid gives way to the FFLO state, and at some upper value of the imbalance, the normal state becomes the true ground state.

So far, the experimental search for the FFLO state has returned intriguing evidence of a transition to an exotic superconducting state, close to the upper critical field in a number of materials. Most notably, the heavy-fermion superconductor $CeCoIn_5$ [66, 67] and the organic superconductor $\kappa - (BEDT\text{-}TTF)_2Cu(NCS)_2$ [68, 69] has provided evidence for the existence of an FFLO state through measurements of the specific heat close to the transition, and NMR studies of the state.

A direct detection of the state is difficult, since normally the FFLO state is expected to exist only in a very narrow parameter range. See, for instance, Fig. 2 in [70] for an example of the phase diagram for a 2D electron gas. The same figure shows the effect of spin-orbit-coupling the fermions, which also dramatically increases the region favoring the FFLO state. Spin-orbit-coupling exploits a further mechanism for forcing a center-of-mass momentum on the Cooper pairs, which is a deformation of the Fermi surface.

It is known that long-range interactions stabilize FFLO superconductivity compared to contact interactions. A bilayer system of dipolar fermions has been studied previously [71], where the correct choice of layer distance was shown to favor the FFLO state. However, the Bose-Fermi mixture is even more promising due the the ability to tune the long-range part of the interaction, in addition to the layer distance.

5.3 Results

The gap equations for the superfluid state are found via the Gor'kov formalism and solved self-consistently. This has to be done for each choice of COM momentum, $\mathbf{Q}$, to find the one that minimizes the energy. While the optimal choice approximately follows Ginzburg-Landau theory

$$Q = \frac{2mh}{k_F}\sqrt{1 - T/T_C} \tag{5.2}$$

the energy differences between the FFLO state and the normal state at the upper field limit are so small that a numerical minimization is needed. The simulations were performed on the `Grendel` cluster at the Centre for Scientific Computing, Aarhus.

The bilayer Bose-Fermi mixture turns out to be advantageous to FFLO superconductivity for several reasons. At $T = 0$, the ability to increase the interaction range greatly increases the range of chemical potential imbalances where the FFLO state survives as the ground state. We do not see a significant change in the lower limit, but the upper limit to the imbalance can be increased by at least 50% while staying within experimentally reasonable parameters. This result improves quite a bit on previous results for dipolar gasses in [71]. It should be noted that our analysis only considered a single $\mathbf{Q}$-component, which has a higher ground state energy than other FFLO states in most conditions [60]. While the energy differences between the different $\mathbf{Q}$-configurations are small, the single-component ansatz might explain why we saw no substantial change of the lower field limit when the range of the interaction was increased.

This stabilizing of the FFLO state seems to require the bilayer topology, however. With the induced Yukawa interaction, the effect was greatest on two spatially separated populations of fermions. We tested to see whether the upper field limit would also increase for a single layer of a two-component fermion gas (that is, a layer distance of zero), and the effect was much less substantial. In this way, the bilayer structure of the fermion system is also crucial, not only the tunability of the interaction range. It could be seen as a simple application of geometry: when the two layers are separated, the close-range interactions are suppressed much more than the long-range interactions.

The critical temperature of the FFLO state was calculated as a BKT melting temperature, similar to what was done previously for the p-wave superconductors. In this case, the analog to the XY-model's rotors was not a global phase of the order parameter, but the center-of-mass momentum $\mathbf{Q}$. In this case we have to consider both parallel, as well as perpendicular perturbations of the vector, where before we discarded the parallel contribution. The FFLO state is gapless, and this ends up being detrimental to the critical temperature of the state. Even though it takes up a larger part of the phase diagram in the bilayer system, the region rapidly shrinks for larger temperatures. We can achieve critical temperatures up to the order of $0.02T_F$, which is unfortunately still about an order of magnitude lower than current limits for Bose-Fermi mixtures [43].

5.4 Contribution

I initiated this project and held the main responsibility for writing the paper. All numerical calculations and all figures were made by me.

Stabilizing Fulde-Ferrell-Larkin-Ovchinnikov superfluidity with long-range interactions in a mixed-dimensional Bose-Fermi system

Jonatan Melkær Midtgaard and Georg M. Bruun
Department of Physics and Astronomy, Aarhus University, DK-8000 Aarhus C, Denmark

(Received 29 May 2018; published 24 July 2018)

We analyze the stability of inhomogeneous superfluid phases in a system consisting of identical fermions confined in two layers that are immersed in a Bose-Einstein condensate (BEC). The fermions in the two layers interact via an induced interaction mediated by the BEC, which gives rise to pairing. We present zero-temperature phase diagrams varying the chemical potential difference between the two layers and the range of the induced interaction, and show that there is a large region where an inhomogeneous superfluid phase is the ground state. This region grows with increasing range of the induced interaction and it can be much larger than for a corresponding system with a short-range interaction. The range of the interaction is controlled by the healing length of the BEC, which makes the present system a powerful tunable platform to stabilize inhomogeneous superfluid phases. We furthermore analyze the melting of the superfluid phases in the layers via phase fluctuations as described by the Berezinskii-Kosterlitz-Thouless mechanism and show that the normal, homogeneous, and inhomogeneous superfluid phases meet in a tricritical point. The superfluid density of the inhomogeneous superfluid phase is reduced by inherent gapless excitations, and we demonstrate that this leads to a significant suppression of the critical temperature as compared to the homogeneous superfluid phase.

DOI: 10.1103/PhysRevA.98.013624

I. INTRODUCTION

The interplay between population imbalance and superfluid pairing has been subjected to intense study ever since Fulde and Ferrell (FF) as well as Larkin and Ovchinnikov (LO) predicted that they can coexist [1,2]. In condensed matter systems, an external magnetic field leads to a population imbalance between the two electron spin projections, which in general is at odds with superconductivity. FFLO however realized that the superconductor can accommodate some population imbalance at the price of giving the Cooper pairs a nonzero center-of-mass (COM) momentum, thereby forming a spatially inhomogeneous but periodic order parameter with no vortices. The fate of superfluid pairing in the presence of population imbalance is a fundamental question relevant for many systems in nature including cold atoms [3–5], superconductors [6], and quark matter [7–9]. Nevertheless, an unambiguous observation of a FFLO phase is still lacking. A major problem for electronic superconductors is that orbital effects due to the magnetic field lead to the formation of vortices and eventually destroy pairing before any FFLO physics can be observed. One strategy to avoid this problem is to explore low-dimensional systems, where orbital effects are suppressed due to the confinement. Indeed, results consistent with a FFLO phase have been reported for quasi-two-dimensional (quasi-2D) organic and heavy fermion superconductors [10–12]. Theoretical studies have furthermore concluded that the FFLO phase is favored in 2D as compared to 3D [13–15].

Quantum degenerate atomic gases are well suited to investigate FFLO physics, because they do not suffer from orbital effects as the atoms are neutral. In addition, it is relatively straightforward to make low-dimensional systems, and signatures of FFLO physics have indeed been observed in a one-dimensional (1D) atomic Fermi gas [16]. There have been a number of investigations of the FFLO phase for 2D atomic gases with a short-range interaction [17–23]. Recently, it was argued that long-range interactions further increase the region of stability of the FFLO phase for a 2D gas of dipolar atoms as compared to a short-range interaction [24,25].

Here, we investigate how to stabilize FFLO superfluidity using a mixed-dimensional system with a tuneable-range interaction. The system consists of fermions confined in two layers immersed in a BEC. The induced interaction between the layers mediated by the BEC gives rise to pairing, and we analyze the stability of the corresponding superfluid phases. We show that the zero-temperature phase diagram as a function of the chemical potential difference in the two layers and the range of the interaction has a large region where an inhomogeneous superfluid phase is the ground state. This region grows with increasing range of the interaction and becomes much wider than for a zero-range interaction. The interaction range can be tuned by varying the healing length of the BEC. We furthermore investigate the melting of the 2D superfluid phases via the Berezinskii-Kosterlitz-Thouless mechanism. The normal phase and the homogeneous and inhomogeneous superfluid phases are shown to meet in a tricritical point in the phase diagram, which determines the maximum critical temperature of the inhomogeneous superfluid. This maximum temperature is, however, significantly suppressed compared to the homogeneous superfluid phase, due to inherent gapless excitations, which decrease the superfluid density.

II. THE BILAYER SYSTEM

We consider the system illustrated in Fig. 1. Two layers contain fermions of a single species with mass m, and they are immersed in a 3D weakly interacting BEC consisting of bosons

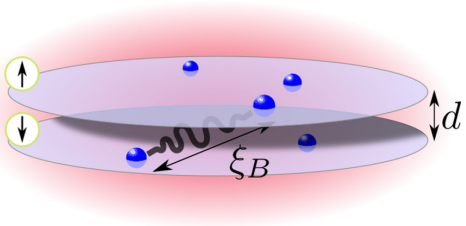

FIG. 1. A sketch of the considered system. The fermions (blue) are confined in two layers immersed in a three-dimensional BEC (red), with a layer distance d. The BEC mediates an interaction between fermions in the two different layers of the Yukawa form, with a range determined by the BEC healing length ξ_B.

with mass m_B and density n_B. The distance between the layers is d and the surface density of fermions in each layer is n_σ with $\sigma = \uparrow, \downarrow$ denoting the two layers. When used in equations, they are taken to mean $\uparrow = +1$, $\downarrow = -1$, respectively. Occasionally we will also use the notation $\bar{\sigma}$ to mean the opposite layer from σ. The boson-fermion interaction is short range and characterized by the strength $g = 2\pi a_{\rm eff}/\sqrt{m_r m_B}$, with $m_r = mm_B/(m + m_B)$ the reduced mass and $a_{\rm eff}$ the effective 2D-3D scattering length [26]. Throughout, this interaction strength is taken to be weak in the sense $k_{F\sigma} a_{\rm eff} \ll 1$, where $k_{F\sigma} = \sqrt{4\pi n_\sigma}$ is the Fermi momentum of layer σ.

We treat the BEC using zero-temperature Bogoliubov theory. This is a good approximation since the critical temperature of the superfluid phases of the fermions is much smaller than the critical temperature of the BEC. The bosonic degrees of freedom can then be integrated out, which yields an effective interaction between the fermions. In the static limit, this interaction is on the Yukawa form, and we end up with an effective Hamiltonian for the fermions in the two layers of the form [27–29]

$$H = H_{\rm kin} + H_{\rm int} = \sum_{\mathbf{k},\sigma} \xi_{\mathbf{k}\sigma} c^\dagger_{\mathbf{k}\sigma} c_{\mathbf{k}\sigma} + \frac{1}{2\mathcal{V}} \sum_{\sigma,\sigma'} \sum_{\mathbf{k},\mathbf{k}',\mathbf{q}} V_{\sigma\sigma'}(\mathbf{q}) c^\dagger_{\mathbf{k}+\mathbf{q}\sigma} c^\dagger_{\mathbf{k}'-\mathbf{q}\sigma'} c_{\mathbf{k}'\sigma'} c_{\mathbf{k}\sigma}. \quad (1)$$

Here, $c^\dagger_{\mathbf{k}\sigma}$ creates a fermion in layer σ with 2D momentum $\mathbf{k} = (k_x, k_y)$, the dispersion in each layer is $\xi_{\mathbf{k}\sigma} = k^2/2m - \mu_\sigma$ with μ_σ the chemical potentials, and $\mathcal{V}$ is the system volume. We define the average chemical potential $\mu = (\mu_\uparrow + \mu_\downarrow)/2$ and the "magnetic field" $h = (\mu_\downarrow - \mu_\uparrow)/2$, so that we can write $\xi_{\mathbf{k}\sigma} = k^2/2m - \mu + \sigma h$. The Yukawa interaction is

$$V_{\sigma\sigma'}(\mathbf{q}) = -\frac{2g^2 n_B m_B}{\sqrt{q^2 + 2/\xi_B^2}} e^{-\sqrt{q^2+2/\xi_B^2}|\sigma-\sigma'|d/2}, \quad (2)$$

where $\xi_B = 1/\sqrt{8\pi n_B a_B}$ is the healing length of the BEC with a_B the boson-boson scattering length. The healing length determines the range of the induced interaction, as can be seen by Fourier transforming Eq. (2) to real space, giving $V(r) = -g^2 n_B m_B \pi^{-1} \exp(-\sqrt{2} r/\xi_B)/r$ with r the 3D distance between the fermions. It follows that the range of the interaction can be tuned by varying the density n_B or the scattering length a_B of the surrounding BEC, which turns out to be a key property for the following. We note that retardation effects can be neglected when the speed of sound in the BEC is much larger than the Fermi velocity in the two planes [28].

III. PAIRING AND GREEN'S FUNCTIONS

The attractive interaction given by Eq. (2) can lead to Cooper pairing within each layer (intralayer pairing), and between the two layers (interlayer pairing). We recently analyzed the competition between intra- and interlayer pairing for the case of equal density in each layer, i.e., for $n_\uparrow = n_\downarrow$ [29]. For a layer distance d large compared to the range ξ_B of the interaction, we found that the ground state is characterized by intralayer p-wave pairing, whereas s-wave interlayer pairing is stable for smaller d/ξ_B. In addition, we identified a crossover phase for intermediate d/ξ_B where both types of pairing coexist.

In this paper, we focus on interlayer s-wave pairing corresponding to $d/\xi_B \lesssim 1$. We shall investigate the case of a nonzero field h giving rise to a population difference between the two layers, and the possibility of FFLO interlayer pairing with nonzero COM momentum. Such interlayer pairing with COM momentum $\mathbf{Q}$ is characterized by the anomalous averages $\langle c_{\mathbf{Q}/2+\mathbf{k}\sigma} c_{\mathbf{Q}/2-\mathbf{k},\bar{\sigma}} \rangle$, which leads us to define the corresponding pairing field

$$\Delta_{\sigma\bar{\sigma}}(\mathbf{k}, \mathbf{Q}) = \frac{1}{\mathcal{V}} \sum_{\mathbf{k}'} V(\mathbf{k} - \mathbf{k}') \langle c_{\mathbf{Q}/2+\mathbf{k}'\sigma} c_{\mathbf{Q}/2-\mathbf{k}',\bar{\sigma}} \rangle. \quad (3)$$

We have dropped the subscripts on the induced interaction $V(\mathbf{q})$, as here and in the following it refers to the interlayer interaction only, i.e., $V(\mathbf{q}) \equiv V_{\sigma\bar{\sigma}}(\mathbf{q})$. The pairing field obeys the Fermi antisymmetry $\Delta_{\sigma\bar{\sigma}}(\mathbf{k}, \mathbf{Q}) = -\Delta_{\bar{\sigma}\sigma}(-\mathbf{k}, \mathbf{Q})$. In real space, it is of the form

$$\Delta_{\sigma\bar{\sigma}}(\mathbf{r}_1, \mathbf{r}_2) = V(\mathbf{r}_1 - \mathbf{r}_2) \langle \psi_\sigma(\mathbf{r}_1) \psi_{\bar{\sigma}}(\mathbf{r}_2) \rangle = \frac{1}{\mathcal{V}} \sum_{\mathbf{Q},\mathbf{k}} \Delta_{\sigma\bar{\sigma}}(\mathbf{k}, \mathbf{Q}) e^{i\mathbf{Q}\cdot\mathbf{R}} e^{i\mathbf{k}\cdot\mathbf{r}}, \quad (4)$$

where $\mathbf{R} = (\mathbf{r}_1 + \mathbf{r}_2)/2$ and $\mathbf{r} = \mathbf{r}_1 - \mathbf{r}_2$ are the COM and relative coordinates respectively, and $\psi_\sigma(\mathbf{r}) = \sum_{\mathbf{k}} c_{\mathbf{k}\sigma} \exp(\mathbf{k}\cdot\mathbf{r})$ is the field operator for particles in layer σ. We note that the pairing field is not translationally symmetric in the FFLO phase, i.e., $\Delta_{\sigma\bar{\sigma}}(\mathbf{r}_1, \mathbf{r}_2) \neq \Delta_{\sigma\bar{\sigma}}(\mathbf{r}_1 - \mathbf{r}_2)$. The interaction becomes in the mean-field BCS approximation

$$H^{\rm MF}_{\rm int} = \sum_{\mathbf{Q},\mathbf{k}} \Delta_{\uparrow\downarrow}(\mathbf{k}, \mathbf{Q}) c^\dagger_{\mathbf{Q}/2-\mathbf{k}\downarrow} c^\dagger_{\mathbf{Q}/2+\mathbf{k}\uparrow} + \text{H.c.}, \quad (5)$$

where we include only the pairing channel as we focus on the superfluid instability. The Hartree-Fock terms will in general lead to small effects in the weak coupling regime, which mostly can be accounted for by a renormalization of the chemical potentials μ_σ.

All results presented here can be obtained by a direct diagonalization of the mean-field BCS Hamiltonian $H^{\rm MF} = H_0 + H^{\rm MF}_{\rm int}$ using a standard Bogoliubov transformation. We, however, use Green's functions to analyze the FFLO states, since this formalism naturally allows us to go beyond mean-field theory to include effects such as retardation, if needed in the future. The normal and anomalous Green's functions for

the superfluid phases are defined in the standard way as

$$\begin{aligned} G_\sigma(\mathbf{k},\mathbf{k}',\tau) &= -\langle T_\tau c_{\mathbf{k}\sigma}(\tau) c^\dagger_{\mathbf{k}'\sigma}(0)\rangle, \\ F_\sigma(\mathbf{k},\mathbf{k}',\tau) &= -\langle T_\tau c_{\mathbf{k}\sigma}(\tau) c_{-\mathbf{k}',\bar\sigma}(0)\rangle, \\ F^\dagger_\sigma(\mathbf{k},\mathbf{k}',\tau) &= -\langle T_\tau c^\dagger_{-\mathbf{k},\sigma}(\tau) c^\dagger_{\mathbf{k}'\bar\sigma}(0)\rangle, \end{aligned} \tag{6}$$

where T_τ denotes imaginary-time ordering. Using $H^{\rm MF} = H_{\rm kin} + H^{\rm MF}_{\rm int}$, the Gor'kov equations for these Green's functions are straightforwardly derived. They read

$$\begin{aligned} &(i\omega_n - \xi_{\mathbf{k}\sigma}) G_\sigma(\mathbf{k},\mathbf{k}',\omega_n) \\ &\quad = \delta_{\mathbf{k},\mathbf{k}'} - \sum_{\mathbf{Q}} \Delta_{\sigma\bar\sigma}(\mathbf{k}-\mathbf{Q}/2,\mathbf{Q}) F^\dagger_{\bar\sigma}(\mathbf{k}-\mathbf{Q},\mathbf{k}',i\omega_n), \end{aligned} \tag{7}$$

$$\begin{aligned} &(i\omega_n - \xi_{\mathbf{k}\sigma}) F_\sigma(\mathbf{k},\mathbf{k}',\omega_n) \\ &\quad = \sum_{\mathbf{Q}} \Delta_{\sigma\bar\sigma}(\mathbf{k}-\mathbf{Q}/2,\mathbf{Q}) G_\sigma(-\mathbf{k}',-\mathbf{k}+\mathbf{Q},-i\omega_n), \end{aligned} \tag{8}$$

$$\begin{aligned} &(i\omega_n + \xi_{-\mathbf{k},\sigma}) F^\dagger_\sigma(\mathbf{k},\mathbf{k}',\omega_n) \\ &\quad = \sum_{\mathbf{Q}} \Delta^*_{\sigma\bar\sigma}(-\mathbf{k}-\mathbf{Q}/2,\mathbf{Q}) G_{\bar\sigma}(\mathbf{k}+\mathbf{Q},\mathbf{k}',i\omega_n), \end{aligned} \tag{9}$$

where we have Fourier transformed to Matsubara frequency space with $\omega_n = (2n+1)\pi T$. The self-consistent gap equation is then from (3) and (6)

$$\begin{aligned} \Delta_{\sigma\bar\sigma}(\mathbf{k},\mathbf{Q}) = -\frac{T}{\mathcal{V}} \sum_{\mathbf{k}',n} V(\mathbf{k}-\mathbf{k}') \\ \times F_\sigma(\mathbf{Q}/2+\mathbf{k}'/2, \mathbf{k}'-\mathbf{Q}/2, i\omega_n) e^{-i\omega_n 0_+}. \end{aligned} \tag{10}$$

IV. FULDE-FERREL SUPERCONDUCTIVITY

The $\mathbf{Q}$ values for which $\Delta_{\sigma\bar\sigma}(\mathbf{k},\mathbf{Q})$ is nonzero determine the structure of the order parameter in the superfluid phase. It has been shown that $\Delta_{\sigma\bar\sigma}(\mathbf{r}_1,\mathbf{r}_2)$ can form very complicated 2D structures corresponding to $\Delta_{\sigma\bar\sigma}(\mathbf{k},\mathbf{Q}) \neq 0$ for many $\mathbf{Q}$'s in Eq. (4) [30,31]. However, the FFLO phase exhibits a second-order transition to the normal phase in 2D at an upper critical field h_{c2} [13,14], and at this transition it is sufficient to consider the case of $\Delta_{\sigma\bar\sigma}(\mathbf{k},\mathbf{Q}) \neq 0$ only for a single $\mathbf{Q}$ vector. The reason is that any linear combination of the $\Delta_{\sigma\bar\sigma}(\mathbf{k},\mathbf{Q})$'s, which are unstable towards pairing, is degenerate at h_{c2}, since it is only the nonlinear part of the gap equation that determines the optimal combination that minimizes the energy.

In the following, we therefore consider the case $\Delta_{\sigma\bar\sigma}(\mathbf{k},\mathbf{Q}) \neq 0$ only for a single $\mathbf{Q}$. This will give the correct upper critical field h_{c2} for the second-order transition between the FFLO and the normal phase. We also expect that it will give a fairly precise value for the lower critical field h_{c1} determining the first-order transition between the FFLO and the superfluid phase, since the energy difference between the FFLO phases with various spatial structures is small [30,31]. Our scheme recovers the usual homogenous BCS pairing for $\mathbf{Q} = 0$, and it corresponds to a plane wave Fulde-Ferrel (FF) type of pairing when $\mathbf{Q} \neq 0$, as can be seen from Eq. (4). Since we only have one $\mathbf{Q}$ vector, we can simplify the notation for the gap as $\Delta_{\sigma\bar\sigma}(\mathbf{k},\mathbf{Q}) \to \Delta_{\sigma\bar\sigma}(\mathbf{k})$. The Gor'kov equations (7)–(9) are then easily solved, giving

$$\begin{aligned} G_\sigma(\mathbf{k},\mathbf{k}' i\omega_n) &= \delta_{\mathbf{k},\mathbf{k}'} \left(i\omega_n - \xi_{\mathbf{k},\sigma} - \frac{|\Delta_{\sigma\bar\sigma}(\mathbf{k}-\mathbf{Q}/2)|^2}{i\omega_n + \xi_{-\mathbf{k}+\mathbf{Q},\bar\sigma}} \right)^{-1}, \\ F_\sigma(\mathbf{k},\mathbf{k}',i\omega_n) &= \frac{\Delta_{\sigma\bar\sigma}(\mathbf{k}-\mathbf{Q}/2)}{i\omega_n - \xi_{\mathbf{k}\sigma}} G_\sigma(\mathbf{k},\mathbf{k}' i\omega_n). \end{aligned} \tag{11}$$

Using Eq. (11) in Eq. (10), we obtain the gap equation

$$\Delta(\mathbf{k}) = -\int d^2\check{k}' V(\mathbf{k}-\mathbf{k}') \frac{\Delta(\mathbf{k}')}{2E_{\mathbf{k}'}} [1 - f^+_{\mathbf{k}'} - f^-_{\mathbf{k}'}], \tag{12}$$

where $E^\pm_{\mathbf{k}'} = E_{\mathbf{k}'} \pm (h + \frac{\mathbf{k}'\cdot\mathbf{Q}}{2m})$, with $E_{\mathbf{k}'} = [(\mathbf{k}'^2/2m + \mathbf{Q}^2/8m - \mu)^2 + |\Delta(\mathbf{k}')|^2]^{1/2}$, and the Fermi distribution function is $f^\pm_{\mathbf{k}} = [\exp(\beta E^\pm_{\mathbf{k}}) + 1]^{-1}$. In Eq. (12) and the rest of this paper, we have further simplified the notation by defining $\Delta_{\uparrow\downarrow}(\mathbf{k}) \to \Delta(\mathbf{k})$ and $d^2\check{k}' = d^2k'/(2\pi)^2$. We solve Eq. (12) along with the number equation

$$N = \sum_{\mathbf{k}} \left[1 - \frac{\xi_{\mathbf{k}} + q^2/8m}{E_{\mathbf{k}}} \left(1 - f^+_{\mathbf{k}} - f^-_{\mathbf{k}}\right) \right]. \tag{13}$$

Note that in order to compare with previous results in the literature, we keep the *total* number of particles, $N = N_\uparrow + N_\downarrow$, fixed, and not the number of particles in each plane. To solve the gap equation (12), we perform a partial wave expansion of the induced interaction $V(\mathbf{k}) = \sum_n V_n(k) \exp(in\phi_{\mathbf{k}})$, where $\phi_{\mathbf{k}}$ is the azimuthal angle of $\mathbf{k}$. In the numerics, we keep the two leading terms, $n = 0, 1$ corresponding to s-wave singlet and p-wave triplet pairing respectively. When solving the above equations, we find three different phases: The homogeneous BCS phase with $\mathbf{Q} = 0$, the FF state with $\mathbf{Q} \neq 0$, and the normal phase with no superfluid pairing. To determine which of these phases is the ground state, we compare their energy E. We have from mean-field theory

$$\begin{aligned} E - \mu_\uparrow N_\uparrow - \mu_\downarrow N_\downarrow = \sum_{\mathbf{k}} \xi_{\mathbf{k}} - \sum_{E^-_{\mathbf{k}}>0} E^-_{\mathbf{k}} + \sum_{E^+_{\mathbf{k}}<0} E^+_{\mathbf{k}} \\ + \sum_{\mathbf{k}} \frac{|\Delta(\mathbf{k})|^2}{2E_{\mathbf{k}}} (1 - f^+_{\mathbf{k}} - f^-_{\mathbf{k}}). \end{aligned} \tag{14}$$

V. RESULTS FOR ZERO TEMPERATURE

We now solve the Gor'kov equations for $T = 0$, varying the interaction range and density imbalance through the healing length ξ_B and the field $h = (\mu_\uparrow - \mu_\downarrow)/2$, respectively. The resulting phase diagrams are shown in Figs. 2 and 3 for two different values of the layer distance, $k_F d = 1$ and $k_F d = 0$. The Fermi momentum is defined as $k_F = \sqrt{2\pi(n_\uparrow + n_\downarrow)}$. We set the effective scattering length to $k_F a_{\rm eff} = 0.05$. This small value ensures that we stay in the valid range of mean-field theory for all parameter sets shown in the figures. As is standard in the literature, we measure the field h in units of $\Delta_0 = \Delta(k_F, \mathbf{0})$, which is the pairing field at the Fermi surface for $h = 0$, that is, with no density imbalance.

Consider first the case of the layer distance $k_F d = 1$. Figure 2 clearly shows that there is a large region in the phase diagram, where the FF phase is stable. We find that the phase transition between the BCS and the FF phase is first order at the lower critical field h_{c_1}, whereas it is second order for the transition between the FF phase and the normal phase at the

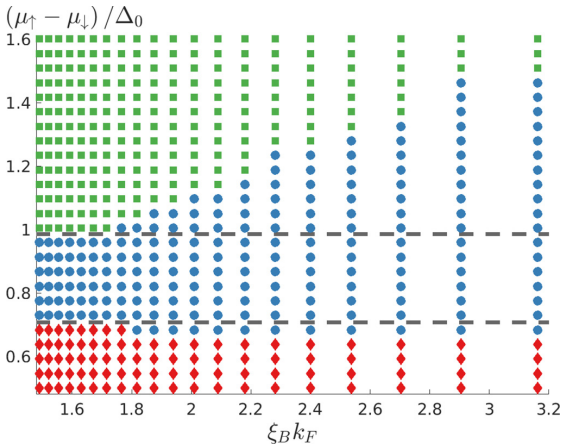

FIG. 2. The $T = 0$ phase diagram of the bilayer fermions for $k_F d = 1$ and $k_F a_{\text{eff}} = 0.05$, as a function of the interaction range ξ_B and the field h. The (red) diamonds, (blue) circles, and (green) squares indicate the BCS, FF, and normal phase, respectively. The horizontal dashed lines give the upper and lower critical fields for the FF phase for a short-range interaction [13,14].

upper critical field h_{c_2}. This is in agreement with the results for a short-range interaction [13,14]. Moreover, the range of values of h for which the FF phase is the ground state increases with the interaction range ξ_B. This shows that a long-range interaction stabilizes the FF phase. The reason is that the relative strength of the p-wave component compared to the s-wave component of the interaction increases with increasing range, which favors FF pairing. To illustrate this important point further, we plot as horizontal lines in Fig. 2 the critical fields for a short-range interaction [1,24], $h_{c_1} \approx \Delta_0/\sqrt{2} \approx 0.7\Delta_0$ and $h_{c_2} = \Delta_0$. While the FF region approaches that of

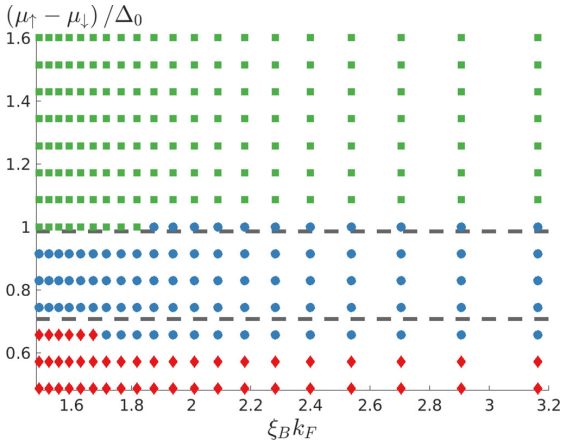

FIG. 3. The $T = 0$ phase diagram of the bilayer fermions as a function of the interaction range ξ_B and the field h for zero layer distance and boson-fermion interaction strength $k_F a_{\text{eff}} = 0.05$. The symbols and lines mean the same as in Fig. 2.

a short-range interaction for decreasing $k_F d$, it becomes much larger with increasing range $k_F \xi_B$.

Consider next the case of zero layer distance $d = 0$ shown in Fig. 3. While a large $k_F \xi_B$ still stabilizes the FF phase, the effect here is much less pronounced as compared to the case $k_F d = 1$. Increasing ξ_B leads to a smaller increase in the range of values of h for which the FF phase is the ground state than for $k_F d = 1$. The reason is that the short-range $1/r$ divergence of the Yukawa interaction between the fermions in the two layers given by Eq. (2) is cut off at $1/d$ for a finite layer distance d. A non-zero value of d makes the p-wave part of the interaction stronger compared to the s-wave part. As a result, the FF phase where there is pairing in both the s- and p-wave channels is favored compared to the pure s-wave BCS state for a nonzero layer distance. Note that the reason the superfluid region (BCS and FF) seems larger for $k_F d = 1$ compared to $d = 0$ even though the strength of the interaction obviously is smaller for a nonzero layer distance, is that we measure h in units of Δ_0, which is also smaller. Had we used the unit ϵ_F instead for instance, the superfluid region of the $d = 0$ phase would be larger.

VI. BEREZINSKII-KOSTERLITZ-THOULESS MELTING

Since the fermions are confined in 2D layers, phase fluctuations of the order parameter are significant and will eventually melt the superfluid through the Berezinskii-Kosterlitz-Thouless (BKT) mechanism at a critical temperature T_{BKT}. To describe this, we first calculate the superfluid stiffness, or equivalently the superfluid density, by imposing a linear phase twist on the order parameter and calculating the corresponding energy cost to second order in the twist. For a given vector $\mathbf{Q}$, the real space pairing becomes, using Eq. (4),

$$\Delta(\mathbf{R}, \mathbf{R}) = \Delta \cdot e^{i(\mathbf{Q}+\delta\mathbf{q})\cdot\mathbf{R}}, \tag{15}$$

where $\Delta = \sum_{\mathbf{k}} \Delta(\mathbf{k})/\mathcal{V}$ and $\delta\mathbf{q} \cdot \mathbf{R} = \delta\theta(\mathbf{R})$ is the imposed spatially linear phase twist. From Eq. (15), it is clear that the direction of the phase twist relative to the COM of the Cooper pairs is important: When $\delta\mathbf{q}$ is parallel to $\mathbf{Q}$, the phase twist corresponds to adding/removing COM momentum to the Cooper pairs which compresses/expands the wavelength of the plane wave pairing field $\Delta(\mathbf{R}, \mathbf{R})$; when $\delta\mathbf{q}$ is perpendicular to $\mathbf{Q}$, the phase twist corresponds to a small rotation of the COM momentum to the Cooper pairs which rotates the plane wave pairing field. These two effects are illustrated in Fig. 4(a).

The phase twist $\delta\theta(\mathbf{R})$ gives a free energy cost δF of the form

$$\begin{aligned}\delta F &= \frac{1}{2}\int d^2\mathbf{r}[J_\parallel(\partial_\parallel\delta\theta)^2 + J_\perp(\partial_\perp\delta\theta)^2] \\ &= \frac{J}{2}\int d^2\mathbf{r}(\nabla\delta\theta)^2,\end{aligned} \tag{16}$$

where $\partial_\parallel$ and $\partial_\perp$ are spatial derivatives parallel or perpendicular to the COM momentum of the Cooper pairs, corresponding to $\delta\mathbf{q} \parallel \mathbf{Q}$ and $\delta\mathbf{q} \perp \mathbf{Q}$ respectively. The associated superfluid stiffness constants are $J_\parallel$ and $J_\perp$. In the second line of Eq. (16), we have rescaled the spatial coordinate perpendicular to $\mathbf{Q}$ by the factor $\sqrt{J_\parallel/J_\perp}$ to obtain an isotropic XY model with the effective stiffness constant $J = \sqrt{J_\parallel J_\perp}$ [32]. Alternatively, defining the superfluid densities parallel and perpendicular to

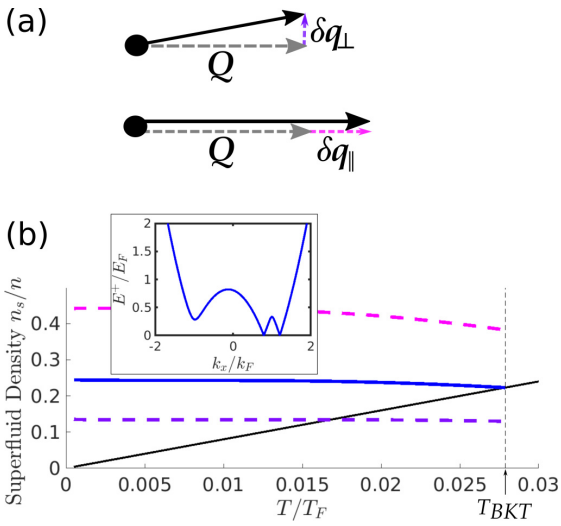

FIG. 4. (a) The two kinds of phase fluctuations with $\delta\mathbf{q}$ perpendicular and parallel to the COM momentum $\mathbf{Q}$ of the Cooper pairs give rise to a rotation and a compression/expansion of the plane wave pairing field respectively. (b) The corresponding superfluid densities $n_{s\parallel}$ (top dashed magenta line) and $n_{s\perp}$ (bottom dashed purple line). The solid blue line is to the effective superfluid density $n_s = \sqrt{n_{s\parallel} n_{s\perp}}$. The critical temperature $T_{\rm BKT}$ is reached when n_s crosses the thin solid black line as indicated by the vertical dashed line. The inset shows one branch of the quasiparticle spectrum along $k_y = 0$ with the COM momentum $\mathbf{Q}$ along the x axis for $T = 0$. The gapless excitations leading to the reduction in the superfluid density are clearly visible.

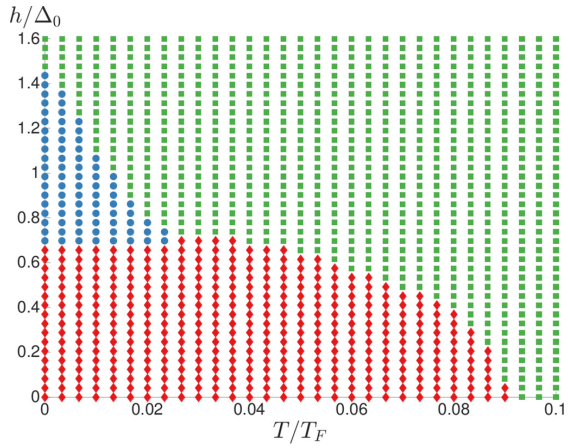

FIG. 5. The phase diagram as a function of temperature T and field h for layer distance $k_F d = 1$, boson-fermion interaction strength $k_F a_{\rm eff} = 0.05$, and range $k_F \xi_B = 3$. The symbols mean the same as in Figs. 2 and 3.

$\mathbf{Q}$ as $n_{s\perp} = 4mJ_\perp$ and $n_{s\parallel} = 4mJ_\parallel$, we can write the free energy cost as

$$\delta F = m \int d^2\mathbf{r}\left[n_{s\parallel} v_{s\parallel}^2 + n_{s\perp} v_{s\perp}^2\right]/2. \tag{17}$$

Here $v_{s\parallel} = \partial_\parallel \delta\theta/2m$ is the superfluid velocity parallel to $\mathbf{Q}$ and likewise for $v_{s\perp}$. One way to calculate the energy shift due to the phase twist is by considering a corresponding gauge transformed lattice Hamiltonian [33]:

$$H^{\rm MF}_{\rm latt.}(\theta) = \exp\left(-i\frac{\delta\theta}{2}\sum_l x_{||,l}/a\right) \times H^{\rm MF}_{\rm latt.} \exp\left(-i\frac{\delta\theta}{2}\sum_l x_{||,l}/a\right),$$

where a is the lattice constant and $x_{||,l}$ is the position along the axis parallel to $\mathbf{Q}$ of the lth particle. This can then be expanded to second order and the continuum limit $a \to 0$ taken while keeping the total density constant. This yields

$$n_{s\parallel} = n - \frac{\beta}{m}\int d^2\check{k}[f^+_{\mathbf{k}}(1 - f^+_{\mathbf{k}}) + f^-_{\mathbf{k}}(1 - f^-_{\mathbf{k}})]k_\parallel^2 \tag{18}$$

for the superfluid density along $\mathbf{Q}$, where $k_\parallel = \mathbf{k}\cdot\mathbf{Q}/Q$. Here, n is the total surface density of fermions coming from the two layers. An equivalent formula holds for $n_{s\perp}$. Note that the continuum result above can also be obtained directly without considering a lattice system first. Equation (18) is the 2D version of the usual expression for the superfluid density allowing for the effects of the spatial anisotropy of the FF state [34,35]. We can now determine the critical temperature of the superfluid using the BKT condition

$$T_{\rm BKT} = \frac{\pi}{2}J = \frac{\pi}{8m}n_s, \tag{19}$$

where we have defined the effective superfluid density as $n_s = \sqrt{n_{s\parallel} n_{s\perp}}$.

In Fig. 4(b), we plot the superfluid densities as a function of T for layer distance $k_F d = 1$ and boson-fermion interaction strength $k_F a_{\rm eff} = 0.05$. We see that $n_{s\parallel} > n_{s\perp}$, reflecting that the energy cost related to compressing/expanding the COM momentum is higher than that related to rotating it as expected. Note that both superfluid densities are smaller than the total density n even for $T \to 0$. This is due to the inherent presence of gapless quasiparticle states in the FF phase. These gapless excitations, which are shown in the inset of Fig. 4(b), reduce the superfluid density. We also plot the effective superfluid density $n_s = \sqrt{n_{s\parallel} n_{s\perp}}$ as well as the line $8mT/\pi$. It follows from Eq. (19) that the superfluid phase melts when n_s crosses this line.

Having set up the theory for BKT melting, we can now analyze the BCS and FF phases at nonzero temperatures. In Fig. 5, we present an example of a phase diagram for $k_F d = 1$ and $k_F a_{\rm eff} = 0.05$. We see that the critical temperature of the FF phase increases with decreasing field h. The highest critical temperature is obtained just above the lowest critical field h_{c_1}, where the FF, BCS, and normal phase meet in a *tricritical point* at $h_{c_1} \approx 0.7\Delta_0$ and $T \approx 0.025T_F$. This critical temperature is well below the theoretical maximum of $T_F/8$ obtained by setting $n_s = n$ in Eq. (19). The reason is that the gapless excitations in the FF phase decrease the superfluid density below n, as we discussed above in connection with Fig. 4. Indeed, we note that the values of the two components of the superfluid density in Fig. 4 at $T = T_c$ are almost unchanged

from their values at $T \to 0$. This is a general result: While the flexibility of the bilayer system allows us to optimize the induced interaction to favor FF pairing, the gapless nature of this state prevents us from reaching critical temperatures close to $T_F/8$.

The critical temperature of the BCS phase is much higher, as can be seen from Fig. 5. Due to its fully gapped spectrum, T_{BKT} can in fact relatively easily be tuned to be close to maximum $T_F/8$ by varying the layer distance d and the interaction range ξ_B, even while keeping the boson-fermion interaction strength a_{eff} weak.

VII. CONCLUSION

We analyzed a mixed-dimensional system consisting of two layers of identical fermions immersed in a BEC. This system was shown to support superfluid pairing due to an attractive induced interaction between the two layers mediated by the BEC. When the densities of the two layers are different, the resulting superfluid phase is inhomogeneous. Using a plane wave FF ansatz to describe this phase, we demonstrated that it is stabilized by the nonzero range of the induced interaction. Importantly, the FF phase can occupy much larger regions of the phase diagram as compared to the case of a short-range interaction. The range of the induced interaction can be tuned by varying the BEC healing length, which makes the present system promising for realizing FFLO physics experimentally. We furthermore analyzed the melting of the superfluid phases due to phase fluctuations using BKT theory, and demonstrated that the normal, homogenous, and inhomogeneous superfluid phases meet in a tricritical point in the phase diagram. The superfluid density of the FF phase was shown to be suppressed by intrinsic gapless excitations, and this leads to a significant reduction in the critical temperature compared to the homogeneous superfluid, which can be tuned to have a critical temperature close to the maximum $T_F/8$.

ACKNOWLEDGMENT

We wish to acknowledge the support of the Danish Council of Independent Research - Natural Sciences via Grant No. DFF-4002-00336.

[1] P. Fulde and R. A. Ferrell, Phys. Rev. **135**, A550 (1964).
[2] A. I. Larkin and Yu. N. Ovchinnikov, Zh. Eksp. Teor. Fiz. **47**, 1136 (1964) [Sov. Phys. JETP **20**, 762 (1965)].
[3] F. Chevy and C. Mora, Rep. Prog. Phys. **73**, 112401 (2010).
[4] L. Radzihovsky and D. E. Sheehy, Rep. Prog. Phys. **73**, 076501 (2010).
[5] J. J. Kinnunen, J. E. Baarsma, J.-P. Martikainen, and P. Törmä, Rep. Prog. Phys. **81**, 046401 (2018).
[6] Y. Matsuda and H. Shimahara, J. Phys. Soc. Jpn. **76**, 051005 (2007).
[7] R. Casalbuoni and G. Nardulli, Rev. Mod. Phys. **76**, 263 (2004).
[8] M. G. Alford, A. Schmitt, K. Rajagopal, and T. Schäfer, Rev. Mod. Phys. **80**, 1455 (2008).
[9] R. Anglani, R. Casalbuoni, M. Ciminale, N. Ippolito, R. Gatto, M. Mannarelli, and M. Ruggieri, Rev. Mod. Phys. **86**, 509 (2014).
[10] R. Beyer and J. Wosnitza, Low Temp. Phys. **39**, 225 (2013).
[11] H. Mayaffre, S. Krämer, M. Horvatić, C. Berthier, K. Miyagawa, K. Kanoda, and V. F. Mitrović, Nat. Phys. **10**, 928 (2014).
[12] A. Bianchi, R. Movshovich, C. Capan, P. G. Pagliuso, and J. L. Sarrao, Phys. Rev. Lett. **91**, 187004 (2003).
[13] H. Shimahara, Phys. Rev. B **50**, 12760 (1994).
[14] H. Burkhardt and D. Rainer, Ann. Phys. (NY) **506**, 181 (1994).
[15] P. Pieri, D. Neilson, and G. C. Strinati, Phys. Rev. B **75**, 113301 (2007).
[16] Y.-a. Liao, A. S. C. Rittner, T. Paprotta, W. Li, G. B. Partridge, R. G. Hulet, S. K. Baur, and E. J. Mueller, Nature (London) **467**, 567 (2010).
[17] J. Gukelberger, S. Lienert, E. Kozik, L. Pollet, and M. Troyer, Phys. Rev. B **94**, 075157 (2016).
[18] J. E. Baarsma and P. Törmä, J. Mod. Opt. **63**, 1795 (2016).
[19] G. J. Conduit, P. H. Conlon, and B. D. Simons, Phys. Rev. A **77**, 053617 (2008).
[20] L. Radzihovsky and A. Vishwanath, Phys. Rev. Lett. **103**, 010404 (2009).
[21] M. J. Wolak, B. Grémaud, R. T. Scalettar, and G. G. Batrouni, Phys. Rev. A **86**, 023630 (2012).
[22] S. Yin, J.-P. Martikainen, and P. Törmä, Phys. Rev. B **89**, 014507 (2014).
[23] D. E. Sheehy, Phys. Rev. A **92**, 053631 (2015).
[24] H. Lee, S. I. Matveenko, D.-W. Wang, and G. V. Shlyapnikov, Phys. Rev. A **96**, 061602 (2017).
[25] A. Mazloom and S. H. Abedinpour, Phys. Rev. B **96**, 064513 (2017).
[26] Y. Nishida and S. Tan, Phys. Rev. Lett. **101**, 170401 (2008).
[27] H. Heiselberg, C. J. Pethick, H. Smith, and L. Viverit, Phys. Rev. Lett. **85**, 2418 (2000).
[28] Z. Wu and G. M. Bruun, Phys. Rev. Lett. **117**, 245302 (2016).
[29] J. M. Midtgaard, Z. Wu, and G. M. Bruun, Phys. Rev. A **96**, 033605 (2017).
[30] H. Shimahara, J. Phys. Soc. Jpn. **67**, 736 (1998).
[31] C. Mora and R. Combescot, Europhys. Lett. **66**, 833 (2004).
[32] Z. Wu, J. K. Block, and G. M. Bruun, Sci. Rep. **6**, 19038 (2016).
[33] E. H. Lieb, R. Seiringer, and J. Yngvason, Phys. Rev. B **66**, 134529 (2002).
[34] A. J. Leggett, Rev. Mod. Phys. **47**, 331 (1975).
[35] L. Landau, E. Lifshitz, and L. Pitaevskij, *Statistical Physics, Part 2: Theory of Condensed State*, Landau and Lifshitz Course of Theoretical Physics Vol. 9 (Butterworth-Heinemann, Oxford, 1980).

— 6 —

Non-Hermitian Models for Topological Systems

This chapter concerns a project which was initiated when I was invited to the group of Prof. Hui Zhai at Tsinghua University. The initial plan was to study non-hermitian variations of the Haldane model, but the project ended up being of a more general nature. The first section gives a brief introduction to parts of the Keldysh formalism used in the manuscript, after which our work is discussed and presented.

6.1 Keldysh Formalism

In the following paper, we consider a lattice system connected to an environment with which it can exchange particles. The environment consists of local baths with a large number of degrees of freedom. If we are only interested in the lattice system, we can imagine integrating out the environment as we have integrated out the bosons from the action of the Bose-Fermi mixture in previous chapters. This, however, leaves us with a problem, since the time evolution of the system will appear to be non-hermitian. The effective hamiltonian will contain loss and gain terms, corresponding to particles jumping into the bath or coming back into the system, respectively. Furthermore, the loss and gain might not balance out to some steady-state solution, so the behaviour of the lattice is completely out of equilibrium.

The goal of this section is to sketch how we can go from a normal Hamiltonian describing the system we are interested in along with the environment, to a retarded Green's function for the system only. This Green's function must necessarily encode the dynamics of particles coming and going from the system. The main focus in the article, however, is on the situation where there are many more possible states in the environment than in the system. This means that over time, any population of particles in the lattice sites will have dissipated out into the environment. So we can't expect to describe the lattice system with normal equilibrium techniques

as before. Instead, I will quickly sketch a few steps of the non-equilibrium Keldysh technique that was omitted from the manuscript below.

Let us first consider the retarded Greens' function of a particle-conserving, interacting system of fermions. In the usual technique, we would define it in the Heisenberg representation as

$$G(t,t') = \langle \Omega | T\psi(t)\psi^\dagger(t')|\Omega\rangle \,, \tag{6.1}$$

where T denotes time ordering and $|\Omega\rangle$ is the ground state of the interacting Hamiltonian. ψ and $\psi^\dagger$ are Grassmann variables. Usually, we imagine that we turn on the interactions slowly at some point in the past, and the ground state evolves adiabatically such that $|\Omega\rangle = U(0,-\infty)\,|0\rangle$, where $|0\rangle$ is the non-interacting ground state and U is the time-evolution operator. We now imagine slowly turning the interactions off again far ahead in the future. The ground state should return to the non-interacting ground state – possibly with a phase factor. This assumption allows us to rewrite the Green's function (or indeed a general correlation function) as

$$G(t,t') = \frac{\langle 0|T\psi(t)\psi^\dagger(t')U(\infty,-\infty)|0\rangle}{\langle 0|U(\infty,-\infty)|0\rangle} \tag{6.2}$$

which is the starting point for many equilibrium field-theoretic techniques. But the assumption we made will clearly not hold if the interaction we switch on is an interaction with an environment where we can lose or gain particles. The state at $t=\infty$ is probably wildly different than the one we started out with at $t=-\infty$. Since we need to know something about the state at the end of the time-evolution, Schwinger's insight [72] was that we could evolve the state to $t=+\infty$, but then evolve it back to $t=-\infty$ again, along a closed contour as shown in Fig. 6.1. Then the state at the end of the evolution is *identical* to the state at the beginning. Furthermore, we only have to think about the "turning on" of the interactions. What happens in the far future is neatly taken care of and we do not have to worry about it. The cost is that our time-contour is now twice as long. It turns out that the easiest way to deal with it is to simply define a field for each branch of the contour and then evolve them in one go. So we get a doubling of our degrees of freedom, here we would have ψ_+ and ψ_- instead of just ψ, corresponding to the forwards and backwards branch of the contour. A full exposition is given in e.g. Kamenev [73, 74], which the following is also based upon.

To write up the Keldysh action, consider the Green's function $G(t,t') = \langle T\psi(t)\psi^\dagger(t')\rangle$. Since we double our degrees of freedom, we now have four possible Green's functions. Also recall that we must path-order, $\mathcal{P}$, the Grassmann numbers instead of time ordering them, according to the time-contour we are on, such that $\psi_-(t')$ is always after $\psi(t)$, for instance. We

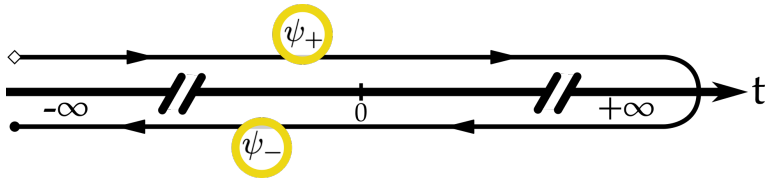

Figure 6.1: The closed time contour of the Keldysh technique. Due to the non-equilibrium nature of the system, we don't know much about the state at $t = +\infty$, so we have to evolve the state back to the known, initial state at $t = -\infty$. Instead of considering a time-contour of twice length, we define another fermion field and double the degrees of freedom.

define

$$\begin{aligned}\langle \mathcal{P}\psi_+(t)\psi_-^\dagger(t')\rangle &\equiv iG^<(t,t')\\ \langle \mathcal{P}\psi_-(t)\psi_+^\dagger(t')\rangle &\equiv iG^>(t,t')\end{aligned} \tag{6.3}$$

A few calculation gives us that the same-branch Green's functions can be expressed in terms of these functions,

$$\begin{aligned}\langle \mathcal{P}\psi_+(t)\psi_+^\dagger(t')\rangle &\equiv iG^T(t,t') = \Theta(t-t')iG^<(t,t') + \Theta(t'-t)iG^>(t,t')\\ \langle \mathcal{P}\psi_-(t)\psi_-^\dagger(t')\rangle &\equiv iG^{\tilde{T}}(t,t') = \Theta(t'-t)iG^<(t,t') + \Theta(t-t')iG^>(t,t')\end{aligned} \tag{6.4}$$

Where in the last line, $\tilde{T}$ refers to reverse time-ordering, since the path-ordering on the backwards branch is opposite to time-ordering. The four Green's functions are not independent, since

$$G^T + G^{\tilde{T}} = G^< + G^> \tag{6.5}$$

and we can use this to eliminate one Green's function through a *Keldysh rotation*. We define two new fields as

$$\begin{aligned}\psi_1(t) &= \frac{1}{\sqrt{2}}(\psi_+(t) + \psi_-(t))\\ \psi_2(t) &= \frac{1}{\sqrt{2}}(\psi_+(t) - \psi_-(t))\end{aligned} \tag{6.6}$$

But we are free to choose a different transformation for $\psi^\dagger$, since they are Grassmann variables, and not hermitian conjugates. Sometimes a bar, $\bar{\psi}$, is used instead of the dagger to eliminate confusion. In the transformation we

choose, we interchange the $1, 2$ indices.

$$\psi_1^\dagger(t) = \frac{1}{\sqrt{2}}(\psi_+(t) - \psi_-(t))$$
$$\psi_2^\dagger(t) = \frac{1}{\sqrt{2}}(\psi_+(t) + \psi_-(t)) \tag{6.7}$$

In these new fields, we have eliminated the $(2,1)$ Green's function, so

$$\hat{G}(t,t') = -i\,\langle \psi_a(t)\psi_b^\dagger(t')\rangle = \begin{pmatrix} G^R(t,t') & G^K(t,t') \\ 0 & G^A(t,t') \end{pmatrix} \tag{6.8}$$

where R, A and K denote the retarded, advanced and Keldysh Green's function respectively, and $a, b = 1, 2$. It is in some ways an arbitrary choice to let the empty component of $\hat{G}$ be in the lower left corner, but having $\hat{G}$ as an upper- or lower-triangular matrix has a benefit. The inverse matrix, $\hat{G}^{-1}$ will then have the same triangular structure, with simple inverses of the retarded and advanced functions along the diagonal. This saves us some technical headaches.

We are now ready to write up an action for a simple system. Consider a single lattice site that can be occupied by a fermion, ψ, with an attached bath of states, b_α. The second-quantized Hamiltonian is $H = H_{\text{sys}} + H_{\text{bath}} + H_{\text{int}}$ where

$$H_{\text{sys}} = \omega_0 \psi^\dagger \psi \tag{6.9}$$

is the single lattice site,

$$H_{\text{bath}} = \sum_\alpha \omega_\alpha b_\alpha^\dagger b_\alpha \tag{6.10}$$

is the bath states and

$$H_{\text{int}} = \kappa \sum_\alpha b^\dagger \psi + \psi^\dagger b_\alpha \tag{6.11}$$

describes the hopping back and forth between the lattice site and the bath states. The partition function in the Keldysh formalism is

$$\mathcal{Z} = \int \mathcal{D}[\Psi^\dagger, \Psi, B^\dagger, B]\, e^{-S} \tag{6.12}$$

and the Keldysh action must then be (in the frequency representation)

$$S = \int \mathrm{d}\omega\, \Psi^\dagger \hat{G}_0^{-1} \Psi + \sum_\alpha B_\alpha^\dagger \hat{G}_\alpha^{-1} B_\alpha + \sum_\alpha \kappa(B_\alpha^\dagger \Psi + \Psi^\dagger B_\alpha) \tag{6.13}$$

where $\Psi^\dagger = (\psi_1^\dagger, \psi_2^\dagger)$, $B_\alpha^\dagger = (b_{1,\alpha}^\dagger, b_{2,\alpha}^\dagger)$ and where $\hat{G}_0, \hat{G}_\alpha$ are the bare Green's functions for the lattice site and the bath modes, respectively. They are

both given by Eq. 6.8. If we are only interested in the dynamics of the lattice sites, it is now easy to integrate the bath out of the partition function. We end up with

$$S_{\text{eff}} = \int \mathrm{d}\omega \, \Psi^\dagger \left(\hat{G}_0^{-1} - \kappa^2 \sum_\alpha \hat{G}_\alpha \right) \Psi \tag{6.14}$$

We can then write up a Dyson's function for the total, retarded Green's function, which is

$$[G^R(\omega)]^{-1} = [G_0^R(\omega)]^{-1} - \Sigma^R(\omega) \tag{6.15}$$

where

$$\Sigma^R(\omega) = \kappa^2 \sum_\alpha G_\alpha^R(\omega) = \kappa^2 \sum_\alpha \left(\omega - \omega_\alpha + i0^+ \right)^{-1} \tag{6.16}$$

in this simple model. The generalisation to many lattice sites and more internal structure is relatively straightforward. In the manuscript below it only leads to a momentum dependence and some further matrix structure in Eq. (11).

6.2 Motivation and Prior Work

After the topological properties of closed, non-interacting systems [20] has had some time to percolate through the field of condensed matter physics, it is only natural to attempt to extend these classifications to interacting or open quantum systems. Some classification schemes can be extended straightforwardly for weakly interacting systems, as long as an energy gap remains [75]. For a recent overview, see also [76]. The other direction, concerning open systems with gain or loss has also been widely studied in recent years. It is not only systems that can physically gain or lose particles to the environment that break hermiticity. We also find non-hermitian descriptions for quasiparticles in e.g. interacting electron systems [77] and mechanical systems [78].

The attempt to systematically extend the topological classification into non-hermitian band theory is ongoing, but has made great advances recently. A full exposition is beyond the scope of the thesis, but see e.g. [79–81]. What is interesting in the context of this paper is the types of toy models used as specific representatives of the topological classes, and their possible microscopic origins in a condensed matter context. Of the well-known lattice models in the field, non-hermitian extensions of the Su-Schrieffer-Heeger (SSH) model [82, 83] and the Haldane model [84] where the hermitian counterpart realises a topological insulator, can be mentioned. A typical

strategy for the toy models is to, by hand, add non-hermitian terms to the Hamiltonian. Often, these are local on-site terms and nearest-neighbour "hopping" terms, as done in the SSH examples above.

An important concept in non-hermitian quantum mechanics is that of parity-time (PT) symmetry. It was shown by Bender and Boettcher [85] that non-hermitian systems could have wholly real spectra if they obeyed the combined transformation of *parity inversion* and *time-reversal*. Since then, the study of PT-symmetric Hamiltonians have been a central part of the field, since they are conceptually close to the familiar hermitian Hamiltonians. Photonics systems have proven to be well-suited for the realization of PT-symmetry [86, 87]. In these systems, the symmetry can be loosely seen as a balancing of the optical loss and the pumping gain, to achieve a stable steady-state. A motivation for our study was then also to see if it was possible to realize non-hermitian systems with real spectra from a passive lattice system.

6.3 Results and Outlook

We set up a general model for a lattice system with on-site baths in an arbitrary number of dimensions. When the environment was integrated out using the Keldysh technique discussed above, we found an inequality between the various non-hermitian terms in the effective Hamiltonian. This only required some minor asssumptions, namely a weak and local system-environment interaction and resonant tunneling between the baths. In fact, I am confident that the last assumption can be relaxed without affecting most of our conclusions, since this was only done for ease of calculations.

The inequality was in turn shown to ensure that the eigenvalues of the effective Hamiltonian were confined to the lower half of the complex plane. This is in conflict with some Hamiltonians that have been used, and show that they are not immediately possible to realize in these types of systems. It seems reasonable that this constraint on the eigenvalues should hold in the general case, as it mirrors the fundamental property of a Fermi liquid, where the imaginary part of the self-energy is negative [88] and gives the lifetime of the quasiparticles. The strength of our method, however, is that it gives us the possibility of finding the real-space behaviour of the non-hermitian terms. We found these to be quite tunable when varying the hopping strength between the baths. For small values of the hopping strength, surprisingly, the non-hermitian terms only appear as nearest-neighbour terms, apart from an onsite dissipation. This validates, for instance, a crucial part of the SSH models considered in [82, 83] as realisable with passive lattice systems. It would be interesting to repeat these calculations for higher-dimensional

lattice systems, to see if the same behaviour is repeated.

6.4 Contribution

I wrote the first draft of the paper and held the primary responsibility for bringing it to publication. In its current state, my primary contributions to the manuscript are in chapters III and IV. I also worked on a previous version of the proof in chapter II, but the current version is a more elegant solution by Yu Chen.

Constraints on the energy spectrum of non-Hermitian models in open environments

Jonatan Melkær Midtgaard,[1,*] Zhigang Wu,[2,3,†] and Yu Chen[4,‡]

[1] *Department of Physics and Astronomy, Aarhus University, DK-8000 Aarhus C, Denmark*
[2] *Shenzhen Institute for Quantum Science and Engineering (SIQSE) and Department of Physics, Southern University of Science and Technology (SUSTech), Shenzhen 518055, China*
[3] *Center for Quantum Computing, Peng Cheng Laboratory, Shenzhen 518055, China*
[4] *Center for Theoretical Physics and Department of Physics, Capital Normal University, Beijing, 100048, China*

Motivated by recent progress on non-Hermitian topological band theories, we study the energy spectrum of a generic two-band non-Hermitian Hamiltonian. We prove rigorously that the complex energy spectrum of such a non-Hermitian Hamiltonian is restricted to the lower complex plane, provided that the parameters of the Hamiltonian satisfy a certain constraint. Furthermore, we consider one specific scenario where such a non-Hermitian Hamiltonian can arise, namely a two-band model coupled to an environment, and show that this aforementioned constraint originates from very general physical considerations. Using this construction we extract the real-space behaviour of the non-hermitian terms. Our findings are relevant in the definition of the energy gap in non-Hermitian topological band theories and also have implications on simulations of such theories using quantum systems.

I. INTRODUCTION

Topological band theory was originally proposed to describe a new type of phase of matter in electronic systems[1–5], namely the symmetry protected topological phases. Now it has found wide applications also in photonic materials, cold atoms, as well as mechanical systems[6–9]. Very recently, the topological band theory was extended to describing open systems governed by non-Hermitian Hamiltonians, where certain topological properties are found to be robust against non-Hermicity[10–107]. A non-Hermitian version of bulk-edge correspondence can be established[33, 41, 42] and the physical connection between Hall conductance and a non-hermitian topological invariant is found[49]. Many new phenomena unique to the non-Hermitian systems, such as the existence of topological bulk Fermi arcs[37, 40, 99], non-Hermitian skin effects[23, 25, 35, 41, 42, 44, 46, 54, 69, 83, 90, 91] and non-Hermitian knotted Fermi ribbons[45, 60] have also been discovered.

Of central importance in the non-Hermitian topological band theory is defining an energy gap, which is not as straightforward as for the Hermitian courterpart due to the fact that the energy spectrum here is generally complex. In previous studies, concepts such as point gap and line gap are introduced[48, 62, 75]; the former means that the complex spectrum encloses the origin of the complex energy plane while the latter depicts a scenario where the complex spectrum can be separated into two parts by a line. Classification theories of non-Hermitian bands are proposed based on whether these mathematical gaps are protected by certain symmetries[48, 62, 75]. An implicit assumption made in these discussions of the non-Hermitian energy gap, however, is that the energy spectrum of the non-Hermitian models exist in both the upper and lower complex plane. But it is not obvious that this is always the case for any non-Hermitian system. In other words, are there any constraints on the non-Hermitian models when the physical origins of such models are taken into account? If so, what are the consequences of such constraints in relation to the energy spectrum of the non-Hermitian models?

In this paper, we address these important questions in the context of a generic two-band system coupled to an environment. We demonstrate that such a coupling generally leads to the following effective non-Hermitian Hamiltonian for the system

$$\mathcal{H}_{\text{eff}}(\mathbf{k}) = [\boldsymbol{d}(\mathbf{k}) + i\boldsymbol{\gamma}(\mathbf{k})] \cdot \boldsymbol{\sigma} + i\gamma_0(\mathbf{k})\sigma_0, \tag{1}$$

where $\boldsymbol{d}(\mathbf{k})$ and $\boldsymbol{\gamma}(\mathbf{k})$ are two three-component vectors, $\boldsymbol{\sigma} = (\sigma_x, \sigma_y, \sigma_z)$ are the Pauli matrices and $\sigma_0 = \mathbb{I}$ is the identity matrix. In deriving the effective Hamiltonian we find the following mathematical constraint for the parameters of the Hamiltonian

$$-\gamma_0(\mathbf{k}) \geq \sqrt{\gamma_x^2(\mathbf{k}) + \gamma_y^2(\mathbf{k}) + \gamma_z^2(\mathbf{k})}. \tag{2}$$

Further, we prove rigorously that this constraint leads to a crucial property of the non-Hermitian Hamiltonian, namely that the imaginary part of all its eigenvalues must be non-positive. We will also show that these seemingly mathematical statements in fact result from very general physical considerations. As a concrete example, we consider a one-dimensional system coupled to a chain of tight-binding baths and determine explicitly the parameters in the effective Hamiltonian as well as the real space behaviour of the non-Hermitian terms. The construction of this class of models allows us to determine the real-space behaviour of the non-hermitian terms, leading to some intriguing results.

* midtgaard@phys.au.dk
† wuzg@sustech.edu.cn
‡ spaceexplorer@163.com

The structure of the paper is as follows. In Section II we will begin with the non-Hermitian Hamiltonian in (1) and prove that all its eigenvalues have non-positive imaginary parts if (2) is obeyed. Next, in Section III we will provide the derivation of such a non-Hermitian Hamiltonian from system-environment coupling and in doing so show that the constraint (2) is indeed satisfied. We then study the behaviour of the non-hermitian terms in real space in Section IV and provide concluding remarks in Section V.

II. PROPERTIES OF THE EIGENVALUES FOR A TWO-BAND NON-HERMITIAN MODEL

We consider the following two-band non-hermitian effective hamiltonian

$$\hat{H}_{\text{eff}} = \sum_{\mathbf{k}} \boldsymbol{\psi}_{\mathbf{k}}^{\dagger} \mathcal{H}_{\text{eff}}(\mathbf{k}) \boldsymbol{\psi}_{\mathbf{k}} \tag{3}$$

where $\mathcal{H}_{\text{eff}}(\mathbf{k})$ is given by (1), the summation is over the crystal momenta in the first Brillouin zone and $\boldsymbol{\psi}_{\mathbf{k}} = (\psi_{\uparrow,\mathbf{k}}, \psi_{\downarrow,\mathbf{k}})^{\mathrm{T}}$ is a two-component spinor.

Such an effective Hamiltonian has been used in most of the studies on topological phases of non-Hermitian systems. We will prove an important property of this Hamiltonian, namely that all its complex eigenvalues must have a non-positive imaginary part, provided that the inequality (2) is satisfied for all $\mathbf{k}$. In the next section, we will show that the constraint (2) in fact follows naturally from general physical considerations.

We denote the eigenvalues of the non-Hermitian matrix $\mathcal{H}_{\text{eff}}(\mathbf{k})$ in (3) by $\lambda^{\pm}(\mathbf{k})$, which are determined by

$$\det\left(\lambda^{\pm}(\mathbf{k})\mathbb{I} - \mathcal{H}_{\text{eff}}(\mathbf{k})\right) = 0.$$

The imaginary part of these eigenvalues can be written as

$$\mathrm{Im}\lambda^{\pm}(\mathbf{k}) = \gamma_0(\mathbf{k}) \pm M(\mathbf{k})$$

where

$$M = \left[(|\boldsymbol{d}|^2 - |\boldsymbol{\gamma}|^2)^2 + (2\boldsymbol{d}\cdot\boldsymbol{\gamma})^2\right]^{1/4} \sin\varphi \tag{4}$$

with

$$\varphi = \frac{1}{2}\tan^{-1}\left(\frac{2\boldsymbol{d}\cdot\boldsymbol{\gamma}}{|\boldsymbol{d}|^2 - |\boldsymbol{\gamma}|^2}\right). \tag{5}$$

Defining the function $f = \left[\left(|\boldsymbol{d}|^2 - |\boldsymbol{\gamma}|^2\right)^2 + (2\boldsymbol{d}\cdot\boldsymbol{\gamma})^2\right]^{1/4}$, we find from (5)

$$\sin^2\varphi = \frac{1}{2}\left(1 - \frac{|\boldsymbol{d}|^2 - |\boldsymbol{\gamma}|^2}{f^2}\right).$$

Substituting this expression in (4) we obtain

$$|M| = f|\sin\varphi| = \frac{1}{\sqrt{2}}\sqrt{f^2 - |\boldsymbol{d}|^2 + |\boldsymbol{\gamma}|^2}.$$

Since

$$f^2 \leq \left[(|\boldsymbol{d}|^2 - |\boldsymbol{\gamma}|^2)^2 + 4|\boldsymbol{d}|^2|\boldsymbol{\gamma}|^2\right]^{1/2} = |\boldsymbol{d}|^2 + |\boldsymbol{\gamma}|^2,$$

we have

$$|M(\mathbf{k})| \leq |\boldsymbol{\gamma}(\mathbf{k})|. \tag{6}$$

Together with the condition (2), (6) implies that

$$\mathrm{Im}\lambda^{\pm}(\mathbf{k}) \leq 0, \tag{7}$$

namely all the eigenvalues of $\mathcal{H}_{\text{eff}}(\mathbf{k})$ have a non-positive imaginary part. In other words, the complex eigenvalues of the non-Hermitian Hamiltonian must all lie in the lower half complex plane. We emphasise that the above analysis is a rigorous mathematical discussion on the property of a generic two-band non-Hermitian Hamiltonian and the conclusion stands regardless of the origin of this Hamiltonian. In the following section, we will discuss the origin of (2) and the physical implication of (7) in the context of a system coupled to an environment.

So far, we have only considered periodic boundary conditions. Relaxing this condition and allowing particles to move in from the edge of the system will effectively result in external gain terms. However, periodic boundary effects are chosen to focus on bulk properties of the system-environment coupling.

III. CONSTRUCTION OF THE NON-HERMITIAN MODEL FROM SYSTEM-ENVIRONMENT COUPLING

In this section, we show how the effective non-Hermitian Hamiltonian (3) can be obtained by considering a two-band system coupled to an environment. By tracing out the degrees of freedom of the environment within certain approximations, we not only derive the effective Hamiltonian (3) but also prove that the constraint in (2) is always fulfilled. To be specific, we consider a general two-band model described by the Hamiltonian

$$\hat{H}_{\text{sys}} = \sum_{\mathbf{k}} \boldsymbol{\psi}_{\mathbf{k}}^{\dagger} \left[\mathbf{d}_0(\mathbf{k})\cdot\boldsymbol{\sigma}\right] \boldsymbol{\psi}_{\mathbf{k}} = \sum_{\mathbf{k}} \boldsymbol{\psi}_{\mathbf{k}}^{\dagger} \mathcal{H}_{\text{sys}}(\mathbf{k}) \boldsymbol{\psi}_{\mathbf{k}},$$

where $\mathbf{d}_0(\mathbf{k})$ is a three-component vector. Such a model is realised in a bipartite lattice with N unit cells and the up and down arrows in $\boldsymbol{\psi}_{\mathbf{k}} = (\psi_{\uparrow,\mathbf{k}}, \psi_{\downarrow,\mathbf{k}})^{\mathrm{T}}$ are used to distinguish the sites within a unit cell. The particles on each site are locally coupled to an individual bath with many internal modes. In addition, the particles in the same internal mode can hop between the baths such that the collection of the baths forms the environment described by the Hamiltonian

$$\hat{H}_{\text{bath}} = \sum_{\mathbf{k},\alpha} \boldsymbol{b}_{\mathbf{k},\alpha}^{\dagger} \mathcal{H}_{\text{bath}} \boldsymbol{b}_{\mathbf{k},\alpha}$$

where $\boldsymbol{b}_{\mathbf{k},\alpha} = (b_{\uparrow,\mathbf{k},\alpha}, b_{\downarrow,\mathbf{k},\alpha})^{\mathrm{T}}$ and

$$\mathcal{H}_{\text{bath}} = \begin{pmatrix} \omega_\alpha & J_{\mathbf{k}} \\ J_{\mathbf{k}}^{*} & \omega_\alpha \end{pmatrix}. \tag{8}$$

Here ω_α is the mode energy in the bath and

$$J_{\mathbf{k}} = |J_{\mathbf{k}}| e^{i\phi_{\mathbf{k}}}$$

describes the coupling between the baths. $\mathcal{H}_{\rm bath}$ can be diagonalised by an unitary transformation $U_{\mathbf{k}}$

$$U_{\mathbf{k}} = \frac{\sqrt{2}}{2}\begin{pmatrix} e^{i\phi_{\mathbf{k}}} & -e^{i\phi_{\mathbf{k}}} \\ 1 & 1 \end{pmatrix}, \tag{9}$$

such that

$$\hat{H}_{\rm bath} = \sum_{\mathbf{k},\alpha} \boldsymbol{\beta}^\dagger_{\mathbf{k},\alpha} \begin{pmatrix} \epsilon^+_{\mathbf{k},\alpha} & 0 \\ 0 & \epsilon^-_{\mathbf{k},\alpha} \end{pmatrix} \boldsymbol{\beta}_{\mathbf{k},\alpha},$$

where $\boldsymbol{\beta}_{\mathbf{k},\alpha} = U^\dagger_{\mathbf{k}} \boldsymbol{b}_{\mathbf{k},\alpha}$ and

$$\epsilon^\pm_{\mathbf{k},\alpha} = \omega_\alpha \pm |J_{\mathbf{k}}|.$$

Finally, since the system-bath coupling is local, the part of the Hamiltonian describing the interaction between the system and the environment can be written as

$$\hat{H}_{\rm int} = \sum_{\mathbf{n},\alpha} \left[\boldsymbol{\psi}^\dagger_{\mathbf{n}} K \boldsymbol{b}_{\mathbf{n},\alpha} + \text{h.c.}\right],$$

where $\mathbf{n}$ labels the unit cells, $K = \text{diag}(\kappa_1, \kappa_2)$ contains real coupling strengths κ_1 and κ_2, and

$$\boldsymbol{b}_{\mathbf{n},\alpha} = \frac{1}{\sqrt{N}} \sum_{\mathbf{k}} e^{i\mathbf{k}\cdot\mathbf{R}_{\mathbf{n}}} \boldsymbol{b}_{\mathbf{k},\alpha}$$
$$\boldsymbol{\psi}_{\mathbf{n}} = \frac{1}{\sqrt{N}} \sum_{\mathbf{k}} e^{i\mathbf{k}\cdot\mathbf{R}_{\mathbf{n}}} \boldsymbol{\psi}_{\mathbf{k}}.$$

Here $\mathbf{R}_{\mathbf{n}}$ denotes the lattice vector. Transforming back to Fourier space and adopting the diagonalised basis for the baths, we obtain

$$\begin{aligned}\hat{H}_{\rm int} &= \sum_{\mathbf{k},\alpha} \left[\boldsymbol{\psi}^\dagger_{\mathbf{k}} K \boldsymbol{b}_{\mathbf{k},\alpha} + \text{h.c.}\right] \\ &= \sum_{\mathbf{k},\alpha} \left[\boldsymbol{\psi}^\dagger_{\mathbf{k}} K U^\dagger_{\mathbf{k}} \boldsymbol{\beta}_{\mathbf{k},\alpha} + \text{h.c.}\right].\end{aligned}$$

The full Hamiltonian for the system-environment is thus given by

$$\hat{H}_{\rm f} = \hat{H}_{\rm sys} + \hat{H}_{\rm bath} + \hat{H}_{\rm int}. \tag{10}$$

To obtain an effective Hamiltonian from (10), we study the retarded Green's function for the system defined as

$$\begin{aligned} &G^{\rm R}(\mathbf{k}, t-t') = -i\Theta(t-t') \\ &\times \left(\left\langle \begin{Bmatrix} \psi_{\uparrow,\mathbf{k}}(t), \psi^\dagger_{\uparrow,\mathbf{k}}(t') \\ \psi_{\downarrow,\mathbf{k}}(t), \psi^\dagger_{\uparrow,\mathbf{k}}(t') \end{Bmatrix} \right\rangle \left\langle \begin{Bmatrix} \psi_{\uparrow,\mathbf{k}}(t), \psi^\dagger_{\downarrow,\mathbf{k}}(t') \\ \psi_{\downarrow,\mathbf{k}}(t), \psi^\dagger_{\downarrow,\mathbf{k}}(t') \end{Bmatrix} \right\rangle \right),\end{aligned}$$

where $\psi_{\uparrow,\mathbf{k}}(t) \equiv e^{i\hat{H}_{\rm f} t} \psi_{\uparrow,\mathbf{k}} e^{-i\hat{H}_{\rm f} t}$ and $\langle \cdots \rangle$ stands for the average over the system and the environment. Using the standard Keldysh formalism, we integrate out the degrees of freedom of the baths and obtain the Dyson's equation for the retarded Green's function in the momentum-frequency space as

$$[G^{\rm R}(\mathbf{k},\epsilon)]^{-1} = [G^{\rm R}_0(\mathbf{k},\epsilon)]^{-1} - \Sigma^{\rm R}(\mathbf{k},\epsilon). \tag{11}$$

Here $G^{\rm R}_0(\mathbf{k},\epsilon)$ is the Green's function in the absence of coupling to the baths, whose inverse is given by

$$[G^{\rm R}_0(\mathbf{k},\epsilon)]^{-1} = \epsilon\mathbb{I} - \mathcal{H}_{\rm sys}(\mathbf{k}).$$

$\Sigma^{\rm R}(\mathbf{k},\epsilon)$ is the self-energy given by

$$\Sigma^{\rm R}(\mathbf{k},\epsilon) = K U_{\mathbf{k}} \left[\sum_\alpha \Pi^{\rm R}_{0,\alpha}(\mathbf{k},\epsilon)\right] U^\dagger_{\mathbf{k}} K^\dagger,$$

where $\Pi^{\rm R}_{0,\alpha}(\mathbf{k},\epsilon) = [\epsilon\mathbb{I} - \text{diag}(\epsilon^+_{\mathbf{k},\alpha}, \epsilon^-_{\mathbf{k},\alpha}) + \text{i}0^+]^{-1}$ is the retarded Green's function for the bath mode α. Introducing the spectral function $A(\mathbf{k},\epsilon) = \text{diag}(A_+(\mathbf{k},\epsilon), A_-(\mathbf{k},\epsilon))$, where

$$A_\pm(\mathbf{k},\epsilon) \equiv 2\pi \sum_\alpha \delta(\epsilon - \epsilon^\pm_{\mathbf{k},\alpha}), \tag{12}$$

we can write

$$\begin{aligned}\sum_\alpha \Pi^{\rm R}_{0,\alpha}(\mathbf{k},\epsilon) &= \int \frac{d\omega}{2\pi} \frac{A(\mathbf{k},\omega)}{\epsilon - \omega + i0^+} \\ &= \mathcal{P}\int \frac{d\omega}{2\pi} \frac{A(\mathbf{k},\omega)}{\epsilon-\omega} - i\frac{1}{2}A(\mathbf{k},\epsilon).\end{aligned}$$

Thus $\Sigma^{\rm R}(\mathbf{k},\epsilon)$ contains a dispersion (real) part and a dissipation (imaginary) part. We shall assume that the self-energy is slowly varying in ϵ around the Fermi energy μ, whereby we can approximate it to be independent of ϵ, i.e.,

$$\Sigma^{\rm R}(\mathbf{k},\epsilon) \approx \Sigma^{\rm R}(\mathbf{k},\mu).$$

This is a good approximation for weak couplings between the environment and the system. Under this approximation we can write

$$\Sigma^{\rm R}(\mathbf{k},\epsilon) \approx \mathcal{H}_{\rm disp} + i\mathcal{H}_{\rm diss},$$

where

$$\begin{aligned}\mathcal{H}_{\rm disp} &= K U^\dagger_{\mathbf{k}} \left[\mathcal{P}\int \frac{d\omega}{2\pi} \frac{A(\mathbf{k},\omega)}{\mu-\omega}\right] U_{\mathbf{k}} K^\dagger \\ \mathcal{H}_{\rm diss} &= -\frac{1}{2} K U_{\mathbf{k}} A(\mathbf{k},\mu) U^\dagger_{\mathbf{k}} K^\dagger.\end{aligned} \tag{13}$$

Now in order to extract an effective Hamiltonian for the system, we recall that in the absence of coupling to the baths, the single particle Hamiltonian of the system can be obtained directly from (11) as

$$\mathcal{H}_{\rm sys} = \epsilon\mathbb{I} - [G^{\rm R}_0(\mathbf{k},\epsilon)]^{-1}.$$

Analogously, in the presence of the baths we obtain the effective single particle Hamiltonian as

$$\begin{aligned}\mathcal{H}_{\text{eff}} &= \epsilon\mathbb{I} - [G^{\text{R}}(\mathbf{k},\epsilon)]^{-1} \\ &\approx \mathcal{H}_{\text{sys}} + \mathcal{H}_{\text{disp}} + i\mathcal{H}_{\text{diss}}. \end{aligned} \tag{14}$$

By writing

$$\mathcal{H}_{\text{sys}} + \mathcal{H}_{\text{disp}} = \mathbf{d}(\mathbf{k})\cdot\boldsymbol{\sigma}$$

and

$$\mathcal{H}_{\text{diss}} = \gamma_0\sigma_0 + \sum_{i=x,y,z}\gamma_i\sigma_i, \tag{15}$$

we arrive at the effective Hamiltonian given in (3).

We next show that the previously assumed constraint (2) follows from the physical consideration that the baths have finite density of states. From (15) we can calculate the γ_i coefficients as

$$\gamma_i = \frac{1}{2}\text{Tr}(\sigma_i\mathcal{H}_{\text{diss}}) \tag{16}$$

where $i = 0, x, y, z$. Using (13) and (9) in (16) we find

$$\gamma_0(\mathbf{k}) = -\frac{\kappa_1^2+\kappa_2^2}{8}\left[A_+(\mathbf{k},\mu) + A_-(\mathbf{k},\mu)\right] \tag{17}$$

$$\gamma_x(\mathbf{k}) = -\frac{\kappa_1\kappa_2\cos\phi_{\mathbf{k}}}{4}\left[A_+(\mathbf{k},\mu) - A_-(\mathbf{k},\mu)\right] \tag{18}$$

$$\gamma_y(\mathbf{k}) = -\frac{\kappa_1\kappa_2\sin\phi_{\mathbf{k}}}{4}\left[A_+(\mathbf{k},\mu) - A_-(\mathbf{k},\mu)\right]$$

$$\gamma_z(\mathbf{k}) = -\frac{\kappa_1^2-\kappa_2^2}{8}\left[A_+(\mathbf{k},\mu) + A_-(\mathbf{k},\mu)\right]. \tag{19}$$

It is clear from (17) that γ_0 is always non-positive because the spectral functions of the baths are non-negative. A straightforward calculation yields

$$\frac{\gamma_x^2+\gamma_y^2+\gamma_z^2}{\gamma_0^2} = 1 - \frac{16{\kappa_2}^2{\kappa_1}^2A_+A_-}{(\kappa_1^2+\kappa_2^2)^2(A_++A_-)^2}.$$

Again, since the spectral functions of the bath are non-negative, it is easy to show from the above expression that

$$0 \le \frac{\gamma_x^2+\gamma_y^2+\gamma_z^2}{\gamma_0^2} \le 1$$

This result, along with the fact that γ_0 is non-positive, immediately leads to the constraint in (2).

In the previous section we have proven that the constraint in (2) means that the imaginary part of the eigenvalues of the effective non-Hermitian Hamiltonian must be non-positive. Now we are in a position to discuss the physical implication of this property. From (14) we can write

$$G^{\text{R}}(\mathbf{k},\epsilon) = \left(\epsilon\mathbb{I} - \mathcal{H}_{\text{eff}}(\mathbf{k}) + i0^+\right)^{-1}.$$

The density of states of the system is thus given by

$$\begin{aligned}D_{\text{eff}}(\epsilon) &= -\frac{1}{\pi N\Omega}\sum_{\mathbf{k}}\text{Tr}\left[\text{Im}G^{\text{R}}(\mathbf{k},\epsilon)\right] \\ &= -\frac{1}{\pi N\Omega}\sum_{\mathbf{k}}\sum_{s=\pm}\frac{\text{Im}\lambda^s(\mathbf{k})}{(\epsilon-\text{Re}\lambda^s(\mathbf{k}))^2+(\text{Im}\lambda^s(\mathbf{k}))^2}.\end{aligned}$$

We now see that the property in (7) ensures that the density of states of the system is non-negative, which is a physical requirement for any non-Hermitian effective Hamiltonian.

It should be noted that this construction can not result in parity-time (PT) symmetric systems, often realised in photonics[108]. These systems contain external gains, and the PT-symmetry ensures that eigenvalues appear in complex-conjugated pairs. In special cases, the spectrum is real [109]. These systems have been heavily studied in recent years, but are not the main focus of this article.

IV. REAL SPACE BEHAVIOUR OF THE NON-HERMITIAN TERMS

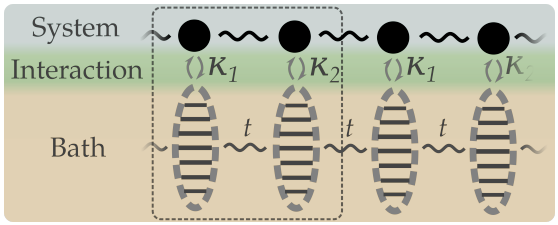

FIG. 1. (Color online) One-dimensional example of a SSH chain, coupled to an environment composed of tight-binding local baths. The unit cell is comprised of two sites, yielding a two-band model.

In the previous section we have seen that the γ_i parameters in the non-Hermitian effective Hamiltonian are momentum dependent, indicating that the dissipation of the system is generally non-local in real space. Although this is to be expected because the baths are coupled to each other, it is instructive to examine a specific example and study how the properties of the baths affect the real space behaviour of the non-hermitian terms. In this section, we consider a two-band chain (e.g. a Su-Schrieffer-Heeger (SSH) model) with a bath at every lattice site, as illustrated in Fig. 1. The coupling between the baths is described by (8). For simplicity, we take the tight-binding coupling between the baths for which

$$J_k = -t(1+e^{ika}),$$

where t is the nearest neighbour hopping parameter, a is the spacing between the adjacent unit cells and $-\pi/a < k \le \pi/a$ is the wave vector in the first Brillouin zone. We

thus find the bath band dispersion is given by

$$\epsilon^{\pm}_{k,\alpha} = \omega_\alpha \pm 2t\cos\frac{ka}{2}.$$

and the phase of the coupling is determined by

$$e^{i\phi_k} = e^{ika/2}.$$

Lastly, we assume that each local bath is Ohmic, namely the density of states of the local bath can be written as

$$D_{\rm bath}(\epsilon) \equiv 2\pi\sum_\alpha \delta(\epsilon-\omega_\alpha) = D_0\epsilon\Theta(\epsilon).$$

Under this assumption and using (12), the spectral function of the collection of baths is given by

$$A_\pm(k,\mu) = D_0\left(\mu \mp 2t\cos\frac{ka}{2}\right)\Theta\left(\mu\mp 2t\cos\frac{ka}{2}\right). \tag{20}$$

Now we can determine the real space behaviour of the non-hermitian parameters by performing the Fourier transform

$$\tilde{\gamma}_i(n) \equiv \frac{a}{2\pi}\int_{-\pi/a}^{\pi/a} dk e^{ikna}\gamma_i(k), \tag{21}$$

where $n = 0, \pm1, \pm2, \cdots$ is the relative distance (in units of a) between two unit cells. It is clear from (17) and (19) that

$$\tilde{\gamma}_0(n) = \frac{\kappa_1^2+\kappa_2^2}{\kappa_1^2-\kappa_2^2}\tilde{\gamma}_z(n).$$

Using (20) and (18)-(19) in (21), we find

$$\tilde{\gamma}_x(n) = \frac{\kappa_1\kappa_2}{8\pi}D_0 t\left[4(\pi-\theta)\delta_{n,0} + 2\pi(\delta_{n,1}+\delta_{n,-1}) + \frac{2\sin 2n\theta}{(4n^2-1)n}(1-\delta_{n,0}) + \frac{\sin 2(n+1)\theta}{2n^2+3n+1} - \frac{\sin 2(n-1)\theta}{2n^2-3n+1}\right] \tag{22}$$

$$\tilde{\gamma}_y(n) = i\frac{\kappa_1\kappa_2}{8\pi}D_0 t\left[2\pi(\delta_{n,1}-\delta_{n,-1}) + \frac{4\sin 2n\theta}{4n^2-1} - \frac{\sin 2(n+1)\theta}{2n^2+3n+1} - \frac{\sin 2(n-1)\theta}{2n^2-3n+1}\right]$$

$$\tilde{\gamma}_z(n) = -\frac{\kappa_1^2-\kappa_2^2}{8\pi}D_0 t\left[4(\pi-\theta)\cos\theta\delta_{n,0} + \frac{2\sin 2n\theta\cos\theta}{(4n^2-1)n}(1-\delta_{n,0}) - \frac{4\cos 2n\theta\sin\theta}{4n^2-1}\right], \tag{23}$$

where $\theta = 0$ for $\mu \geq 2t$ and $\theta = \cos^{-1}(\mu/2t)$ for $\mu < 2t$. From (22)-(23) we immediately see that for small hopping amplitudes of the bath particles, more specifically for $t \leq \mu/2$, the dissipation of the system is restricted to on-site or to the nearest neighbour sites. Interestingly, the real-space non-Hermitian terms exhibit a type of universal behaviour in this parameter region, namely we see that $\gamma_i(n)/t$ are independent of the hopping parameter t when $t \leq \mu/2$. This is a good sign for realising toy models of non-hermitian lattice systems with tight-binding non-hermitian terms. For $t > \mu/2$, in contrast, the dissipation spreads beyond the nearest neighbour sites, which is expected due to the increasing mobility of the bath particles.

V. CONCLUDING REMARKS

In this paper, we study one possible origin of the non-Hermitian Hamiltonians used in the non-Hermitian topological band theories, namely a quantum system coupled to an environment. We show that the effective non-Hermitian Hamiltonian of such a system will generally carry a constraint, which can affect the complex energy spectrum of the Hamiltonian in a significant way. In the Hermitian case, it is known that the topological band theory can be simulated by quantum systems such as cold atomic gases as well as by classical systems such as photonic crystals. For non-Hermitian topological band theories, however, our study suggests that their simulation using passive quantum systems may encounter some difficulties, due to the constraint on the complex energy spectrum of the resulting non-Hermitian Hamiltonian. On the other hand, it will be interesting to investigate the topological properties of such constrained non-Hermitian models. This will be the subject of future studies.

ACKNOWLEDGMENTS

We thank Prof. Hui Zhai for initiating this project and for his valuable suggestions. J. M. Midtgaard wishes to acknowledge the support of the Danish Council of Independent Research – Natural Sciences via Grant No. DFF - 4002-00336. Y. Chen acknowledges that this work was supported by NSFC under Grant No. 11604225(YC) and No. 11734010(YC), Beijing Natural Science Foundation (Z180013)(YC), Foundation of Beijing Education Committees under Grant No. KM201710028004(YC).

AUTHOR CONTRIBUTION STATEMENT

All authors contributed to the analysis and writing of the manuscript. Every author has discussed and reviewed the manuscript before publication.

[1] M. Z. Hasan, and C. L. Kane, Rev. Mod. Phys. **82**, 3045 (2010).
[2] X. L. Qi, and S. C. Zhang, Rev. Mod. Phys. **83**, 1057(2011).
[3] A. Bansil, H. Lin, and T. Das, Rev. Mod. Phys. **88**, 021004(2016).
[4] C. K. Chiu, J. C. Y. Teo, A. P. Schnyder, and S. Ryu, Rev. Mod. Phys. **88**, 035005(2016).
[5] N. P. Armitage, E. J. Mele, and A. Vishwanath, Rev. Mod. Phys. **90**, 015001 (2018).
[6] N. Goldman, J. C. Budich, and P. Zoller, Nat. Phys. **12**, 639 (2016)
[7] N. R. Cooper, J. Dalibard, and I. B. Spielman, arXiv:1803.00249 (2018).
[8] T. Ozawa, H. M. Price, A. Amo, N. Goldman, M. Hafezi, L. Lu, M. Rechtsman, D. Schuster, J. Simon, O. Zilberberg, and I. Carusotto, arXiv:1802.04173 (2018)
[9] M. Aidelsburger, S. Nascimbene, N. Goldman, arXiv:1710.00851(2017)
[10] M. S. Rudner and L. S. Levitov, Phys. Rev. Lett. **102**, 065703 (2009).
[11] M. S. Rudner and L. S. Levitov, Phys. Rev. B **82**, 155418 (2010)
[12] Y. C. Hu and T. L. Hughes, Phys. Rev. B **84**, 153101 (2011).
[13] K. Esaki, M. Sato, K. Hasebe, and M. Kohmoto, Phys. Rev. B **84**, 205128 (2011).
[14] M. Sato, K. Hasebe, K. Esaki, and M. Kohmoto, Prog. Theor. Phys. **127**, 937 (2012)
[15] D. I. Pikulin and Y. V. Nazarov, Phys. Rev. B **87**, 235421 (2013).
[16] S.-D. Liang and G.-Y. Huang, Phys. Rev. A **87**, 012118 (2013).
[17] H. Schomerus, Opt. Lett. **38**, 1912 (2013).
[18] S. Malzard, C. Poli, and H. Schomerus, Phys. Rev. Lett. **115**, 200402 (2015).
[19] P. SanJose, J. Cayao, E. Prada, and R. Aguado, Sci. Rep. **6**, 21427 (2016).
[20] J. González and R. A. Molina, Phys. Rev. Lett. **116**, 156803 (2016)
[21] J. González and R. A. Molina, Phys. Rev. B **96**, 045437 (2017)
[22] R. A. Molina and J. González, Phys. Rev. Lett. **120**, 146601 (2018)
[23] T. E. Lee, Phys. Rev. Lett. **116**, 133903(2016).
[24] A. K. Harter, T. E. Lee, and Y. N. Joglekar, Phys. Rev. A **93**, 062101 (2016).
[25] D. Leykam, K. Y. Bliokh, C. Huang, Y. D. Chong, and F. Nori, Phys. Rev. Lett. **118**, 040401 (2017).
[26] Y. Xu, S.-T. Wang, and L.-M. Duan, Phys. Rev. Lett. **118**, 045701 (2017).
[27] H. Menke and M. M. Hirschmann, Phys. Rev. B **95**, 174506 (2017).
[28] L. Campos Venuti, Z. Ma, H. Saleur, and S. Haas, Phys. Rev. A **96**, 053858 (2017).
[29] S. Lieu, Phys. Rev. B **97**, 045106 (2018).
[30] A. A. Zyuzin and A. Yu. Zyuzin, Phys. Rev. B **97**, 041203(R) (2018).
[31] A. Cerjan, M. Xiao, L. Yuan, and S. Fan, Phys. Rev. B **97**, 075128 (2018).
[32] V. M. Martinez Alvarez, J. E. Barrios Vargas, and L. E. F. Foa Torres, Phys. Rev. B **97**, 121401(R) (2018).
[33] H. Shen, B. Zhen and L. Fu, Phys. Rev. Lett. **120**, 146402(2018).
[34] H. Shen, and L. Fu, Phys. Rev. Lett. **121**, 026403 (2018).
[35] Y. Xiong, J. Phys. Commun. 2, 035043 (2018).
[36] C. Yin, H. Jiang, L. Li, R. Lü, and S. Chen, Phys. Rev. A 97, 052115 (2018).
[37] V. Kozii and L. Fu, arXiv: 1708.05841.
[38] K. Kawabata, Y. Ashida, H. Katsura, and M. Ueda, Phys. Rev. B **98**, 085116 (2018).
[39] X. Ni, D. Smirnova, A. Poddubny, D. Leykam, Y. Chong, and A. B. Khanikaev, Phys. Rev. B **98**, 165129 (2018).
[40] M. Papaj, H. Isobe, and L. Fu, arXiv: 1802.00443.
[41] S. Yao, and Z. Wang, Phys. Rev. Lett. **121**, 086803 (2018).
[42] S. Yao, F. Song, and Z. Wang, Phys. Rev. Lett. **121**, 136802 (2018).
[43] K. Kawabata, S. Higashikawa, Z. Gong, Y. Ashida, and M. Ueda, Phys. Rev. X **8**, 031079 (2018).
[44] F. K. Kunst, E. Edvardsson, J. C. Budich, and E. J. Bergholtz, Phys. Rev. Lett. **121**, 026808 (2018).
[45] J. Carlström and E. J. Bergholtz, Phys. Rev. A **98**, 042114 (2018).
[46] K. Kawabata, K. Shiozaki, and M. Ueda, Phys. Rev. B **98**, 165148 (2018).
[47] K. Takata and M. Notomi, Phys. Rev. Lett. **121**, 213902 (2018).
[48] K. Kawabata, S. Higashikawa, Z. Gong, Y. Ashida, and M. Ueda, Nat. Commun. **10**, 297 (2019).
[49] Y. Chen, and H. Zhai, Phys. Rev. B **98**, 245130 (2018).
[50] T. Yoshida, R. Peters, and N. Kawakami, Phys. Rev. B **98**, 035141 (2018)
[51] X. Qiu, T.-S. Deng, Y. Hu, P. Xue, and W. Yi, arXiv: 1806.10268.
[52] Z. Yang and J. Hu, Phys. Rev. B **99**, 081102 (2019).
[53] H. Wang, J. Ruan, and H. Zhang, Phys. Rev. B **99**, 075130 (2019).
[54] C. H. Lee and R. Thomale, arXiv: 1809.02125.
[55] L. Jin and Z. Song, Phys. Rev. B **99**, 081103 (2019)
[56] J. C. Budich, J. Carlström, F. K. Kunst, and E. J. Bergholtz, Phys. Rev. B **99**, 041406 (2019).
[57] R. Okugawa and T. Yokoyama, Phys. Rev. B **99**, 041202 (2019).

[58] T. Liu, Y.-R. Zhang, Q. Ai, Z. Gong, K. Kawabata, M. Ueda, and F. Nori, Phys. Rev. Lett. **122**, 076801 (2019).
[59] H. Zhou, J. Y. Lee, S. Liu, and B. Zhen, Optica **6**, 190 (2019).
[60] J. Carlström, M. Stålhammar, J. C. Budich, and E. J. Bergholtz, Phys. Rev. B **99**, 161115 (2019).
[61] E. Edvardsson, F. K. Kunst, and E. J. Bergholtz, rXiv:1812.09060.
[62] K. Kawabata, K. Shiozaki, M. Ueda, and M. Sato, arXiv: 1812.09133.
[63] H. Zhou, and J. Y. Lee, arXiv:1812.10490.
[64] L. Herviou, J. H. Bardarson, and N. Regnault, arXiv:1901.00010.
[65] K. Y. Bliokh, D. Leykam, M. Lein, and F. Nori, arXiv:1901.00346.
[66] M. G. Silveirinha, Phys. Rev. B **99**, 125155 (2019).
[67] C. Wang, and X. R. Wang, arXiv:1901.06982.
[68] Q. Zeng, Y. Yang, and Y. Xu, arXiv:1901.08060.
[69] H. Jiang, L. Lang, C. Yang, S. Zhu, and S. Chen, arXiv:1901.09399.
[70] M. R. Hirsbrunner, T. M. Philip, and M. J. Gilbert, arXiv:1901.09961.
[71] H.-G. Zirnstein, G. Refael, and B. Rosenow, arXiv:1901.11241.
[72] W. B. Rui, Y. X. Zhao, and A. P. Schnyder, arXiv:1902.06617.
[73] D. S. Borgnia, A. J. Kruchkov, and R.-J. Slager, arXiv:1902.07217.
[74] A. Ghatak, and T. Das, J. Phys.: Condens. Matter **31**, 263001 (2019).
[75] K. Kawabata, T. Bessho, and M. Sato, arXiv:1902.08479.
[76] K. Yokomizo, and S. Murakami, arXiv:1902.10958.
[77] J. D. H. Rivero, and L. Ge, arXiv:1903.02231.
[78] X. Luo, and C. Zhang, arXiv:1903.02448.
[79] T. Deng, and W. Yi, arXiv:1903.03811.
[80] Z. Ge, Y. Zhang, T. Liu, S. Li, H. Fan, and F. Nori, arXiv:1903.09985.
[81] E. J. Bergholtz, and J. C. Budich, arXiv:1903.12187.
[82] P. A. McClarty, and J. G. Rau, arXiv:1904.02160.
[83] X. Yang, Y. Cao, and Y. Zhai, arXiv:1904.02492.
[84] G. Dubach, and Y. Peled, arXiv:1904.04312.
[85] J. Hou, Z. Li, Q. Gu, and C. Zhang, arXiv:1904.05260.
[86] N. Okuma, and M. Sato, arXiv:1904.06355.
[87] S. Lieu, arXiv:1904.07481.
[88] T. Ohashi, S. Kobayashi, and Y. Kawaguchi, arXiv:1904.08724.
[89] K. Snizhko, R. Egger, and Y. Gefen, arXiv:1904.11673.
[90] F. Song, S. Yao, and Z. Wang, arXiv:1904.08432.
[91] F. Song, S. Yao, and Z. Wang, arXiv:1905.02211.
[92] C. Poli, M. Bellec, U. Kuhl, F. Mortessagne, and H. Schomerus, Nature Commun. **6**, 6710 (2015).
[93] J. M. Zeuner, M. C. Rechtsman, Y. Plotnik, Y. Lumer, S. Nolte, M. S. Rudner, M. Segev, and A. Szameit, Phys. Rev. Lett. **115**, 040402 (2015).
[94] B. Zhen, C. W. Hsu, Y. Igarashi, L. Lu, I. Kaminer, A. Pick, S. L. Chua, J. D. Joannopoulos, and M. Soljačić, Nature **525**, 354 (2015).
[95] S. Weimann, M. Kremer, Y. Plotnik, Y. Lumer, S. Nolte, K. G. Makris, M. Segev, M. C. Rechtsman, and A. Szameit, Nature Mater. **16**, 433 (2017).
[96] D. Kim, K. Mochizuki, N. Kawakami, and H. Obuse, arXiv: 1609.09650; L. Xiao, X. Zhan, Z. H. Bian, K. K. Wang, X. Zhang, X. P. Wang, J. Li, K. Mochizuki, D. Kim, N. Kawakami, W. Yi, H. Obuse, B. C. Sanders, and P. Xue, Nature Phys. **13**, 1117 (2017).
[97] X. Zhan, L. Xiao, Z. Bian, K. Wang, X. Qiu, B. C. Sanders, W. Yi, and P. Xue, Phys. Rev. Lett. **119**, 130501 (2017)
[98] P. St-Jean, V. Goblot, E. Galopin, A. Lemaître, T. Ozawa, L. Le Gratiet, I. Sagnes, J. Bloch, and A. Amo, Nature Photon. **11**, 651 (2017).
[99] H. Zhou, C. Peng, Y. Yoon, C. W. Hsu, K. A. Nelson, L. Fu, J. D. Joannopoulos, M. Soljacić, and B. Zhen, Science **359**, 1009 (2018).
[100] H. Zhao, P. Miao, M. H. Teimourpour, S. Malzard, R. El-Ganainy, H. Schomerus, and L. Feng, Nature Commun. **9**, 981 (2018).
[101] M. Pan, H. Zhao, P. Miao, S. Longhi, and L. Feng, Nature Commun. **9**, 1308 (2018).
[102] M. Parto, S. Wittek, H. Hodaei, G. Harari, M. A. Bandres, J. Ren, M. C. Rechtsman, M. Segev, D. N. Christodoulides, and M. Khajavikhan, Phys. Rev. Lett. **120**, 113901 (2018).
[103] G. Harari, M. A. Bandres, Y. Lumer, M. C. Rechtsman, Y. D. Chong, M. Khajavikhan, D. N. Christodoulides, and M. Segev, Science **359**, eaar4003 (2018);
[104] M. A. Bandres, S. Wittek, G. Harari, M. Parto, J. Ren, M. Segev, D. Christodoulides, and M. Khajavikhan, Science **359**, eaar4005 (2018).
[105] K. Wang, X. Qiu, L. Xiao, X. Zhan, Z. Bian, B. C. Sanders, W. Yi, and P. Xue, arXiv: 1808.06446.
[106] A. Cerjan, S. Huang, K. P. Chen, Y. Chong, and M. C. Rechtsman, arXiv: 1808.09541.
[107] L. He, Z. Addison, J. Jin, E. J. Mele, S. G. Johnson, and B. Zhen, arXiv:1902.08560.
[108] Feng, Liang and El-Ganainy, Ramy and Ge, Li, Nat. Phot. **11** 752-762 (2017).
[109] A. Mostafazadeh, Journal of Mathematical Physics **43**, 205 (2002)

— 7 —

Summary

In this thesis I have summarized my work during my PhD at the Institute of Physics and Astronomy at Aarhus University, and briefly at Tsinghua University in Beijing. The bulk of the work has been centered around topological superfluidity in mixed-dimensional Bose-Fermi mixtures, which seems to be a promising testbed for realizing topological phases of matter. Initially, I have thought the experimental realization of these systems would be quite a few years off, but the work by Schäfer *et al.* on Yb-^{7}Li mixtures has bolstered my confidence that a chiral superfluid in a cold atomic gas might be within reach before long. The main hurdle is achieving low enough temperatures.

For detecting the subtle signatures of these states there is still a need for clear probes, as in the case of topological insulators. The heating rate measurements I explored in chapter 4 are an elegant use of the broken chiral symmetry, but it remains to be seen how challenging the experimental implementation is. This and other ways of detecting topological superfluidity thus remains an interesting avenue of research.

The analysis of superconductivity in atomic gases was then extended to consider FFLO-type superconductivity. At zero temperature we saw that the ability to impose a population imbalance in the bilayer geometry, along with the fine control of the fermion interactions allowed the FFLO-state to be favored over the normal state for a large part of the phase diagram.

The last part of the thesis concerned non-hermitian systems. We studied how to realize some of the models used in non-hermitian topological band theory with passive systems connected to environments. A notable result here was the validation of models with only nearest-neighbour non-hermitian terms. A subject for further studies would be the much discussed class of PT-symmetric non-hermitian Hamiltonians. These are heavily studied in photonic systems, but it would be interesting to study what the conditions for PT-symmetry would be in the context of a lattice system coupled to an environment.

List of Figures

Bibliography

[1] Jonatan Melkær Midtgaard, Zhigang Wu, and G. M. Bruun. "Topological superfluidity of lattice fermions inside a Bose-Einstein condensate." In: *Phys. Rev. A* 94 (6 Dec. 2016), p. 063631.

[2] Jonatan Melkær Midtgaard, Zhigang Wu, and G. M. Bruun. "Time-reversal-invariant topological superfluids in Bose-Fermi mixtures." In: *Phys. Rev. A* 96 (3 Sept. 2017), p. 033605.

[3] Jonatan Melkær Midtgaard and Georg M. Bruun. "Stabilizing Fulde-Ferrell-Larkin-Ovchinnikov superfluidity with long-range interactions in a mixed-dimensional Bose-Fermi system." In: *Phys. Rev. A* 98 (1 July 2018), p. 013624.

[4] Jonatan Melkær Midtgaard, Zhigang Wu, and Yu Chen. "Constraints on the energy spectrum of non-Hermitian models in open environments." In: *Eur. Phys. J. B (accepted)* (2019).

[5] Jonatan Melkær Midtgaard, Zhigang Wu, and G. M. Bruun. "Detecting Topological Superfluidity with a Dichroism probe." In: *(in preparation)* (2019).

[6] Oleksandr V. Marchukov, Emil H. Eriksen, Jonatan M. Midtgaard, Alex A.S. Kalaee, Dmitri V. Fedorov, Aksel S. Jensen, and Nikolaj T. Zinner. "Computation of local exchange coefficients in strongly interacting one-dimensional few-body systems: local density approximation and exact results." In: *The European Physical Journal D* 70.2 (Feb. 2016), p. 32.

[7] M. H. Anderson, J. R. Ensher, M. R. Matthews, C. E. Wieman, and E. A. Cornell. "Observation of Bose-Einstein Condensation in a Dilute Atomic Vapor." In: *Science* 269.5221 (July 1995), pp. 198–201.

[8] W Ketterle, M R Andrews, K B Davis, D S Durfee, D M Kurn, M -O Mewes, and N J van Druten. "Bose–Einstein condensation of ultracold atomic gases." In: *Physica Scripta* T66 (Jan. 1996), pp. 31–37.

[9] B. DeMarco and D. S. Jin. "Onset of Fermi Degeneracy in a Trapped Atomic Gas." In: *Science* 285.5434 (1999), pp. 1703–1706. eprint: https://science.sciencemag.org/content/285/5434/1703.full.pdf.

[10] Andrew G. Truscott, Kevin E. Strecker, William I. McAlexander, Guthrie B. Partridge, and Randall G. Hulet. "Observation of Fermi Pressure in a Gas of Trapped Atoms." In: *Science* 291.5513 (2001), pp. 2570–2572. eprint: https://science.sciencemag.org/content/291/5513/2570.full.pdf.

[11] F. Schreck, L. Khaykovich, K. L. Corwin, G. Ferrari, T. Bourdel, J. Cubizolles, and C. Salomon. "Quasipure Bose-Einstein Condensate Immersed in a Fermi Sea." In: *Phys. Rev. Lett.* 87 (8 Aug. 2001), p. 080403.

[12] Jacob F. Sherson, Christof Weitenberg, Manuel Endres, Marc Cheneau, Immanuel Bloch, and Stefan Kuhr. "Single-atom-resolved fluorescence imaging of an atomic Mott insulator." In: *Nature* 467.7311 (2010), pp. 68–72. arXiv: arXiv:1006.3799v1.

[13] A. J. Moerdijk, B. J. Verhaar, and A. Axelsson. "Resonances in ultracold collisions of ^{6}Li, ^{7}Li, and ^{23}Na." In: *Phys. Rev. A* 51 (6 June 1995), pp. 4852–4861.

[14] Cheng Chin, Rudolf Grimm, Paul Julienne, and Eite Tiesinga. "Feshbach resonances in ultracold gases." In: *Rev. Mod. Phys.* 82 (2 Apr. 2010), pp. 1225–1286.

[15] Mohit Randeria and Edward Taylor. "Crossover from Bardeen-Cooper-Schrieffer to Bose-Einstein Condensation and the Unitary Fermi Gas." In: *Annual Review of Condensed Matter Physics* 5.1 (2014), pp. 209–232. eprint: https://doi.org/10.1146/annurev-conmatphys-031113-133829.

[16] M. Holland, S. J. J. M. F. Kokkelmans, M. L. Chiofalo, and R. Walser. "Resonance Superfluidity in a Quantum Degenerate Fermi Gas." In: *Phys. Rev. Lett.* 87 (12 Aug. 2001), p. 120406.

[17] S. J. J. M. F. Kokkelmans, J. N. Milstein, M. L. Chiofalo, R. Walser, and M. J. Holland. "Resonance superfluidity: Renormalization of resonance scattering theory." In: *Phys. Rev. A* 65 (5 May 2002), p. 053617.

[18] Giancarlo Calvanese Strinati, Pierbiagio Pieri, Gerd Röpke, Peter Schuck, and Michael Urban. "The BCS-BEC crossover: From ultracold Fermi gases to nuclear systems." In: *Physics Reports* 738 (2018), pp. 1–76.

[19] Alexei Kitaev. "Periodic table for topological insulators and superconductors." In: *AIP Conference Proceedings* 1134.1 (2009), pp. 22–30. eprint: `https://aip.scitation.org/doi/pdf/10.1063/1.3149495`.

[20] Alexander Altland and Martin R. Zirnbauer. "Nonstandard symmetry classes in mesoscopic normal-superconducting hybrid structures." In: *Phys. Rev. B* 55 (2 Jan. 1997), pp. 1142–1161.

[21] Andreas P. Schnyder. *Topological insulators and superconductors*. 2015.

[22] Andreas W W Ludwig. "Topological phases: classification of topological insulators and superconductors of non-interacting fermions, and beyond." In: *Physica Scripta* T168 (Dec. 2015), p. 014001.

[23] Shinsei Ryu, Andreas P Schnyder, Akira Furusaki, and Andreas W W Ludwig. "Topological insulators and superconductors: tenfold way and dimensional hierarchy." In: *New Journal of Physics* 12.6 (June 2010), p. 065010.

[24] Chetan Nayak, Steven H. Simon, Ady Stern, Michael Freedman, and Sankar Das Sarma. "Non-Abelian anyons and topological quantum computation." In: *Rev. Mod. Phys.* 80 (3 Sept. 2008), pp. 1083–1159.

[25] Michael Stone and Suk-Bum Chung. "Fusion rules and vortices in $p_x + ip_y$ superconductors." In: *Phys. Rev. B* 73 (1 Jan. 2006), p. 014505.

[26] Antonio Fornieri et al. "Evidence of topological superconductivity in planar Josephson junctions." In: *Nature* 569.7754 (2019), pp. 89–92.

[27] Hao-Hua Sun and Jin-Feng Jia. "Detection of Majorana zero mode in the vortex." In: *npj Quantum Materials* 2.1 (2017), p. 34.

[28] F. D. M. Haldane. "Model for a Quantum Hall Effect without Landau Levels: Condensed-Matter Realization of the "Parity Anomaly"." In: *Phys. Rev. Lett.* 61 (18 Oct. 1988), pp. 2015–2018.

[29] Li He, Zachariah Addison, Jicheng Jin, Eugene J Mele, Steven G Johnson, and Bo Zhen. "Floquet Chern insulators of light." In: *Nature Communications* 10.1 (2019), p. 4194.

[30] Titus Neupert, Claudio Chamon, Thomas Iadecola, Luiz H Santos, and Christopher Mudry. "Fractional (Chern and topological) insulators." In: *Physica Scripta* T164 (Aug. 2015), p. 014005.

[31] Kenneth Günter, Thilo Stöferle, Henning Moritz, Michael Köhl, and Tilman Esslinger. "p-Wave Interactions in Low-Dimensional Fermionic Gases." In: *Phys. Rev. Lett.* 95 (23 Nov. 2005), p. 230401.

[32] Liang Jiang, Takuya Kitagawa, Jason Alicea, A. R. Akhmerov, David Pekker, Gil Refael, J. Ignacio Cirac, Eugene Demler, Mikhail D. Lukin, and Peter Zoller. "Majorana Fermions in Equilibrium and in Driven Cold-Atom Quantum Wires." In: *Phys. Rev. Lett.* 106 (22 June 2011), p. 220402.

[33] Stefan Kuhr. "Quantum-gas microscopes: a new tool for cold-atom quantum simulators." In: *National Science Review* 3.2 (Apr. 2016), pp. 170–172. eprint: `http://oup.prod.sis.lan/nsr/article-pdf/3/2/170/7434551/nww023.pdf`.

[34] Ryuta Yamamoto, Jun Kobayashi, Takuma Kuno, Kohei Kato, and Yoshiro Takahashi. "An ytterbium quantum gas microscope with narrow-line laser cooling." In: *New Journal of Physics* 18.2 (Feb. 2016), p. 023016.

[35] N. D. Mermin and H. Wagner. "Absence of Ferromagnetism or Antiferromagnetism in One- or Two-Dimensional Isotropic Heisenberg Models." In: *Phys. Rev. Lett.* 17 (22 Nov. 1966), pp. 1133–1136.

[36] V. L. Berezinskiĭ. "Destruction of Long-range Order in One-dimensional and Two-dimensional Systems having a Continuous Symmetry Group I. Classical Systems." In: *Soviet Journal of Experimental and Theoretical Physics* 32 (Jan. 1971), p. 493.

[37] V. L. Berezinskiĭ. "Destruction of Long-range Order in One-dimensional and Two-dimensional Systems Possessing a Continuous Symmetry Group. II. Quantum Systems." In: *Soviet Journal of Experimental and Theoretical Physics* 34 (Jan. 1972), p. 610.

[38] J M Kosterlitz and D J Thouless. "Ordering, metastability and phase transitions in two-dimensional systems." In: *Journal of Physics C: Solid State Physics* 6.7 (Apr. 1973), pp. 1181–1203.

[39] J M Kosterlitz and D J Thouless. "Long range order and metastability in two dimensional solids and superfluids. (Application of dislocation theory)." In: *Journal of Physics C: Solid State Physics* 5.11 (June 1972), pp. L124–L126.

[40] J. CLERK-MAXWELL. "On the Dynamical Evidence of the Molecular Constitution of Bodies." In: *Nature* 11.279 (Mar. 1875), pp. 357–359.

[41] Francesca M. Marchetti, Charles J. M. Mathy, David A. Huse, and Meera M. Parish. "Phase separation and collapse in Bose-Fermi mixtures with a Feshbach resonance." In: *Phys. Rev. B* 78 (13 Oct. 2008), p. 134517.

[42] H. P. Büchler and G. Blatter. "Phase separation of atomic Bose-Fermi mixtures in an optical lattice." In: *Phys. Rev. A* 69 (6 June 2004), p. 063603.

[43] F. Schäfer, N. Mizukami, P. Yu, S. Koibuchi, A. Bouscal, and Y. Takahashi. "Experimental realization of ultracold Yb-^{7}Li mixtures in mixed dimensions." In: *Phys. Rev. A* 98 (5 Nov. 2018), p. 051602.

[44] Anne-Louise Gadsbølle and G. M. Bruun. "Dipolar fermions in a two-dimensional lattice at nonzero temperature." In: *Phys. Rev. A* 86 (3 Sept. 2012), p. 033623.

[45] C. L. Kane and E. J. Mele. "Quantum Spin Hall Effect in Graphene." In: *Phys. Rev. Lett.* 95 (22 Nov. 2005), p. 226801.

[46] Zhong Wang and Shou-Cheng Zhang. "Strongly correlated topological superconductors and topological phase transitions via Green's function." In: *Phys. Rev. B* 86 (16 Oct. 2012), p. 165116.

[47] Zhigang Wu and G. M. Bruun. "Topological Superfluid in a Fermi-Bose Mixture with a High Critical Temperature." In: *Phys. Rev. Lett.* 117 (24 Dec. 2016), p. 245302.

[48] Duc Thanh Tran, Alexandre Dauphin, Adolfo G. Grushin, Peter Zoller, and Nathan Goldman. "Probing topology by heating: Quantized circular dichroism in ultracold atoms." In: *Science Advances* 3.8 (2017). eprint: `https://advances.sciencemag.org/content/3/8/e1701207.full.pdf`.

[49] Anindya Das, Yuval Ronen, Yonatan Most, Yuval Oreg, Moty Heiblum, and Hadas Shtrikman. "Zero-bias peaks and splitting in an Al-InAs nanowire topological superconductor as a signature of Majorana fermions." In: *Nature Physics* 8.12 (Sept. 2012), pp. 887–895. eprint: `1205.7073`.

[50] V. Mourik, K. Zuo, S. M. Frolov, S. R. Plissard, E. P. A. M. Bakkers, and L. P. Kouwenhoven. "Signatures of Majorana Fermions in Hybrid Superconductor-Semiconductor Nanowire Devices." In: *Science* 336.6084 (2012), pp. 1003–1007. eprint: `https://science.sciencemag.org/content/336/6084/1003.full.pdf`.

[51] M. T. Deng, C. L. Yu, G. Y. Huang, M. Larsson, P. Caroff, and H. Q. Xu. "Anomalous Zero-Bias Conductance Peak in a Nb–InSb Nanowire–Nb Hybrid Device." In: *Nano Letters* 12.12 (2012), pp. 6414–6419. eprint: `https://doi.org/10.1021/nl303758w`.

[52] Clifford W. Hicks, John R. Kirtley, Thomas M. Lippman, Nicholas C. Koshnick, Martin E. Huber, Yoshiteru Maeno, William M. Yuhasz, M. Brian Maple, and Kathryn A. Moler. "Limits on superconductivity-related magnetization in Sr_2RuO_4 and $PrOs_4Sb_{12}$ from scanning SQUID microscopy." In: *Phys. Rev. B* 81 (21 June 2010), p. 214501.

[53] Andrew P Mackenzie, Thomas Scaffidi, Clifford W Hicks, and Yoshiteru Maeno. "Even odder after twenty-three years: the superconducting order parameter puzzle of Sr2RuO4." In: *npj Quantum Materials* 2.1 (2017), p. 40.

[54] Immanuel Bloch, Jean Dalibard, and Wilhelm Zwerger. "Many-body physics with ultracold gases." In: *Rev. Mod. Phys.* 80 (3 July 2008), pp. 885–964.

[55] N. Fläschner, B. S. Rem, M. Tarnowski, D. Vogel, D.-S. Lühmann, K. Sengstock, and C. Weitenberg. "Experimental reconstruction of the Berry curvature in a Floquet Bloch band." In: *Science* 352.6289 (2016), pp. 1091–1094. eprint: `https://science.sciencemag.org/content/352/6289/1091.full.pdf`.

[56] Tomoki Ozawa and Hannah M Price. "Topological quantum matter in synthetic dimensions." In: *Nature Reviews Physics* 1.5 (2019), pp. 349–357.

[57] Luca Asteria, Duc Thanh Tran, Tomoki Ozawa, Matthias Tarnowski, Benno S Rem, Nick Fläschner, Klaus Sengstock, Nathan Goldman, and Christof Weitenberg. "Measuring quantized circular dichroism in ultracold topological matter." In: *Nature Physics* 15.5 (2019), pp. 449–454.

[58] P. D. Sacramento, M. A. N. Araújo, and E. V. Castro. "Hall conductivity as bulk signature of topological transitions in superconductors." In: *EPL (Europhysics Letters)* 105.3 (Feb. 2014), p. 37011.

[59] Alexander Altland and Ben D. Simons. *Condensed Matter Field Theory.* 2nd ed. Cambridge University Press, 2010.

[60] Jami J Kinnunen, Jildou E Baarsma, Jani-Petri Martikainen, and Päivi Törmä. "The Fulde-Ferrell-Larkin-Ovchinnikov state for ultracold fermions in lattice and harmonic potentials: a review." In: *Reports on Progress in Physics* 81.4 (Feb. 2018), p. 046401.

[61] Wei Zhang and Wei Yi. "Topological Fulde–Ferrell–Larkin–Ovchinnikov states in spin–orbit-coupled Fermi gases." In: *Nature Communications* 4.1 (2013), p. 2711.

[62] Peter Fulde and Richard A. Ferrell. "Superconductivity in a Strong Spin-Exchange Field." In: *Phys. Rev.* 135 (3A Aug. 1964), A550–A563.

[63] Jeroen P. A. Devreese and Jacques Tempere. "Effect of phase fluctuations on the Fulde-Ferrell-Larkin-Ovchinnikov state in a three-dimensional Fermi gas." In: *Phys. Rev. A* 89 (1 Jan. 2014), p. 013616.

[64] Hiroshi Shimahara. "Structure of the Fulde-Ferrell-Larkin-Ovchinnikov State in Two-Dimensional Superconductors." In: *Journal of the Physical Society of Japan* 67.3 (1998), pp. 736–739. eprint: `https://doi.org/10.1143/JPSJ.67.736`.

[65] A. I. Larkin and Y. N. Ovchinnikov. "Nonuniform state of superconductors." In: *Zh. Eksp. Teor. Fiz.* 47 (1964). [Sov. Phys. JETP20,762(1965)], pp. 1136–1146.

[66] A. Bianchi, R. Movshovich, C. Capan, P. G. Pagliuso, and J. L. Sarrao. "Possible Fulde-Ferrell-Larkin-Ovchinnikov Superconducting State in $CeCoIn_5$." In: *Phys. Rev. Lett.* 91 (18 Oct. 2003), p. 187004.

[67] K. Kumagai, H. Shishido, T. Shibauchi, and Y. Matsuda. "Evolution of Paramagnetic Quasiparticle Excitations Emerged in the High-Field Superconducting Phase of $CeCoIn_5$." In: *Phys. Rev. Lett.* 106 (13 Mar. 2011), p. 137004.

[68] H Mayaffre, S Krämer, M Horvatić, C Berthier, K Miyagawa, K Kanoda, and V F Mitrović. "Evidence of Andreev bound states as a hallmark of the FFLO phase in κ-(BEDT-TTF)2Cu(NCS)2." In: *Nature Physics* 10 (Oct. 2014), p. 928.

[69] R. Lortz, Y. Wang, A. Demuer, P. H. M. Böttger, B. Bergk, G. Zwicknagl, Y. Nakazawa, and J. Wosnitza. "Calorimetric Evidence for a Fulde-Ferrell-Larkin-Ovchinnikov Superconducting State in the Layered Organic Superconductor $\kappa-(BEDT-TTF)_2Cu(NCS)_2$." In: *Phys. Rev. Lett.* 99 (18 Oct. 2007), p. 187002.

[70] Zhen Zheng, Ming Gong, Yichao Zhang, Xubo Zou, Chuanwei Zhang, and Guangcan Guo. "FFLO Superfluids in 2D Spin-Orbit Coupled Fermi Gases." In: *Scientific Reports* 4 (Oct. 2014), p. 6535.

[71] Hao Lee, S. I. Matveenko, Daw-Wei Wang, and G. V. Shlyapnikov. "Fulde-Ferrell-Larkin-Ovchinnikov state in bilayer dipolar systems." In: *Phys. Rev. A* 96 (6 Dec. 2017), p. 061602.

[72] Julian Schwinger. "Brownian Motion of a Quantum Oscillator." In: *Journal of Mathematical Physics* 2.3 (1961), pp. 407–432. eprint: `https://doi.org/10.1063/1.1703727`.

[73] Alex Kamenev. *Field Theory of Non-Equilibrium Systems*. Cambridge University Press, 2011.

[74] Alex Kamenev. *Many-body theory of non-equilibrium systems*. 2004. arXiv: `cond-mat/0412296 [cond-mat.dis-nn]`.

[75] Andreas P. Schnyder, Shinsei Ryu, Akira Furusaki, and Andreas W. W. Ludwig. "Classification of topological insulators and superconductors in three spatial dimensions." In: *Phys. Rev. B* 78 (19 Nov. 2008), p. 195125.

[76] Ching-Kai Chiu, Jeffrey C. Y. Teo, Andreas P. Schnyder, and Shinsei Ryu. "Classification of topological quantum matter with symmetries." In: *Rev. Mod. Phys.* 88 (3 Aug. 2016), p. 035005.

[77] Tsuneya Yoshida, Robert Peters, and Norio Kawakami. "Non-Hermitian perspective of the band structure in heavy-fermion systems." In: *Phys. Rev. B* 98 (3 July 2018), p. 035141.

[78] Krishanu Roychowdhury and Michael J. Lawler. "Classification of magnetic frustration and metamaterials from topology." In: *Phys. Rev. B* 98 (9 Sept. 2018), p. 094432.

[79] Kohei Kawabata, Ken Shiozaki, Masahito Ueda, and Masatoshi Sato. "Symmetry and Topology in Non-Hermitian Physics." In: *Phys. Rev. X* 9 (4 Oct. 2019), p. 041015.

[80] Chun-Hui Liu, Hui Jiang, and Shu Chen. "Topological classification of non-Hermitian systems with reflection symmetry." In: *Phys. Rev. B* 99 (12 Mar. 2019), p. 125103.

[81] Huitao Shen, Bo Zhen, and Liang Fu. "Topological Band Theory for Non-Hermitian Hamiltonians." In: *Phys. Rev. Lett.* 120 (14 Apr. 2018), p. 146402.

[82] Simon Lieu. "Topological phases in the non-Hermitian Su-Schrieffer-Heeger model." In: *Phys. Rev. B* 97 (4 Jan. 2018), p. 045106.

[83] Hui Jiang, Chao Yang, and Shu Chen. "Topological invariants and phase diagrams for one-dimensional two-band non-Hermitian systems without chiral symmetry." In: *Phys. Rev. A* 98 (5 Nov. 2018), p. 052116.

[84] Shunyu Yao, Fei Song, and Zhong Wang. "Non-Hermitian Chern Bands." In: *Phys. Rev. Lett.* 121 (13 Sept. 2018), p. 136802.

[85] Carl M. Bender and Stefan Boettcher. "Real Spectra in Non-Hermitian Hamiltonians Having PT Symmetry." In: *Phys. Rev. Lett.* 80 (24 June 1998), pp. 5243–5246.

[86] Liang Feng, Ramy El-Ganainy, and Li Ge. "Non-Hermitian photonics based on parity–time symmetry." In: *Nature Photonics* 11.12 (2017), pp. 752–762.

[87] Ş K Özdemir, S Rotter, F Nori, and L Yang. "Parity–time symmetry and exceptional points in photonics." In: *Nature Materials* 18.8 (2019), pp. 783–798.

[88] A. L. Fetter and J. D. Walecka. *Quantum Theory of Many-Particle Systems*. Boston: McGraw-Hill, 1971.